

AD-A095 114 NATIONAL RESEARCH COUNCIL OF CANADA OTTAWA (ONTARIO) --ETC F/6 20/4
CONFINED MIXING OF COAXIAL FLOWS (MELANGE D'ECOULEMENTS COAXIAUX--ETC(U)
OCT 80 R A TYLER, R G WILLIAMSON
UNCLASSIFIED DME-LR-602 NRC-18831 NL

1 of 1
AD 95-114

END
DATE
FILMED
3 4 81
DTIC



National Research
Council Canada

Conseil national
de recherches Canada

LEVEL

6

CONFINED MIXING OF COAXIAL FLOWS

DTIC
ELECTE
FEB 17 1981
S C

by

R.A. Tyler, R.G. Williamson

Division of Mechanical Engineering

OTTAWA

OCTOBER 1980

DISTRIBUTION STATEMENT A

Approved for public release;
Distribution Unlimited

Canada

AERONAUTICAL REPORT

LR-602

NRC NO. 18831

81 2 13 008

AD A095114

BBC FILE COPY

CONFINED MIXING OF COAXIAL FLOWS

MÉLANGE D'ÉCOULEMENTS COAXIAUX DANS DES CONDUITS

by/par

R.A. Tyler, R.G. Williamson

**R.A. Tyler, Head/Chef
Gas Dynamics Laboratory/
Laboratoire de la dynamique des gaz**

**E.H. Dudgeon
Director/Directeur**

SUMMARY

An empirical approach is used to correlate the mixing of isothermal incompressible coaxial air flows in straight pipes of constant circular cross-section. An assumed decay function for kinetic momentum is correlated in terms of initial geometry and initial velocities of the mixing streams. The method allows the rapid estimation of quantities of engineering interest including the axial distribution of both static pressure and total momentum. The method has been tested against published data on thrust augmenting ejectors of the parietal type, and found to provide satisfactory reproduction of measured performance as affected by mixing pipe length and area ratio.

RÉSUMÉ

On exploite une approche empirique pour établir la corrélation du mélange d'écoulements d'air coaxiaux incompressibles et isothermiques dans des conduites droites de section circulaire constante. La corrélation, établie en fonction de la géométrie initiale et des vitesses initiales des courants de mélange, utilise une fonction de décroissance hypothétique de la quantité de mouvement cinétique. La méthode retenue rend possible une estimation rapide des grandeurs d'intérêt technique, y compris la répartition axiale de la pression statique et de la quantité de mouvement totale. Les résultats obtenus ont été comparés aux données publiées sur les éjecteurs d'augmentation de la poussée de type pariétal, et on a trouvé que cette méthode reproduisait de façon satisfaisante la performance mesurée, telle que modifiée par la longueur de mélange et le rapport des sections.

Accession For	
NTIS GFA&I	<input checked="" type="checkbox"/>
DTIC TAB	<input type="checkbox"/>
Unannounced	<input type="checkbox"/>
Justification	
By _____	
Distribution/	
Availability Codes	
Avail. and/or	
Dist. Statement	
A	

CONTENTS

	Page
SUMMARY.....	(iii)
SYMBOLS.....	(vii)
1.0 INTRODUCTION.....	1
2.0 ANALYSIS.....	1
2.1 The Momentum Equation in Confined Mixing.....	1
2.2 The Momentum Coefficient Decay Model.....	3
2.3 Initial Momentum Coefficient, β_1 , for Coaxial Flows.....	4
3.0 EXPERIMENTAL DETAILS.....	4
3.1 Apparatus.....	4
4.0 PROCEDURE AND RESULTS.....	5
4.1 Results with $V_i > V_o$	5
4.2 Correlation of Results ($V_i > V_o$).....	5
4.3 Results with $V_o > V_i$	7
4.4 Correlation of Results ($V_o > V_i$).....	8
5.0 SUMMARY OF PREDICTION METHOD.....	9
6.0 APPLICATION OF PREDICTION METHOD TO EJECTOR PERFORMANCE.....	10
7.0 CONCLUSIONS.....	11
8.0 REFERENCES.....	11

ILLUSTRATIONS

Figure		Page
1	Typical Experimental Results.....	13
2	Mixing Process Nomenclature.....	14
3	Idealized Model.....	15
4	Ideal Momentum Coefficient as a Function of Geometry and Velocity Ratio.....	16
5	Maximum Attainable Momentum Coefficient for a Given Velocity Ratio.....	17

ILLUSTRATIONS (Cont'd)

Figure		Page
6	Test Arrangements	18
7(a)	Measured Static Pressure Distribution ($V_i > V_o$).....	19
7(b)	Measured Static Pressure Distribution ($V_i > V_o$).....	20
7(c)	Measured Static Pressure Distribution ($V_i > V_o$).....	21
7(d)	Measured Static Pressure Distribution ($V_i > V_o$).....	22
7(e)	Measured Static Pressure Distribution ($V_i > V_o$).....	23
7(f)	Measured Static Pressure Distribution ($V_o = 0$).....	24
8	Derived Values of d for $V_i > V_o$	25
9	Correlation of Derived d Values with Geometry ($V_i > V_o$).....	26
10	Correlation of Derived k Values with Velocity Ratio ($V_i > V_o$).....	27
11	Final Correlation of Derived k Values ($V_i > V_o$).....	28
12(a)	Predicted and Measured Values of C_p Compared ($V_i > V_o$)	29
12(b)	Predicted and Measured Values of C_p Compared ($V_i > V_o$)	30
12(c)	Predicted and Measured Values of C_p Compared ($V_i > V_o$)	31
12(d)	Predicted and Measured Values of C_p Compared ($V_i > V_o$)	32
12(e)	Predicted and Measured Values of C_p Compared ($V_i > V_o$)	33
12(f)	Predicted and Measured Values of C_p Compared ($V_o = 0$)	34
13	Predicted and Measured Values of \hat{C}_p Compared ($V_i > V_o$)	35
14	Predicted and Measured Values of \hat{x} Compared ($V_i > V_o$)	36
15	Data of Reference 5 Compared with Prediction of Present Method.....	37
16(a)	Measured Static Pressure Distribution ($V_o > V_i$).....	38
16(b)	Measured Static Pressure Distribution ($V_o > V_i$).....	39
16(c)	Measured Static Pressure Distribution ($V_o > V_i$).....	40
17(a)	Measured Velocity Profiles in Mixing Pipe ($V_i > V_o$)	41

ILLUSTRATIONS (Cont'd)

Figure		Page
17(b)	Measured Velocity Profiles in Mixing Pipe ($V_o > V_i$)	42
18	Wall Friction Measurements by Preston Tube	43
19	Alternative Derivations of Δ Compared	44
20	Correlation of Derived Δ Values	45
21	$(V_o/\bar{V} - 1)$ Factor for 'Maximum β ' Geometry	46
22	Correlation of Derived d Values with Geometry ($V_o > V_i$)	47
23	Final Correlation of Derived d Values ($V_o > V_i$)	48
24	Correlation of Derived k Values with Velocity Ratio ($V_o > V_i$)	49
25	Final Correlation of Derived k Values ($V_o > V_i$)	50
26(a)	Predicted and Measured Values of C_p Compared ($V_o > V_i$)	51
26(b)	Predicted and Measured Values of C_p Compared ($V_o > V_i$)	52
26(c)	Predicted and Measured Values of C_p Compared ($V_o > V_i$)	53
27	Predicted and Measured Values of \hat{C}_p Compared ($V_o > V_i$)	54
28	Predicted and Measured Values of \hat{x} Compared ($V_o > V_i$)	55
29(a)	Results of Calculation Procedure Applied to Central Jet Ejectors ($S = 25$)	56
29(b)	Results of Calculation Procedure Applied to Parietal Jet Ejectors ($S = 25$)	57
30	Ejector Performance Corresponding to Calculated Results of Figure 29	58
31	Predicted Performance of Central and Parietal Jet Ejectors, $S = 25$	59
32	Predicted Maximum Mass Flow Ratio and Required Length vs. Area Ratio	60
33	Predicted Maximum Thrust Augmentation Ratio and Required Length vs. Area Ratio	61
34	Predicted Parietal Ejector Performance Compared with Measured Data of Reference 6 ($S = 10$ and 20)	62
35	Predicted Parietal Ejector Performance Compared with Measured Data of Reference 6 ($S = 10$ to 131)	63

SYMBOLS

Symbol	Description
A	flow cross-sectional area
C_p	$\frac{p - p_1}{1/2\rho\bar{V}^2}$
\hat{C}_p	peak value of C_p
d	see Section 2.2
D_i	inside diameter of inner pipe
D_o	inside diameter of outer (mixing) pipe
\bar{D}	D_i/D_o
f	local friction factor, $\frac{\tau}{1/2\rho\bar{V}^2}$
f'	friction factor corresponding to 'fully developed' flow
k	see Section 2.2
L	ejector mixing pipe overall length (D_o)
M	total mass flow rate
p	mean static pressure in flow section
p_1	mean static pressure at initial mixing plane
S	ejector mixing pipe area (primary area)
V	local axial velocity
\bar{V}	mean velocity in mixing pipe
	mean velocity in general $\frac{\int V dA}{A} (= \frac{M}{\rho A} \text{ for constant density})$
V_i	mean velocity of inner flow
V_o	mean velocity of outer flow
V_p	mean velocity of ejector primary flow at initial mixing plane
V_s	mean velocity of ejector secondary flow at initial mixing plane

SYMBOLS (Cont'd)

Symbol	Description
x	axial distance from initial mixing plane/ D_m
\hat{x}	value of x corresponding to \hat{C}_p
β	momentum coefficient $= \frac{\text{Total kinetic momentum flux}}{M\bar{V}} \left(= \frac{A^A \int fV^2 dA}{(A \int fV dA)^2} \geq 1 \text{ for constant density} \right)$
β'	momentum coefficient corresponding to 'fully developed' flow
$\bar{\beta}$	$\beta - \beta'$
$\bar{\beta}$	value of $\bar{\beta}$ at \hat{x}
β_1	value of β at initial mixing plane
β_D	see Section 2.1
β_1	value of β at ejector mixing pipe exit
Δ	$2(\bar{\beta}_1 - \bar{\beta}_D)$
ρ	density (constant throughout mixing pipe for isothermal incompressible air flow)
τ	local wall shear stress
Φ	ratio of ejector thrust to thrust corresponding to primary flow rate at primary total pressure discharging directly to mixing tube exit static pressure
Ψ	ratio of secondary to primary mass flow rates
Ω	velocity profile distortion factor (maximum velocity/mean velocity of ejector secondary flow at initial mixing plane)

CONFINED MIXING OF COAXIAL FLOWS

1.0 INTRODUCTION

Most test data on the internal aerodynamics of duct components relate to approach flows with thin boundary layers or, less frequently, fully developed velocity profiles. Little information is available on the effects of entry velocity profiles of significant non-uniformity (referred to here as 'distorted' velocity profiles and characterized by values of momentum coefficient, β , > 1.02 say).

Some earlier work was concerned with the overall effects of a particular type of entry flow distortion on the static pressure recovery of diffusers and sudden area enlargements (Refs. 1 and 2). Subsequent to this, it appeared useful to undertake a more general experimental investigation into the behaviour of different types of velocity profile distortion in the flow in straight pipes of circular and annular cross-section.

The process of confined mixing of non-uniform velocities occurs in many applications of engineering interest, the non-uniformities arising from upstream components such as bends, enlargements, diffusers, manifolds, turbomachinery, ejectors, etc. Considerable attention has been directed in the past toward prediction of the turbulent mixing process by relatively sophisticated calculation procedures. These methods necessarily require detailed specification of the flow field leaving the distortion generating device in order to predict the parameters of interest at arbitrary distances downstream. It is noted, however, that in practice appropriately detailed information on the initial flow field is not generally available and that the parameters of engineering interest in the mixing duct are frequently confined to the axial distribution of static pressure and, in particular, to the magnitude and position of peak static pressure recovery together with some indication of the velocity profile characteristics as this region is approached.

From the standpoint of practical need therefore, it appeared worthwhile to investigate the possible usefulness of an empirical correlation technique based on experimental observations. The method assumes a plausible decay function for a single parameter characterizing the velocity profile and uses the momentum equation to predict the longitudinal static pressure distribution in the mixing duct. Appropriate constants are derived from experimental results and correlated for general applicability.

Attention is confined here to mixing of coaxial streams in a duct of constant circular cross-section under essentially incompressible and isothermal conditions. Sudden enlargements are included as a special case where one of the coaxial stream velocities is zero. Other types of distorted velocity profile, and the effects of annular rather than circular mixing pipes, are dealt with in a following report.

2.0 ANALYSIS

2.1 The Momentum Equation in Confined Mixing

The momentum equation for isothermal incompressible flow between planes j and k in a straight pipe of circular cross-section and constant area may be written:

$$\beta_j \rho \bar{V}^2 A + p_j A = \beta_k \rho \bar{V}^2 A + p_k A + \tau \pi D (X_k - X_j)$$

where τ is an effective value of wall shear stress between planes j and k .

Writing $C_{p_{jk}} = \frac{P_k - P_j}{1/2\rho\bar{V}^2}$, $f = \frac{\tau}{1/2\rho\bar{V}^2}$ and $x = \frac{X}{D}$

$$C_{p_{jk}} = 2(\beta_j - \beta_k) - 4f(x_k - x_j) \quad (1)$$

The mixing of coaxial flows of differing velocities results in a characteristic type of longitudinal static pressure distribution which is illustrated in Figure 1 for several geometries and velocity distributions. It is apparent that the mixing process incorporates three main regions, illustrated schematically in Figure 2. An initial region, characterized by relatively minor changes in static pressure (and, by implication, momentum coefficient) is followed by a region of rapid mixing in which the principal rise of static pressure (and corresponding decay of kinetic momentum) occurs, and in which a maximum value of C_p is attained. In the final region the essentially flat and highly turbulent velocity profile near the position of peak static pressure readjusts to become a fully developed velocity profile far downstream. In the vicinity of point 'a' the constant gradient of static pressure coefficient is associated with a constant friction factor, f' , and a momentum coefficient, β' , corresponding to effectively fully developed flow. It is noted that β' is very close to unity ($\beta' \sim 1.01$ to 1.02 depending on Reynolds number). If friction factor were constant throughout the mixing pipe (at f'), the datum value of β at the initial mixing plane (β_D) would be given by Relation (1) as:

$$2(\beta_D - \beta') = 2\bar{\beta}_D = C_{p_a} + 4f'x_a \quad (2)$$

where $C_{p_a} = \frac{P_a - P_1}{1/2\rho\bar{V}^2}$ and subscript 1 refers to the initial mixing plane.

In practice the local value of friction factor will differ from f' , particularly in the initial mixing region. The actual value of the initial momentum coefficient, β_1 , can be written

$$2\beta_1 = 2\bar{\beta}_1 + \Delta \quad (3)$$

where Δ represents an incremental pressure coefficient (positive or negative) due to initial wall friction factor differences from f' .

If it is assumed that these differences are confined to the initial region, i.e. the wall friction factor in the rapid mixing region is essentially constant at f' , then the momentum coefficient at an arbitrary point (n) in the rapid mixing region may be obtained from Relation (1) as

$$2(\beta_n - \beta') = 2\beta_n = C_{p_n} - C_{p_1} + 4f'(x_n - x_1) \quad (4)$$

where $C_{p_n} = \frac{P_n - P_1}{1/2\rho\bar{V}^2}$

or, from (2):

$$2\beta_n = 2\bar{\beta}_D - C_{p_n} - 4f'x_n \quad (4a)$$

This expression allows the evaluation of the momentum coefficient, β_n , at any point in the rapid mixing region from measurements of static pressure coefficient. The present prediction method is based on fitting the experimentally derived values of the momentum coefficient, along the pipe, with a plausible decay function.

2.2 The Momentum Coefficient Decay Model

Assessment of the measured data (e.g. Fig. 1) suggests that momentum decay characteristics in the rapid mixing region can be well represented by an expression of the form:

$$\frac{d\bar{\beta}}{dx} = -k\bar{\beta}$$

Integrating and introducing convenient constants gives

$$\bar{\beta} = \bar{\beta}_1 e^{-k(x-d)} \quad (5)$$

The essence of the prediction method lies in the correlation of the constants k and d with geometry and initial velocity profile. In turn this depends on the adequacy of the postulated model and the degree to which k and d reflect actual physical processes.

In the initial region of small momentum decay it is assumed for consistency and completeness that

$$\frac{d\bar{\beta}}{dx} = -zk\bar{\beta} \quad \text{where } z \ll 1$$

On integrating this leads to

$$\bar{\beta} = \bar{\beta}_1 e^{-zkx} \quad (6)$$

for

$$0 \leq x \leq \frac{d}{1-z}$$

i.e. d is closely representative of the initial region length.

The complete model is summarized in Figure 3. It is noted that if k , d and Δ are known then C_{p_n} in the rapid mixing region, for given β_1 , follows from Equations (3), (4a) and (5). In particular the position and magnitude of the peak static pressure is given by

$$\hat{x} = d + \frac{1}{k} \ln \left[\frac{\bar{\beta}_1 k}{2f'} \right] \quad (7)$$

$$\hat{C}_p = 2\bar{\beta}_1 \left[1 - \frac{2f'}{\bar{\beta}_1 k} \right] - 4f'\hat{x} - \Delta \quad (8)$$

At the peak, $\frac{\hat{\beta}}{\beta} = \frac{2f'}{k}$

The constants d and k were evaluated from the measured data by fitting each faired pressure-rise curve at two points in the rapid mixing region. The points were arbitrarily selected in the area of greatest interest, at 50% and 90% \bar{C}_p . Then k and d followed from application at each point of Equations (4) and (5).

2.3 Initial Momentum Coefficient, β_1 , for Coaxial Flows

The isothermal incompressible coaxial flows considered here are described by the diameter ratio, \bar{D} , and the inlet velocity ratio V_1/V_0 .

For the ideal case of negligible inner pipe wall thickness and uniform inlet velocity profiles

$$(\beta_1)_{ideal} = \frac{(1 - \bar{D}^2) + \bar{D}^2(V_1/V_0)^2}{[(1 - \bar{D}^2) + \bar{D}^2(V_1/V_0)^2]} \quad (9)$$

For non-uniform individual entry profiles

$$\beta_1 = \frac{\beta_0(1 - \bar{D}^2) + \beta_1\bar{D}^2(V_1/V_0)^2}{[(1 - \bar{D}^2) + \bar{D}^2(V_1/V_0)^2]} \quad (9a)$$

It is noted that for turbulent entry flows β_0 and β_1 are close to unity, ($\beta \sim 1.02$ for fully developed turbulent pipe flow) and β_1 is, in general, not significantly different from $(\beta_1)_{ideal}$.

$(\beta_1)_{ideal}$ is shown plotted against \bar{D} for various V_1/V_0 in Figure 4. The marked reduction as initial velocity ratio approaches unity is evident, and is further illustrated in Figure 5 which presents the maximum attainable value of $(\beta_1)_{ideal}$ as a function of initial velocity ratio. It is seen that values of V_1/V_0 or V_0/V_1 in excess of about 0.4 will generally result in β_1 values too low for significant pressure recovery through downstream mixing.

3.0 EXPERIMENTAL DETAILS

3.1 Apparatus

The mixing pipe consisted of 7-1/2 ft. (2.3 m) of 1.8 in. (3.2 mm) wall brass tubing of nominal I.D. 3.75 in. (9.5 cm) with a semi-circular bellmouth of 3/8 in. (9.5 mm) radius at entry. The inner surface was honed smooth resulting in a final I.D. of 3.761 in. (9.553 cm). The pipe was equipped with a single row of static pressure tappings (Fig. 6), and provision was made for the mounting of traversing gear at each longitudinal station. Circumferential traversing and measurement of static pressure at various circumferential positions could be accomplished by pipe rotation, which was facilitated by roller supports and a clamped slip flange with an 'O' ring seal at the downstream junction. Additional static pressure tappings were provided at the initial mixing plane, located 2-1/4 diameters from the pipe entrance. The pipe was sucked from atmosphere through a 6 in. (15.2 cm) diameter connection containing a standard venturi meter and leading via a gate valve for control to a 25 ft. (10.67 m) diameter continuously evacuated sphere. Choked flow through the gate valve resulted in particularly steady flow conditions.

Various coaxial flow situations were provided by a series of inner pipes supplied by blown air and terminating at the initial mixing plane. Outer wall surfaces of the inner pipes were machined down to give wall thicknesses of 1/16 in. (1.6 mm) or less over the final 14 in. (35 cm) of the pipes. In addition, wakes from the pipe walls were minimized by tapering the outer surface (at less than 1°) to achieve a final wall thickness of about 0.005 in. (0.13 mm) at the end of each pipe. Details of inner pipe dimensions and of geometry near the initial mixing plane are also shown in Figure 6.

Mass flows in the inner pipes were measured by a standard orifice installation well upstream, and a subsequent straight run of inner pipe 7 ft. 8 in. (2.36 m, 29 to 90 dia.) long was employed in each setup to ensure essentially fully developed flow at inner pipe exit. Considerable care was taken to position the inner and mixing pipes in a truly coaxial fashion. Boundary layer trip strips were located on the outer wall of the inner pipe and on the mixing pipe bellmouth as shown in Figure 6.

Air temperatures were measured by thermocouples adjacent to the flow measuring device and near the bellmouth inlet. With the exception of orifice and venturi differentials, which were displayed on water manometers, pressures were measured via a scanivalve, a 0-1 psi (0.7 kPa) differential transducer and digital voltmeter.

4.0 PROCEDURE AND RESULTS

4.1 Results with $V_i > V_o$

Most of the tests were conducted at a constant Reynolds number of about 10^5 in the mixing pipe, i.e. at a fixed total flow rate. Mean velocity in the mixing pipe was usually about 60 ft/sec. (18 m/s). Inner velocities were limited to essentially incompressible levels (< 300 ft/sec. (90 m/s)). The suction gate valve was set to give the desired overall flow rate. The velocity ratio between the inner and outer streams could then be varied by adjustment of the air supply control valve on the inner pipe. The limiting condition of $V_o/V_i = 0$, corresponding to a sudden enlargement of the inner pipe, was difficult to establish, implying as it did equality of inner and mixing pipe flow rates. The problem was circumvented by constructing a series of three flanged entry pipes (details given in Fig. 6) to investigate the sudden enlargement situation directly.

In general, for each inner pipe in turn the air flow rate was varied to cover the useful range of initial momentum coefficient, and the longitudinal static pressure distribution for each combination of total and inner pipe flow rates was measured. Experimental results, plotted in the form C_p vs x , are shown for each pipe arrangement with various velocity ratios in Figures 7(a) to (f). Lines have been faired through the experimental points to assist in interpolation. Only flow conditions which embody a central jet (i.e. $V_i > V_o$) are covered in these figures. Discussion of the effects of peripheral jets corresponding to $V_o > V_i$ is deferred to Section 4.3.

It is evident from these results that axial static pressure gradients tend to become constant shortly after the peak pressure region, the gradients being about 10% higher than would be expected with fully developed flow in a smooth pipe at the same Reynolds number. In view of the care taken in finishing the test section it seems likely that this value of pressure drop per unit length reflects the higher than normal turbulence level and associated flatter than fully developed velocity profile prevailing after the main turbulent mixing process. Hot wire measurements suggested axial turbulence levels on the centre-line of 3% to 4%, and pitot tube traverses gave a momentum coefficient of about 1.010 (c.f. 1.5% and 1.020 for fully developed flow at the test Reynolds number, Ref. 3) at the final downstream measuring plane some 20 dia. from the initial mixing plane. As mentioned earlier some indication of the variation of wall friction can be inferred by extrapolating the line of wall friction pressure drop back to the initial mixing plane, and comparing the intercept ($2\bar{\beta}_1$) with the value determined from velocity ratio and geometry ($2\bar{\beta}_1$). Values of $\bar{\beta}_1$ were calculated allowing for inner pipe wall thickness effects and appropriate momentum coefficients on inner and outer flows. The value of β' was taken as 1.01 as suggested by traverses 20 dia. downstream of the initial mixing plane, (point 'a', Equation (2)). Calculated values of $2\bar{\beta}_1$ are shown on the ordinates of Figures 7(a) to (f) for direct comparison with the intercept values. In general the agreement is close, indicating that, for practical purposes, Δ may be taken as zero (Eq. (3)) and substantiating the hypothesis of effectively constant wall friction in the mixing region. (See later discussion under 4.3.)

4.2 Correlation of Results ($V_i > V_o$)

As indicated in Section 2.2 the assumed exponential decay function for β was fitted through points at 50% and 90% C_p on faired curves through the data of Figures 7(a) to (f), providing values of d and k for each test condition.

Calculated values of d are shown plotted against velocity ratio for various diameter ratios in Figure 8. Experimental ranges of velocity ratio and diameter ratio were $0 \leq V_o/V_i \leq 0.42$ and $0.273 \leq \bar{D} \leq 0.849$ respectively. The data indicate a tendency for d to increase with V_o/V_i , suggesting a correlation of the form

$$d = (\text{function of geometry}) \cdot (\text{inverse power of } (1 - V_o/V_i))$$

In Reference 4, Abbott and Kline present data on flow in two-dimensional channels containing a backward facing step and conclude that the reattachment distance for flow over the step appears to scale with step height. Although the physical interpretation of d in the present work is ill-defined and the axisymmetric geometry would be expected to introduce some differences, it

seemed reasonable to attempt a correlation in terms of $\frac{D_o - D_i}{D_o}$. A logarithmic plot of $d(1 - V_o/V_i)$ against $(1 - \bar{D})$ shown in Figure 9 suggested the following correlation for d

$$d = 4.2(1 - \bar{D})^{5/3}(1 - V_o/V_i)^{-1} \quad (10)$$

This relation is compared with the data in Figure 8.

It seemed probable that the exponential rate coefficient, k , would be strongly influenced by the velocity difference between the inner and outer streams. A correlation for k was postulated in terms of this difference normalized by the higher (inner) velocity. A logarithmic plot of k in these terms is presented in Figure 10. It appears that a suitable correlation could take the form

$$k = (\text{function of geometry}) \cdot (1 - V_o/V_i)^{2.5}$$

where the function of geometry is relatively weak. The expression finally adopted was

$$k = 0.75(1 - V_o/V_i)^{2.5} \left[\frac{1}{\bar{D}^2(1 - \bar{D}^2)} \right]^{1/6} \quad (11)$$

Expression 11 is shown relative to the experimental points in Figure 11.

It is noted that for many applications with $0.8 > \bar{D} > 0.4$ a satisfactory approximation is given by the simplified expression

$$k = (1 - V_o/V_i)^{2.5} \quad (12)$$

Although, for present purposes, detailed static pressure behaviour in the initial region is not of prime significance, an estimate is included for completeness using Equation (6) with $z = 0.05$ for all conditions.

The predicted behaviour of static pressure coefficient with streamwise distance, based on the foregoing correlations, is compared to the measured data in Figures 12(a) to (f) for all test configurations and flow conditions. Agreement in the rapid mixing region and in particular in the vicinity of \hat{C}_p is good.

A quantitative indication of the capability of the present correlation is afforded by comparing the predicted values of \hat{C}_p and \hat{x} with those observed in practice (Figs. 13 and 14). The results confirm that the suggested correlation procedure reproduces these practically important quantities to a useful degree of accuracy. In general the value of \hat{C}_p is predicted essentially without error, while the more critical \hat{x} is predicted within half a pipe diameter.

As a check on the applicability of the present method, measured data on coaxial mixing by Razinsky and Brighton (Ref. 5) are compared with the predictions of the present correlation in Figure 15. It is noted that although the value of \bar{D} of 0.167 is well outside the range in which the present experiments were conducted, a satisfactory degree of agreement is evident.

4.3 Results with $V_o > V_i$

For this series of tests the air supply to the centre pipe was disconnected and flow was induced from atmosphere, the value of V_i being controlled by a valve at the entry far upstream of the test section. In other respects the test procedure was essentially as described earlier. Experimental ranges of velocity ratio and diameter ratio were $0 < V_i/V_o < 0.315$ and $0.712 < \bar{D} < 0.907$ respectively.

Experimental results for conditions involving a 'peripheral jet' ($V_o > V_i$) are shown in Figures 16(a) to (c) with lines faired through the data points to assist in interpolation. The main features of the mixing process appear broadly similar to those evident in the earlier results, the extent of the initial delay region increasing, and the subsequent rate of momentum exchange decreasing, with increasing velocity ratio, V_i/V_o (i.e. with inner and outer stream velocities becoming more similar). It is evident, however, that the rate of mixing is in general more rapid with a peripheral jet than with a central primary flow (i.e. $V_i > V_o$). (This difference is well illustrated by data presented in Figure 17 which were obtained from total pressure traverses at various axial stations in the mixing pipe for peripheral and central jet situations of equal area ($\bar{D} = 0.707$) and similar initial lower to higher velocity ratio (and hence similar β_1). The apparent effect of wall friction in assisting velocity profile flattening in one case while delaying it in the other is marked and appears to persist throughout the range of geometry tested.)

As before, extrapolation of the downstream line of constant pressure gradient back to the initial mixing plane allows an assessment of the overall incremental friction force upstream through comparison of the intercepts $2\bar{\beta}_1$ with calculated values of $2\bar{\beta}_1$. In contrast to the results for $V_i > V_o$, significant force increments are indicated. As would be expected these are positive ($\Delta > 0$) and increase with increasing \bar{D} .

It is noted that in the treatment of experimental data it is implicitly assumed that wall static pressure measurements are entirely representative of flow section mean static pressure. Significant radial static pressure gradients, particularly at the initial mixing plane, could account for the indicated differences between β_1 and $\bar{\beta}_1$. Traverses of a specially designed miniature static pressure probe, however, failed to establish the existence of any significant static pressure variations other than apparent effects of high turbulence, confined to the shear layer between the inner and outer flows. Evidence that the observed differences, Δ , were in fact due mainly to excess upstream wall friction force (over that which would have prevailed had local friction coefficient been constant at the downstream value throughout the mixing pipe) was provided by a series of measurements using a Preston tube (inner diameter 0.040 in. (1 mm)).

A selection of results for three geometries is shown in Figure 18 in terms of f/f' vs. x . These indicate a high initial value of wall friction (f/f' at the initial plane $\sim (V_o/\bar{V})^2$) with a subsequent rapid drop to the final value. The assumption that increased frictional effects are largely confined to the initial region appears to be substantiated. Estimates of the overall reduction in pressure coefficient due to initial excess friction were derived from these curves by integration. These are shown compared with the indicated values of Δ , Equation (3), in Figure 19.

Although uncertainties attach to the derivation of both sets of data, the agreement is sufficiently close to suggest that the individual discrepancies, Δ , derive almost wholly from initial wall friction effects.

All values of Δ (including those derived from integrated skin friction) are shown plotted against the velocity ratio V_o/\bar{V} in Figure 20. A satisfactory correlation for the geometries tested is afforded by

$$\Delta = 6.5(V_o/\bar{V} - 1) \cdot (4f') \quad (13)$$

It is noted that

$$(V_o/\bar{V} - 1) = \frac{1 - V_i/V_o}{1/\bar{D}^2 - (1 - V_i/V_o)}$$

This is shown plotted against V_i/V_o for the β_{max} conditions (Fig. 5) in Figure 21.

Assuming the Δ correlation, Expression (13), is physically based, it would seem reasonable to expect it to apply also to cases for which $V_i > V_o$. The factor $(V_o/\bar{V} - 1)$ is shown for these cases also in Figure 21. It is seen that the implied values of Δ are negative and considerably smaller than for $V_o > V_i$, particularly at high values of β_1 . This would seem to point up the difficulties of deriving these values experimentally (by intercept) and to justify their (conservative) neglect for practical purposes.

The overall reduction in pressure coefficient corresponding to Δ is assumed to have taken place by the end of the initial region (Fig. 2), i.e., as before, wall friction coefficient in the region of prime interest (rapid mixing, Fig. 2) is assumed constant at f' . (Estimates of local pressure coefficient in the initial region require some sort of assumption as to the axial distribution of this reduction. Where, for completeness, these estimates have been included the distribution has been assumed linear with x , over $0 \leq x \leq (')$

4.4 Correlation of Results ($V_o > V_i$)

Curve fitting at 50% and 90% C_p points, as before, led to values for d and k which were correlated by a procedure similar to that employed with the results for $V_i > V_o$. A logarithmic plot of $d(1 - V_i/V_o)$ against the effective non-dimensional step height \bar{D} is presented in Figure 22 and indicates a similar relationship to that observed for $V_i > V_o$ (Fig. 9). Data were correlated, at least qualitatively, by the expression

$$d = 1.4(\bar{D})^{5/3} (1 - V_i/V_o)^{-1} \quad (14)$$

which is shown in Figure 23 together with the experimental points.

Experimentally derived values of k are shown in Figure 24 in terms of $(1 - V_i/V_o)$ and again exhibit a similar relationship to that found earlier, leading to a correlation

$$k = 1.9(1 - V_i/V_o)^{2.5} \left[\frac{1}{\bar{D}^2(1 - \bar{D}^2)} \right]^{1/6} \quad (15)$$

The factor 1.9 (c.f. 0.75 in Expression (11)) quantifies the previously noted increased mixing rate pertaining to a 'peripheral jet' ($V_o > V_i$) compared with a 'central jet' ($V_i > V_o$) of the same lower to higher velocity ratio and the same β_1 (i.e. the same total to 'primary' area ratio).

Expression (15) is shown relative to the experimental data in Figure 25. (As before it is noted that the indicated dependence of k on geometry is weak and the use of a simplified expression, viz.

$$k = 2.5(1 - V_1/V_0)^{2.5}$$

would, in most applications, result in no significant differences in prediction, at least for $0.5 < \bar{D} < 0.9$).

The value of z adopted earlier (viz. 0.05) was found satisfactory in providing an approximate representation of the initial region. With this final element it was possible to produce the predictions of static pressure distribution shown compared with experimental data in Figures 26(a) to (c). Agreement is generally good. Predicted and measured values of the magnitude and axial location of peak static pressure recovery, based on Relations (8) and (7), are compared in Figures 27 and 28 respectively. The correlation appears satisfactory.

5.0 SUMMARY OF PREDICTION METHOD

In summary, for the mixing of coaxial air flows in a duct of constant circular cross-section under essentially isothermal incompressible conditions, and given V_1, V_0, D_1, D_0 :

Calculate β_1 from Relation (9) or (9a).

Estimate β' (≈ 1.01) and f' from Reynolds number.

Then for $x \geq \ell'$

$$C_p = 2\bar{\beta}_1 \left[1 - e^{-k(x-d)} \right] - 4f'x - \Delta$$

$$\bar{\beta} = \bar{\beta}_1 e^{-k(x-d)}$$

$$\hat{C}_p = 2\bar{\beta}_1 \left(1 - \frac{2f'}{\bar{\beta}_1 k} \right) - 4f'\hat{x} - \Delta$$

$$\frac{\hat{\beta}}{\bar{\beta}} = \frac{2f'}{k}$$

$$\hat{x} = d + \frac{1}{k} \ln \left[\frac{\bar{\beta}_1 k}{2f'} \right]$$

where for $V_1 > V_0$

$$k = 0.75(1 - V_0/V_1)^{2.5} \left[\frac{1}{\bar{D}^2(1 - \bar{D}^2)} \right]^{1/6}$$

or $k = (1 - V_o/V_i)^{2.5}$ for $0.4 < \bar{D} < 0.8$

$$d = 4.2(1 - V_o/V_i)^{-1} (1 - \bar{D})^{5/3}$$

$$\Delta = 0 \text{ (for practical purposes, but see Section 4.3)}$$

and for $V_o > V_i$

$$k = 1.9(1 - V_i/V_o)^{2.5} \left[\frac{1}{\bar{D}^2(1 - \bar{D}^2)} \right]^{1/6}$$

or $k = 2.5(1 - V_i/V_o)^{2.5}$ for $0.5 < \bar{D} < 0.9$

$$d = 1.4(1 - V_i/V_o)^{-1} (\bar{D})^{5/3}$$

$$\Delta = 6.5(V_o/\bar{V} - 1) \cdot (4f')$$

$$= 6.5 \left[\frac{\bar{D}^2(1 - V_i/V_o)}{1 - \bar{D}^2(1 - V_i/V_o)} \right] (4f')$$

Note: $\varrho' = \frac{d}{1-z}$ where $z \ll 1$. In the present report predictions for the initial region have been included for completeness by taking $z = 0.05$ and using, for $0 \leq x \leq \varrho'$,

$$C_p = 2\bar{\beta}_1(1 - e^{-zkx}) - 4f'x - \left[\frac{x}{\varrho'} \right] \Delta$$

$$\bar{\beta} = \bar{\beta}_1 e^{-zkx}$$

6.0 APPLICATION OF PREDICTION METHOD TO EJECTOR PERFORMANCE

The foregoing correlations for mixing of coaxial air flows may be applied, for example, to the estimation of axisymmetric ejector performance under incompressible and isothermal conditions (for cases with parallel mixing pipes and either central or parietal primary flow). In particular they allow estimates of the effect of mixing pipe length. By way of illustration, such ejector calculations have been carried out and compared, where possible, with experimental results from another source.

For simplicity the calculations pertain in general to stationary conditions with uniform entry flows, negligible secondary flow entry loss, and $\beta' = 1.0$. (Other postulated conditions can be readily incorporated.) For a given mixing pipe length L , mixing pipe area/primary area ratio, S , and downstream friction factor, f , the calculations proceed in principle by relating entry secondary dynamic pressure to the mean static pressure at the initial mixing plane through the identity of secondary entry total pressure and mixing pipe exit static pressure. The resulting expression for initial velocity ratio contains d and k which are themselves related to velocity ratio through the correlations. An iterative procedure is therefore required. Starting from reasonable initial approximations,

e.g. $\Lambda = 0$, $d = 0$, $k = 1$, convergence is generally rapid (3 or 4 iterations), leading to a solution for initial velocity ratio and hence mass flow ratio. The final values of d and k allow estimation of the momentum coefficient along the mixing pipe, in particular at mixing pipe exit, leading to thrust augmentation ratio, Φ (ratio of ejector thrust to the thrust corresponding to the primary flow rate at the primary total pressure discharging directly to mixing tube exit static pressure).

Some sample calculated results for both central and parietal primary jets over a range of values of mixing pipe length, L , at a typical ejector area ratio, $S = 25$, are shown in Figures 29 to 31. Figure 29 shows the calculated values of k , d , $\hat{\Lambda}$, V_1/V_p , β_1 , β_1' and \hat{x} at each selected value of L . The associated performance factors Φ and Ψ are shown in Figure 30. It is noted that while the greater decay rate (k) pertaining to the parietal arrangement leads to a considerably shorter mixing pipe length for maximum performance, the influence of increased initial friction ($\hat{\Lambda}$) results in generally inferior performance particularly with respect to thrust. The differences in predicted overall performance between the two ejector types are further illustrated in Figure 31 where the same data are plotted as Φ vs. Ψ and shown relative to ideal performance.

The results of calculations for other values of area ratio, S , are shown in Figure 32. For clarity only the maximum values of the performance factors Φ and Ψ (together with the associated values of mixing pipe length) are presented in this Figure. The curves exhibit the same qualitative differences between the ejector types as observed for $S = 25$, with the additional result that the predicted maximum Φ attainable with the parietal type *declines* with increase in area ratio beyond $S \approx 10$.

A literature survey revealed only one source of parietal ejector performance under appropriately isothermal, incompressible conditions and with varying mixing pipe length (Reid, Ref. 6). Experimental data from this reference are shown compared with calculations using the present method in Figures 34 and 35. Figure 34 shows thrust augmentation ratio, Φ , against L for parietal ejectors with $S = 10$ and $S = 20$. The generally poor level of thrust performance predicted for this type of ejector is well substantiated by the experimental data. (Calculated values of Φ are shown both for uniform secondary entry velocity, $\Omega = 1.0$ and for a more realistic secondary entry profile, $\Omega = 1.1$.) The experimentally observed effect of mixing pipe length is closely reproduced by the prediction method as is the adverse effect of increasing area ratio from $S = 10$ to $S = 20$.

Measured overall performance, Φ vs. Ψ , for a wide range of area ratio, $S = 10$ to 131, is shown compared with the predictions of the present method in Figure 35. In general the agreement is surprisingly good, both quantitatively and qualitatively, particularly in view of the extrapolations involved in applying the present correlations to parietal geometries of considerably higher values of \bar{D} (up to 0.996) than those used in the present experiments ($\bar{D} \geq 0.907$).

7.0 CONCLUSIONS

An empirical approach has been adopted to correlate the mixing of isothermal incompressible coaxial air flows in straight pipes of constant circular cross-section. An assumed decay function for kinetic momentum is correlated in terms of initial geometry and initial velocities of the mixing streams. The method allows the rapid estimation of quantities of engineering interest including the axial distribution of both static pressure and total momentum. The method has been tested against published data on thrust augmenting ejectors of the parietal type, and found to provide satisfactory reproduction of measured performance as affected by mixing pipe length and area ratio.

8.0 REFERENCES

1. Tyler, R.A.
Williamson, R.G. *Diffuser Performance with Distorted Inflow.*
Paper 11, Symposium on Subsonic Fluid Flow Losses in
Complex Passages and Ducts. Inst. Mech. Eng., October 1967.

2. Tyler, R.A.
Williamson, R.G. *Sudden Area Enlargement Pressure Recovery with Inflow Distortion.*
Aeronautical Journal, March 1968.
3. Sharan, V. Kr. *An Experimental Investigation of Naturally Developing Turbulent Flow and Flow with Fixed Transition in a Parallel Pipe.*
ASME Paper No. 72-WA/FE-38, November 1972.
4. Abbott, D.
Kline, S.J. *Experimental Investigation of Subsonic Turbulent Flow Over Single and Double Backward Facing Steps.*
ASME Paper No. 61-Hyd-15, May 1961.
5. Razinsky, E.
Brighton, J.A. *Confined Jet Mixing for Nonseparating Conditions.*
ASME Paper No. 70-WA/FE-2, November 1970.
6. Reid, E.G. *Annular Jet Ejectors.*
NACA TN-1949, November 1949.

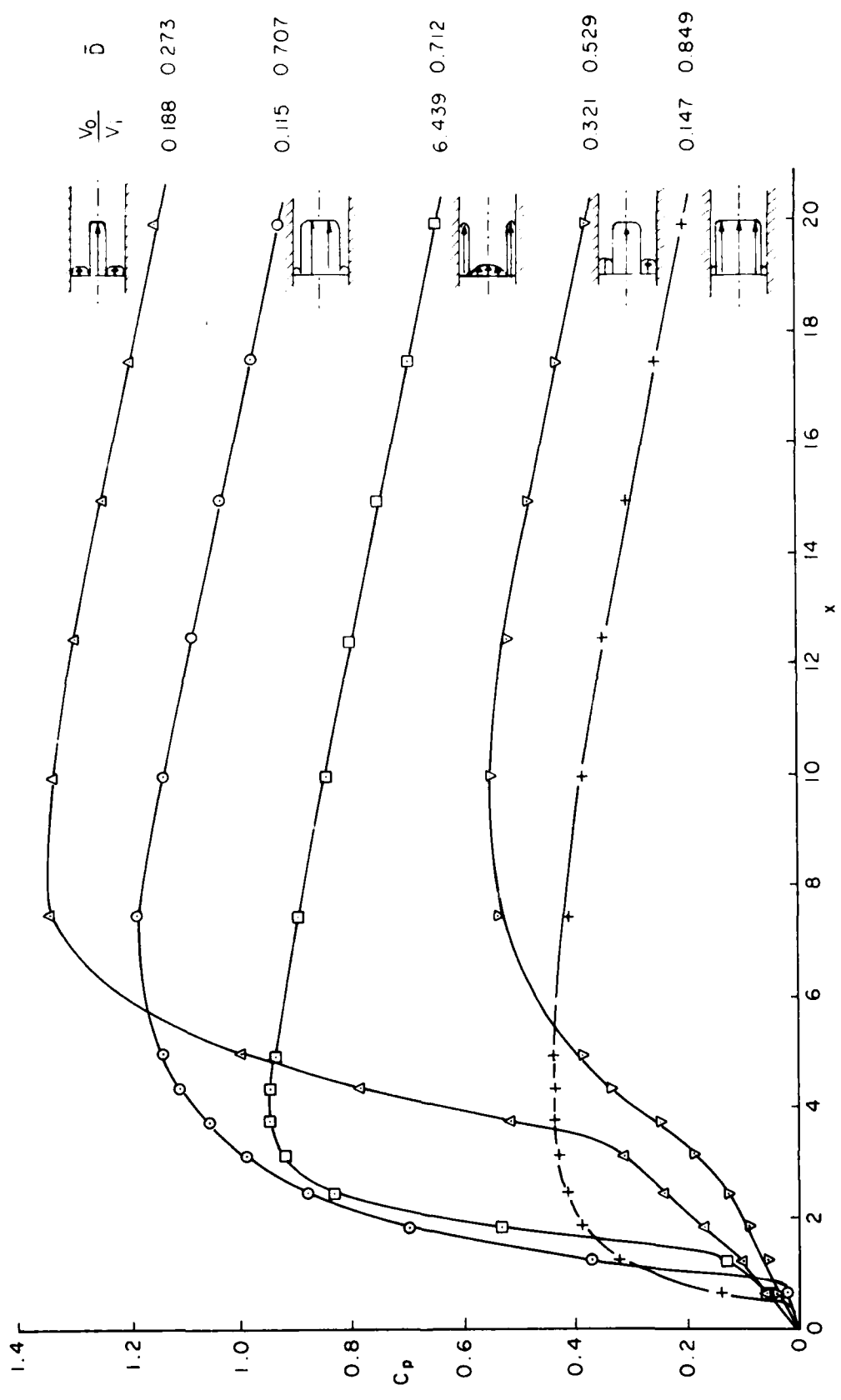


FIG. 1: TYPICAL EXPERIMENTAL RESULTS

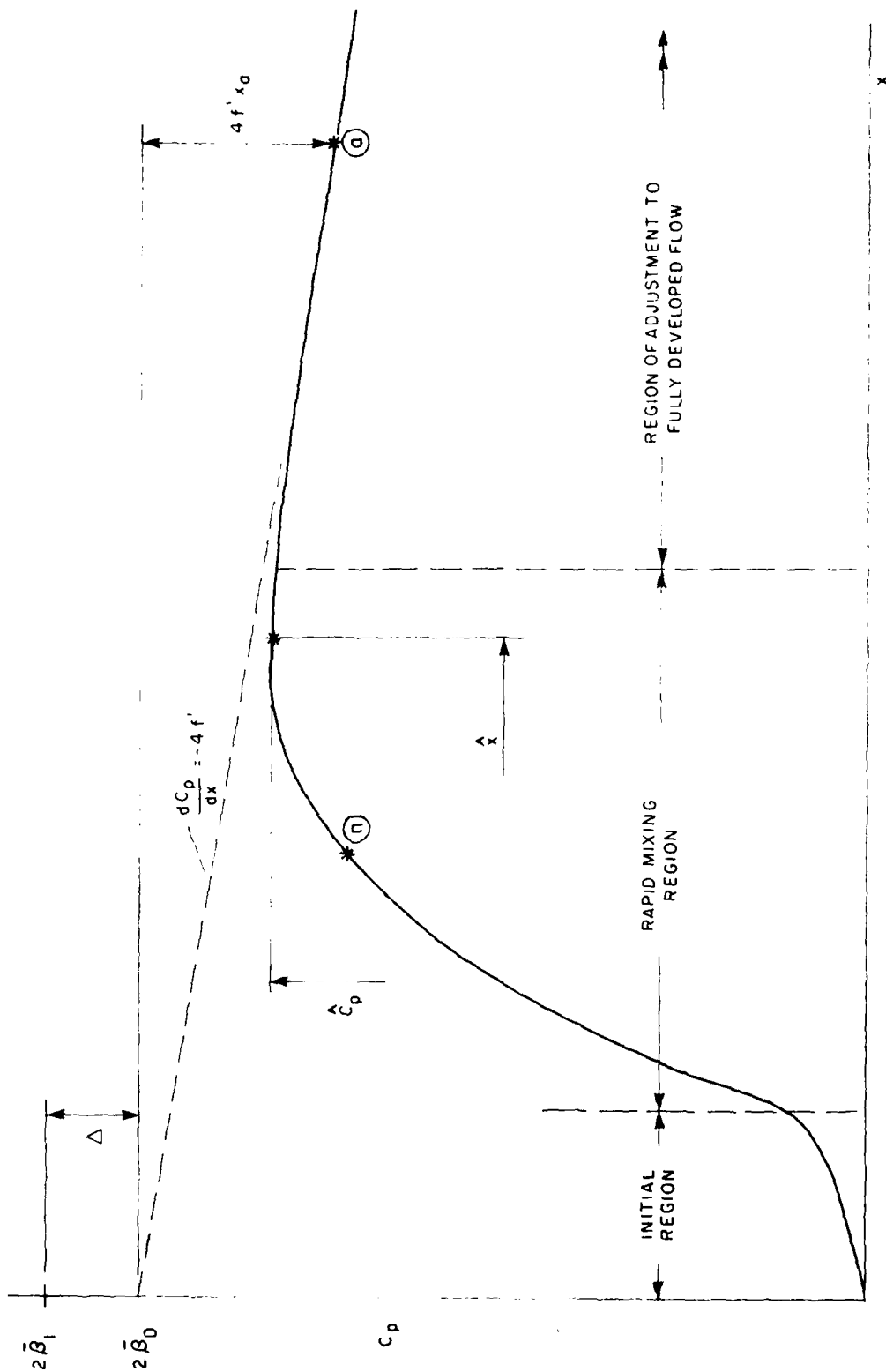


FIG. 2: MIXING PROCESS NOMENCLATURE

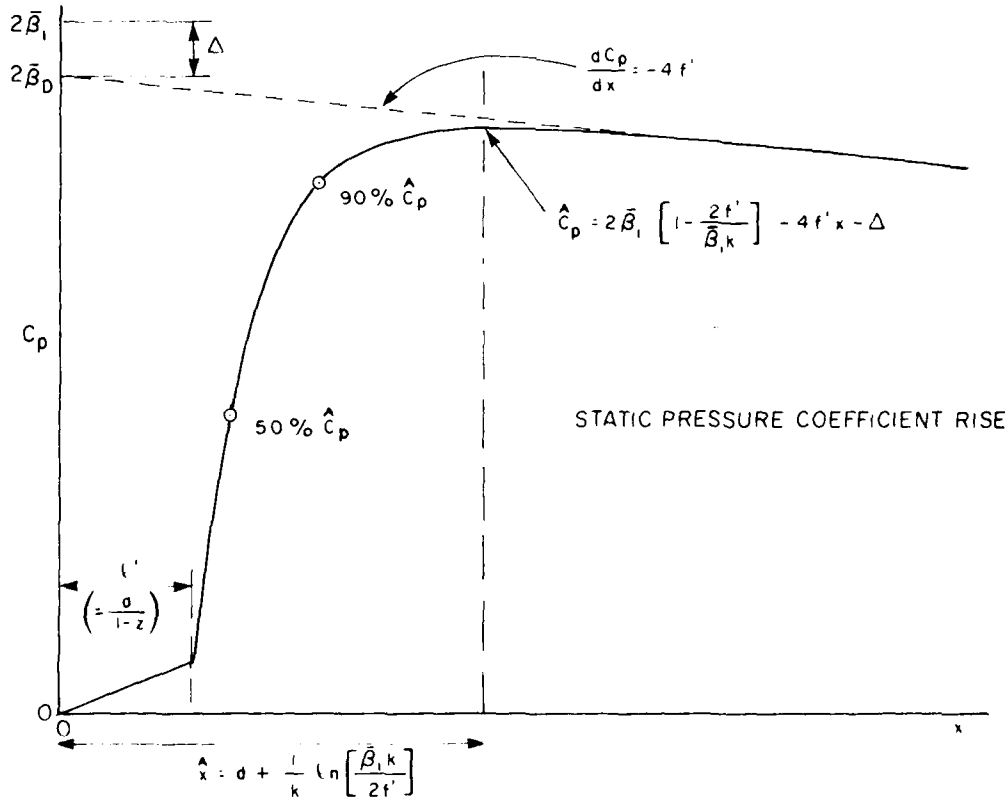
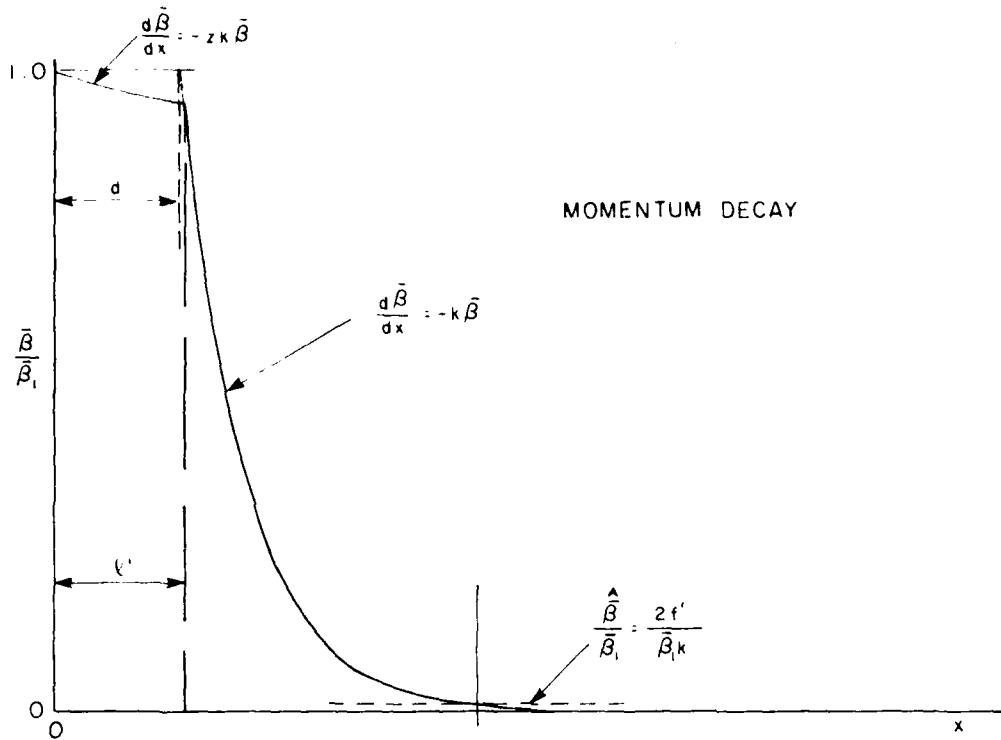


FIG. 3: IDEALIZED MODEL

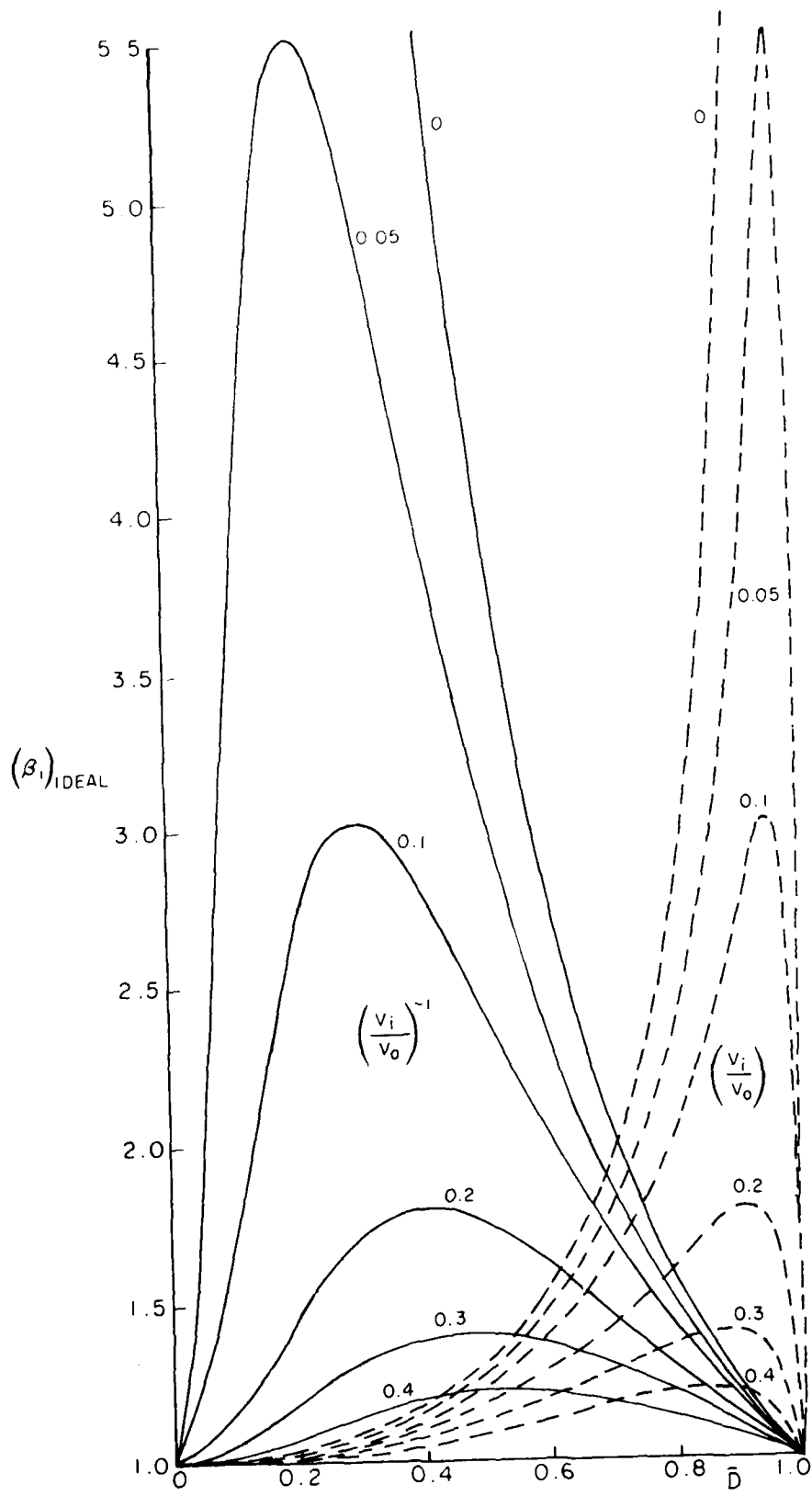


FIG. 4: IDEAL MOMENTUM COEFFICIENT AS A FUNCTION OF GEOMETRY AND VELOCITY RATIO

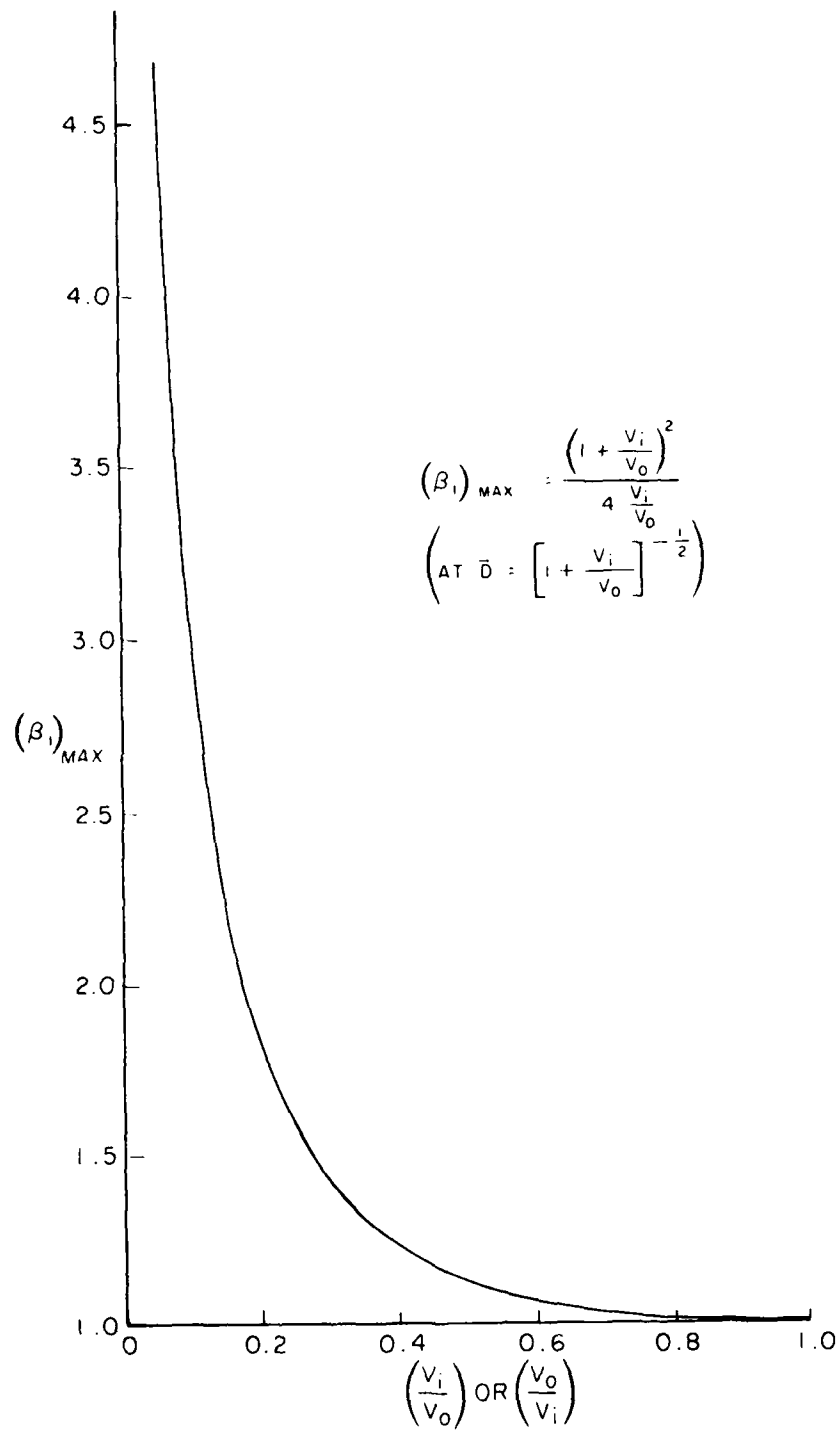


FIG. 5: MAXIMUM ATTAINABLE MOMENTUM COEFFICIENT FOR A GIVEN VELOCITY RATIO

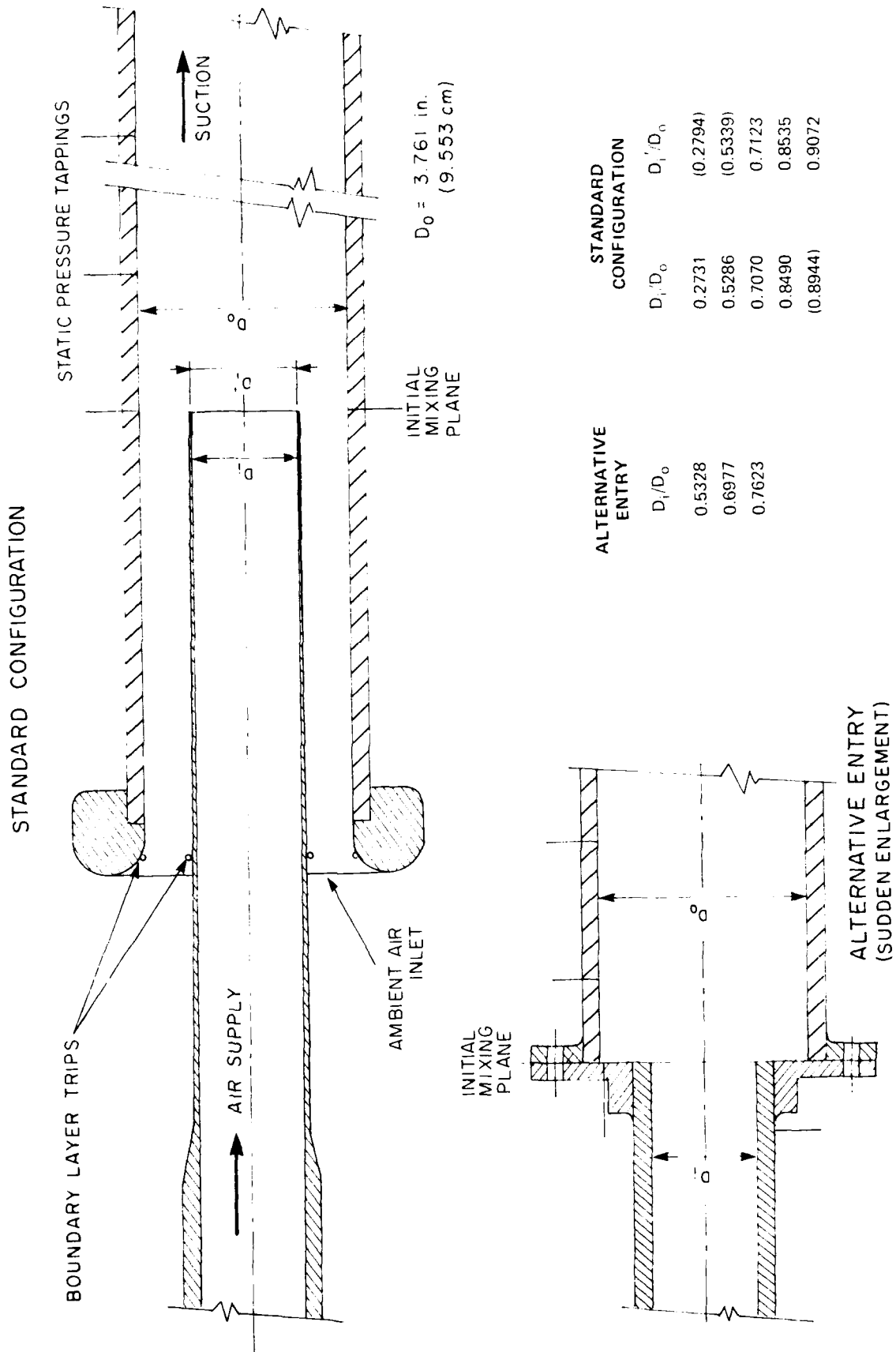


FIG. 6. TEST ARRANGEMENTS

$V_i > V_0$
 $\bar{D} = 0.849$
 $* 2\bar{\beta}_1$

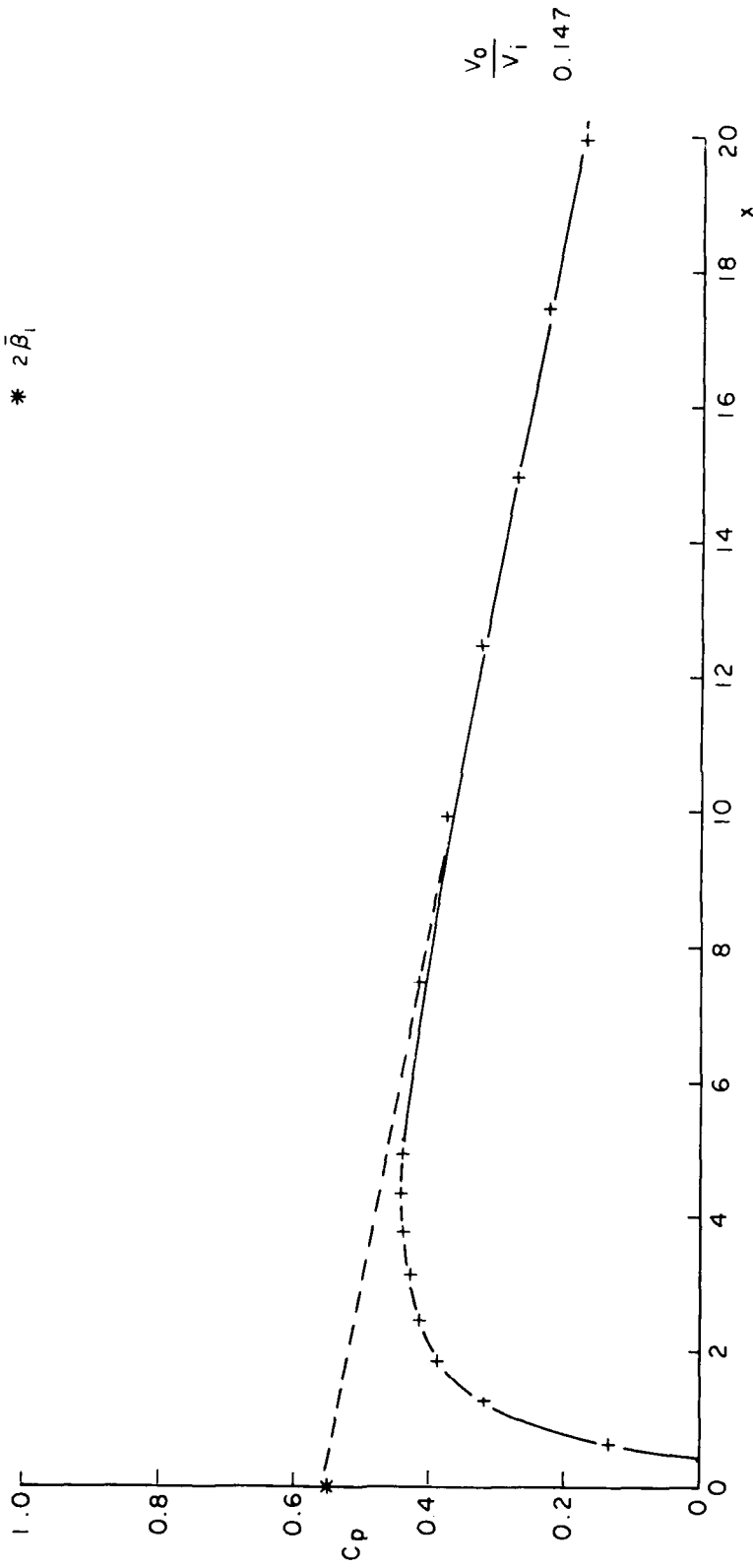


FIG. 7(a): MEASURED STATIC PRESSURE DISTRIBUTION ($V_i > V_0$)

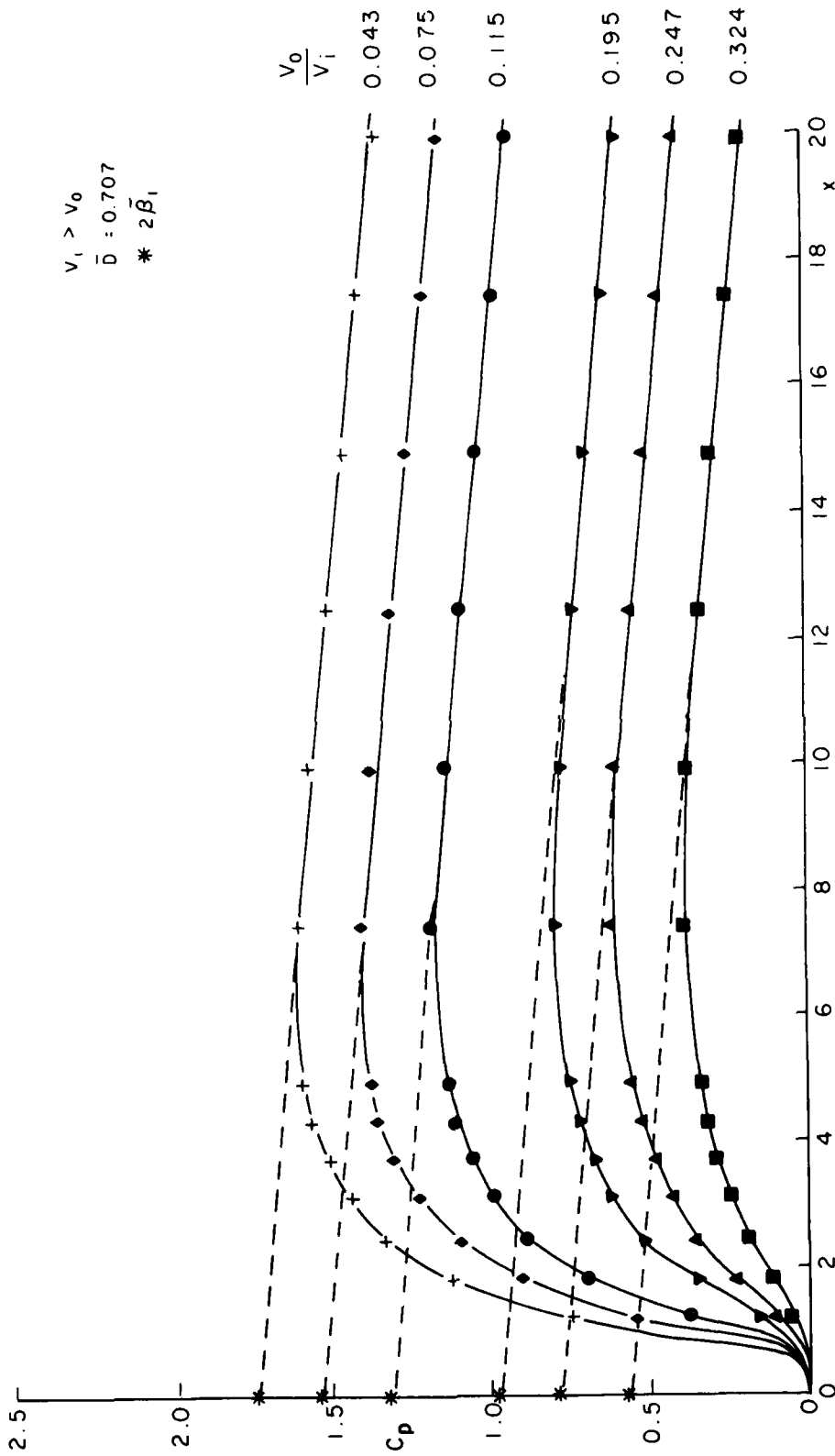


FIG. 7(b). MEASURED STATIC PRESSURE DISTRIBUTION ($V_i > V_0$)

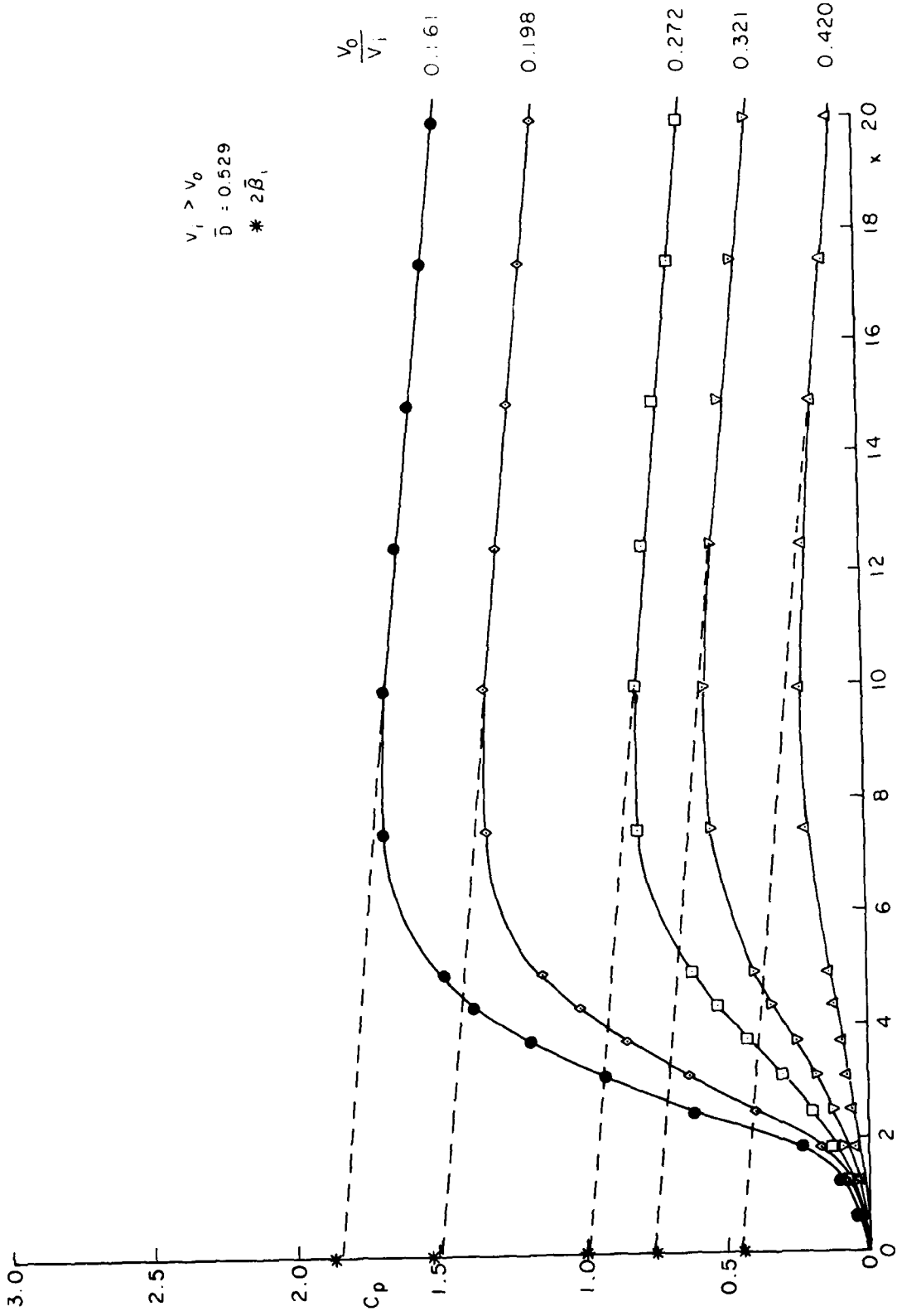


FIG. 7(c): MEASURED STATIC PRESSURE DISTRIBUTION ($V_1 > V_0$)

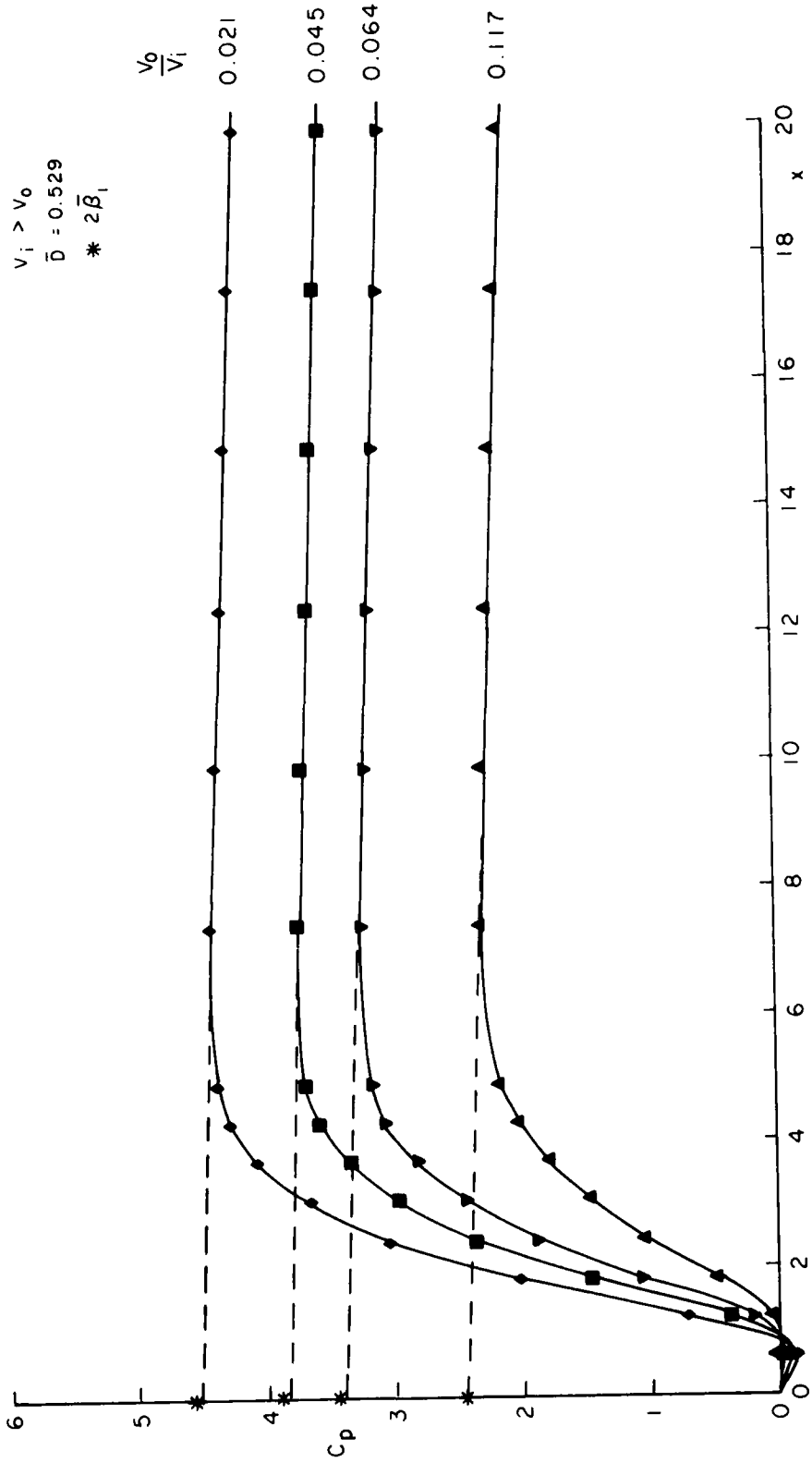


FIG. 7(d): MEASURED STATIC PRESSURE DISTRIBUTION ($V_i > V_0$)

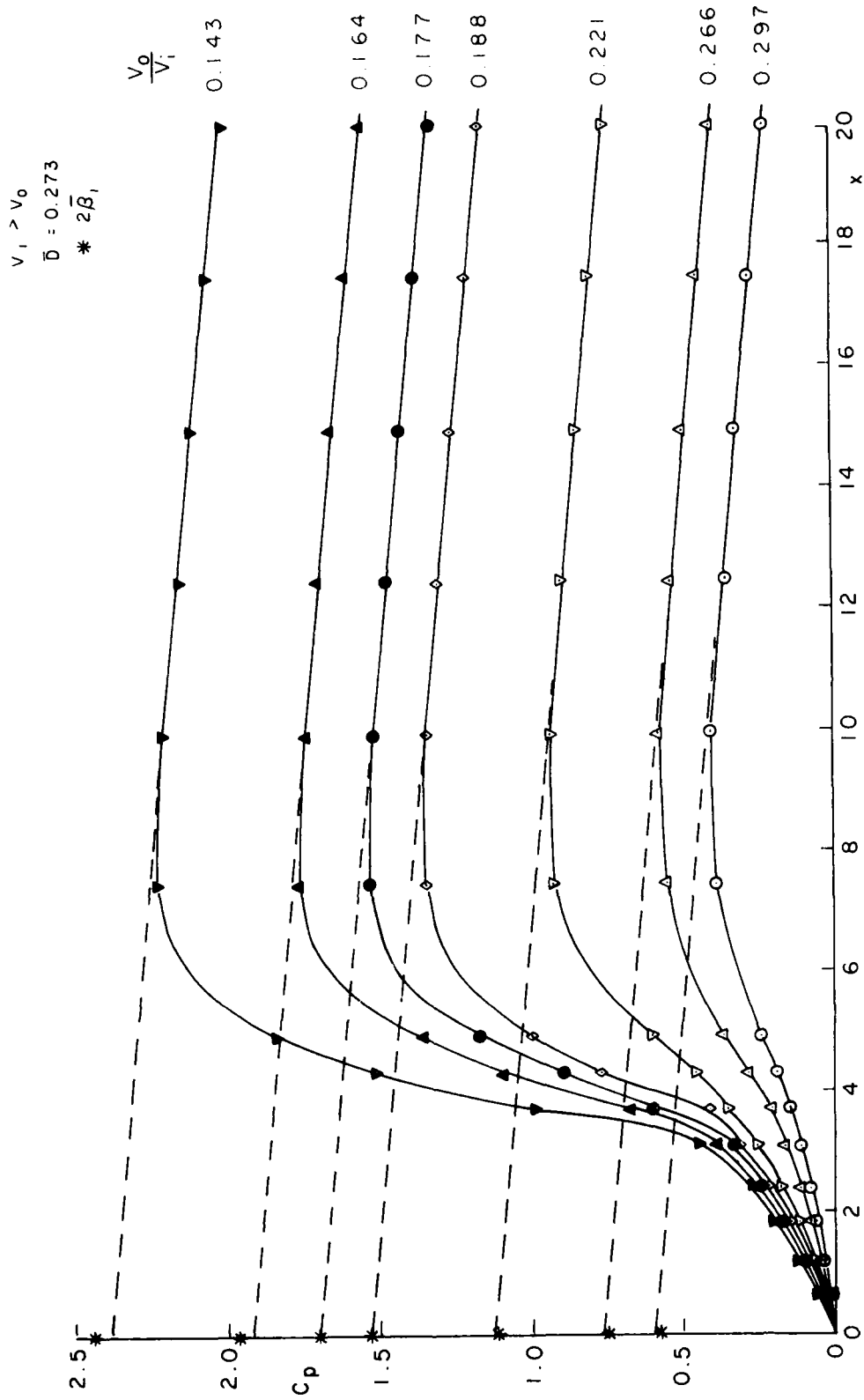


FIG. 7(e): MEASURED STATIC PRESSURE DISTRIBUTION ($V_1 > V_0$)

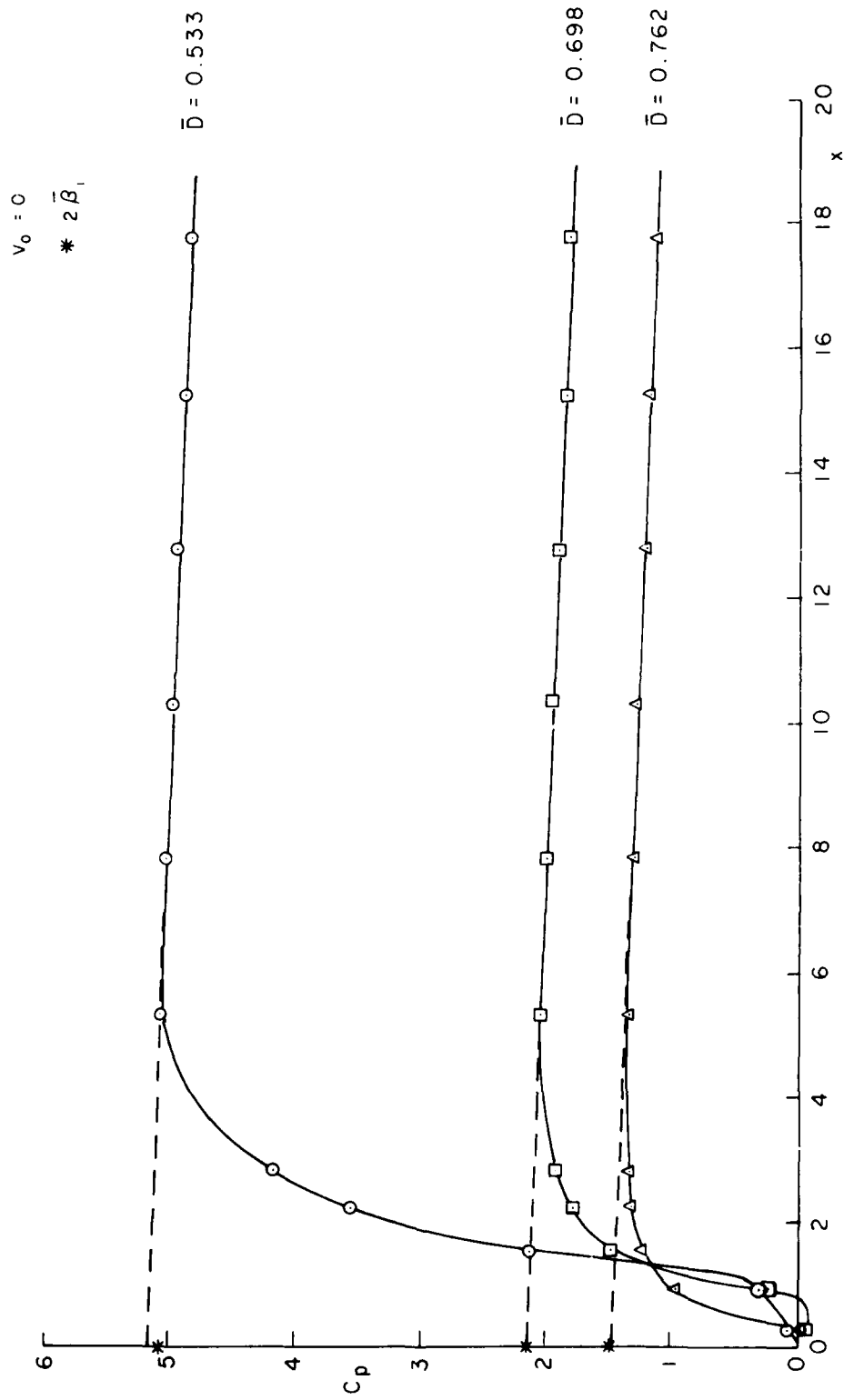


FIG. 7(f): MEASURED STATIC PRESSURE DISTRIBUTION ($V_0 = 0$)

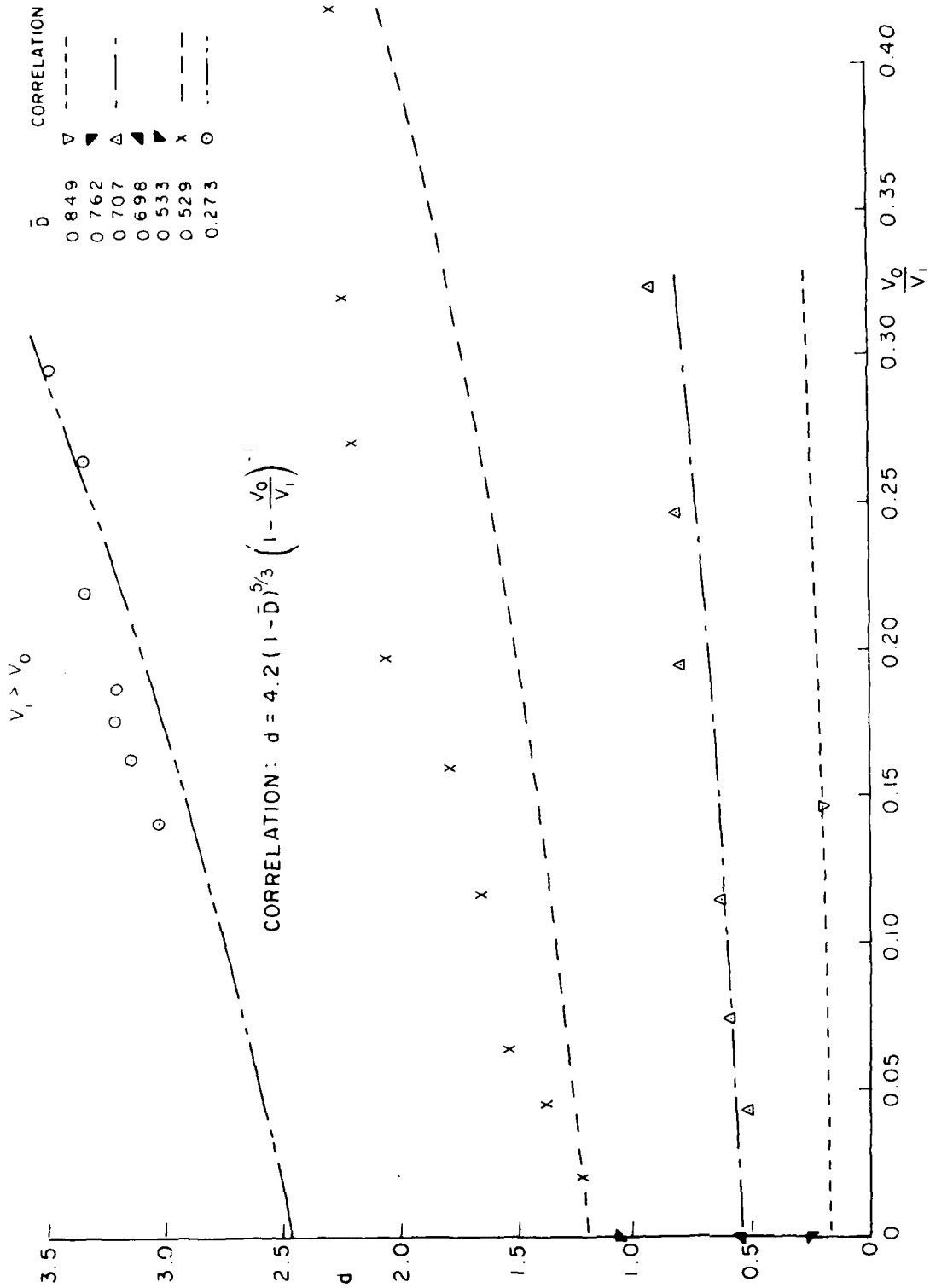


FIG. 8: DERIVED VALUES OF d FOR $V_1 > V_0$

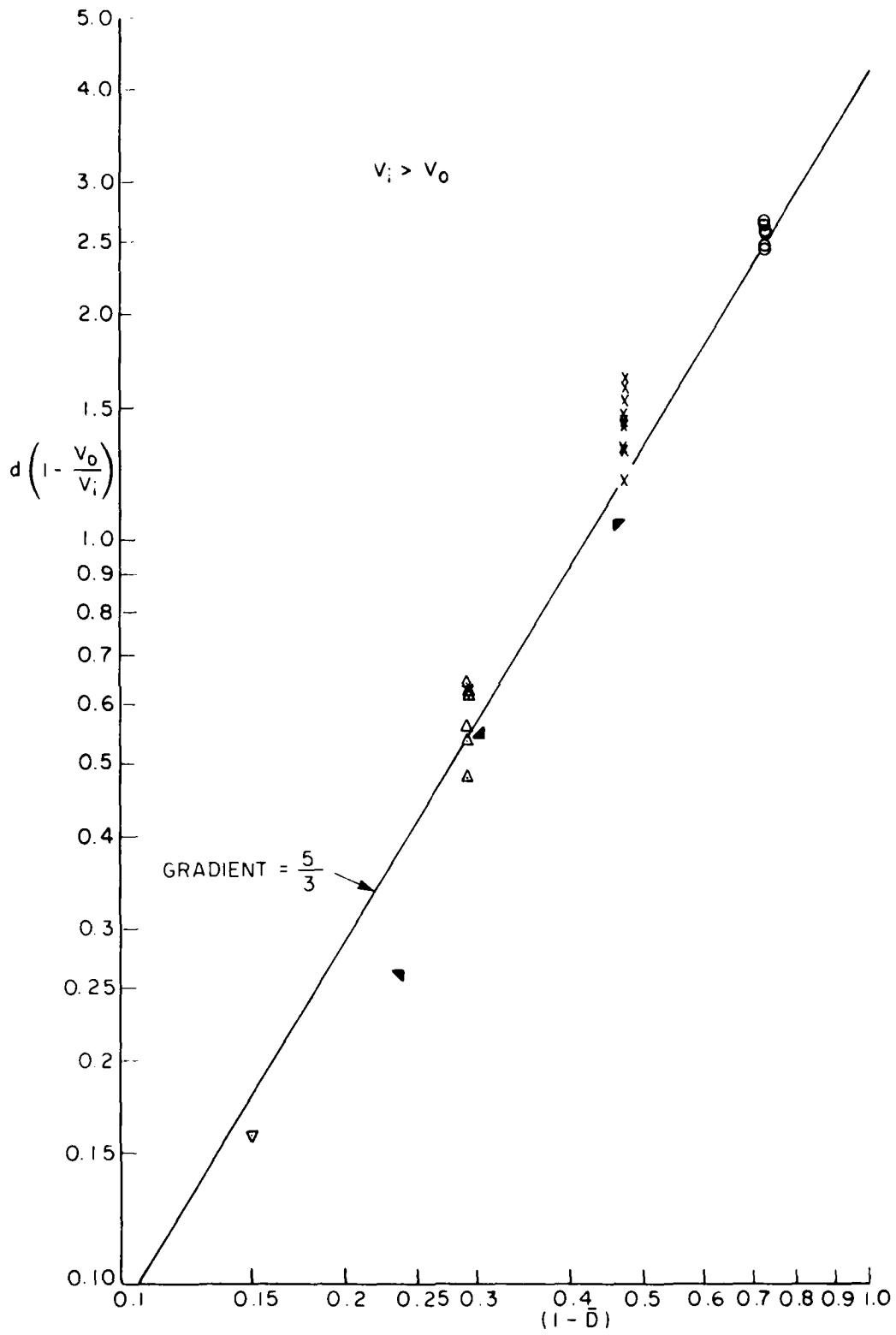


FIG. 9: CORRELATION OF DERIVED d VALUES WITH GEOMETRY ($V_i > V_o$)

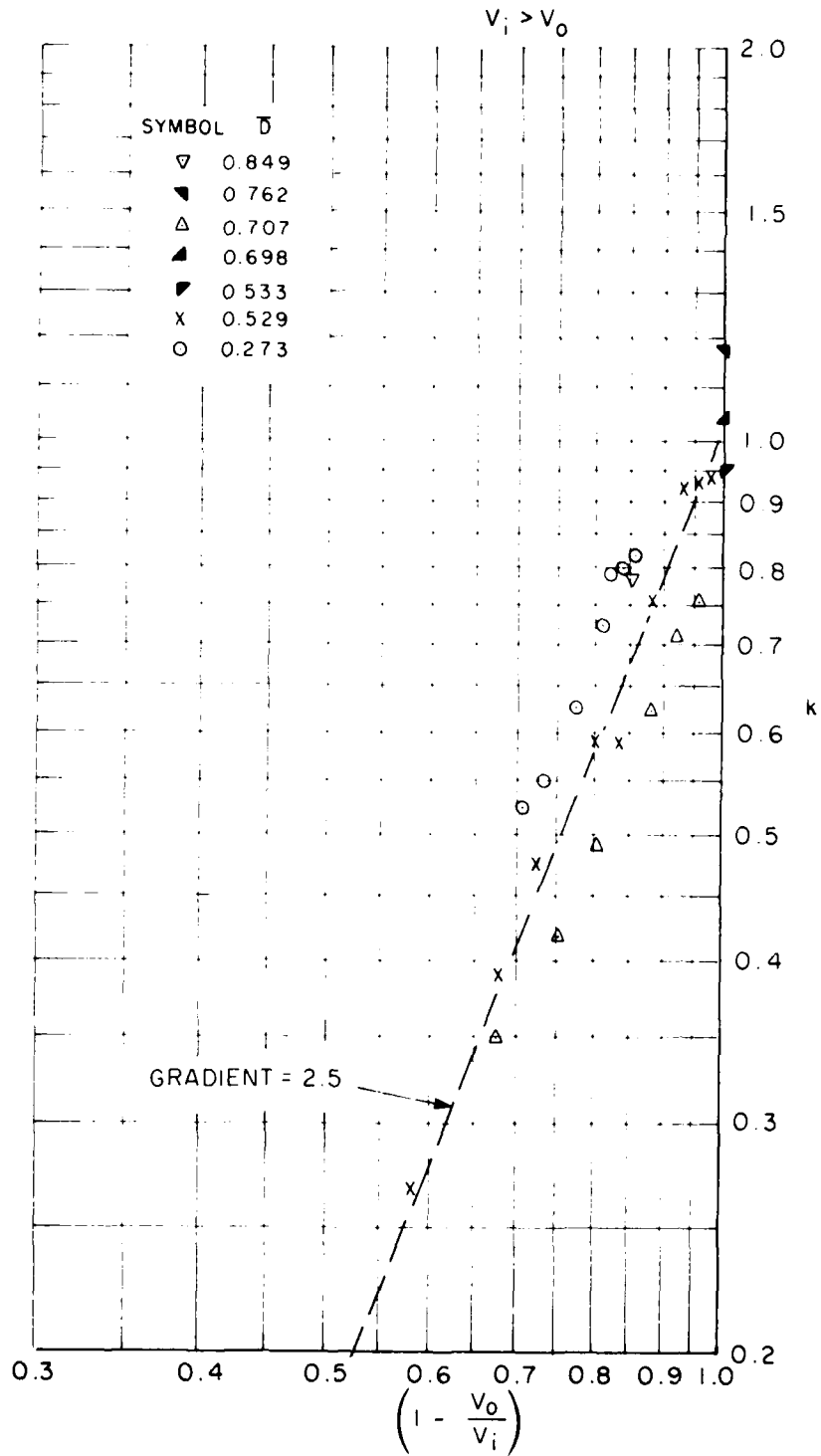


FIG. 10. CORRELATION OF DERIVED k VALUES WITH VELOCITY RATIO ($V_i > V_o$)

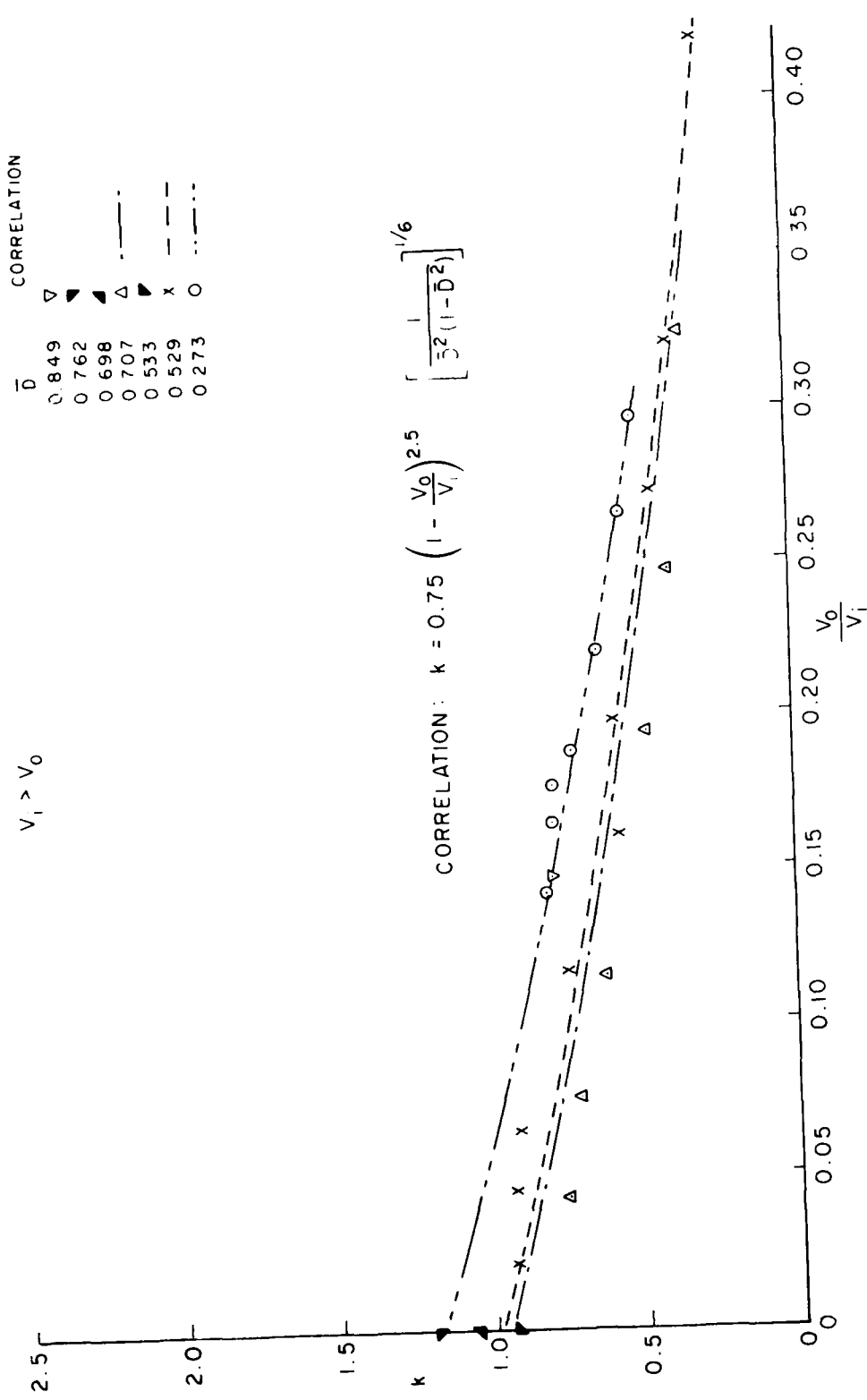


FIG. 11: FINAL CORRELATION OF DERIVED k VALUES ($V_i > V_0$)

$V_i > V_o$
 $\bar{D} = 0.849$

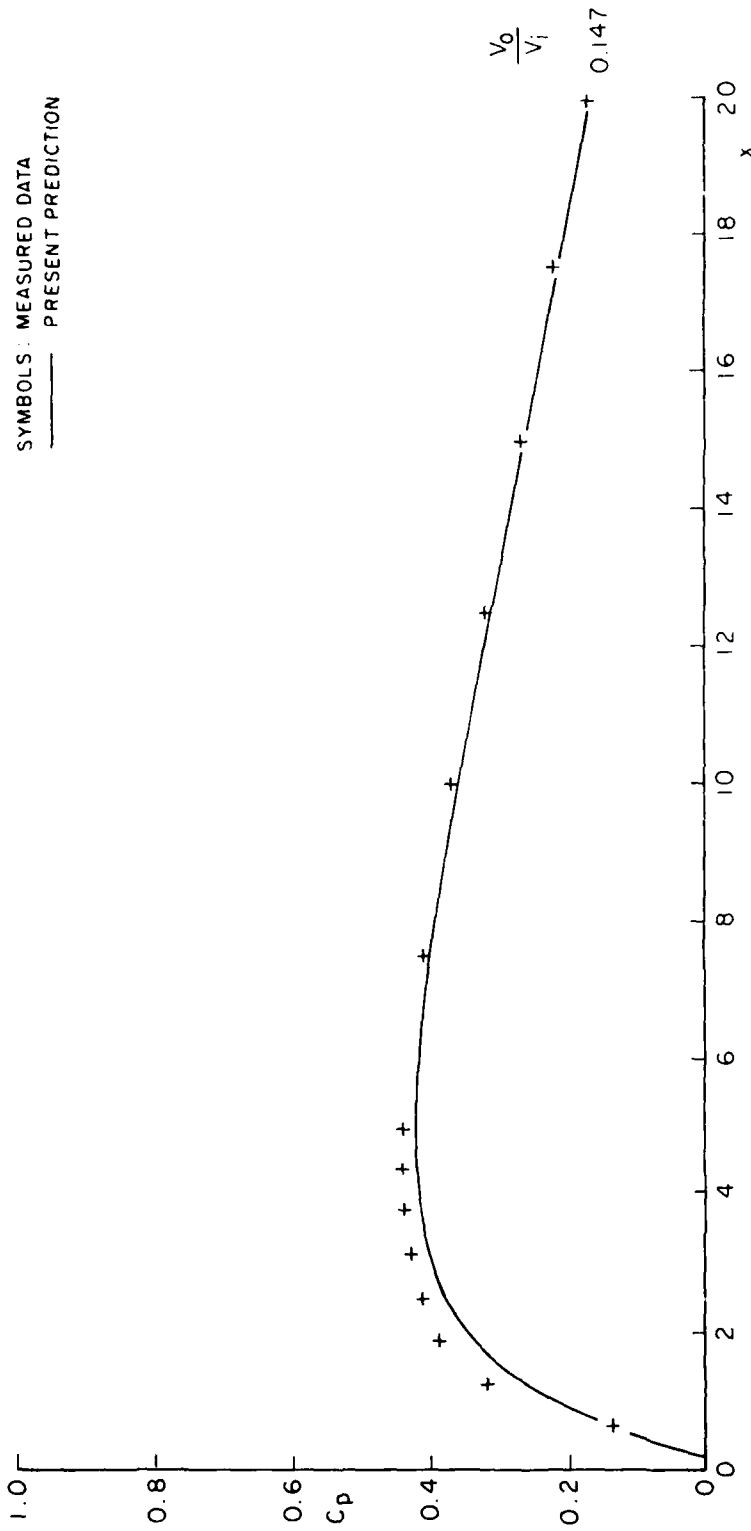


FIG. 12(a): PREDICTED AND MEASURED VALUES OF C_p COMPARED ($V_i > V_o$)

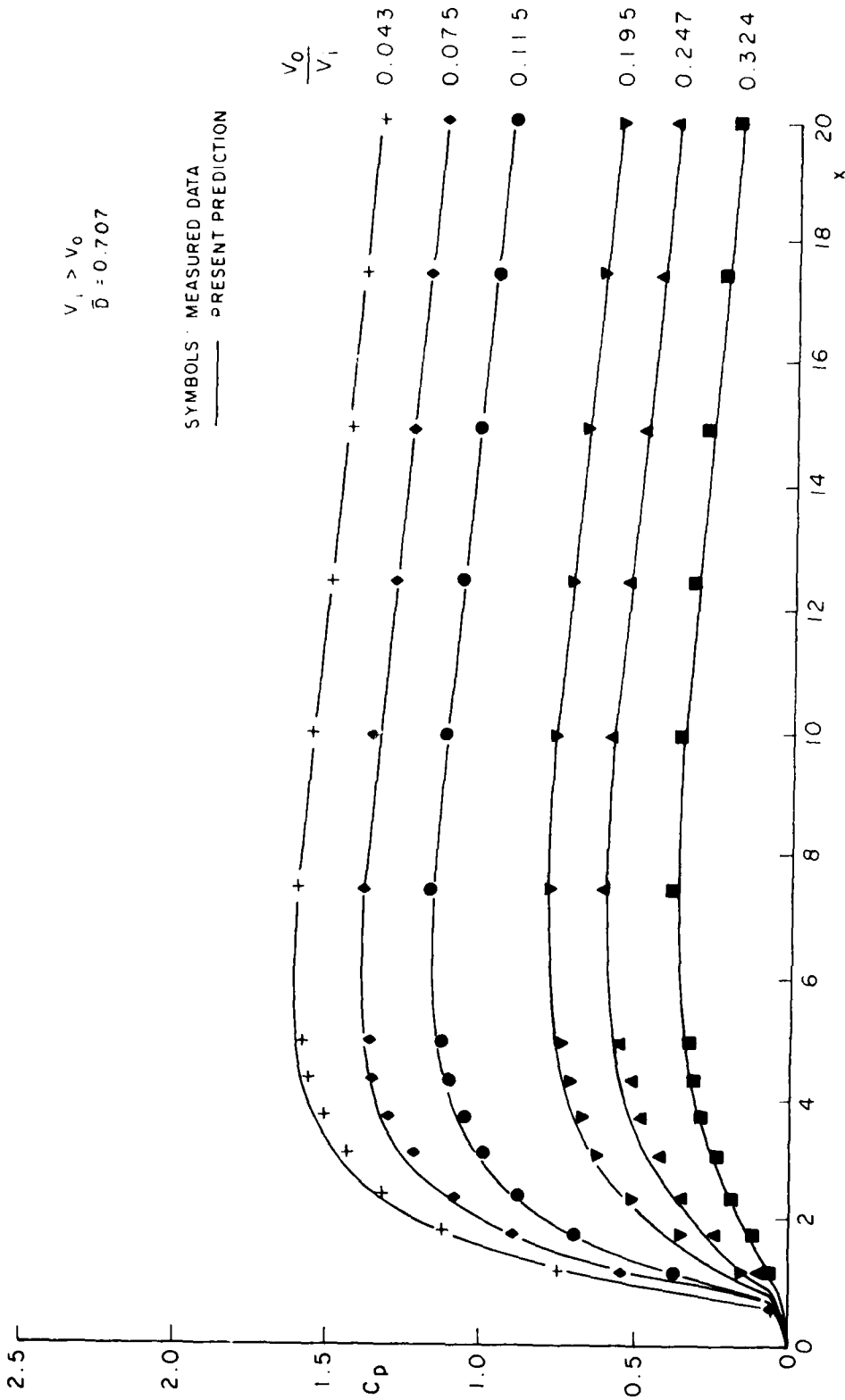


FIG. 12(b): PREDICTED AND MEASURED VALUES OF C_p COMPARED ($V_1 > V_0$)

$V_i > V_0$
 $D = 0.529$

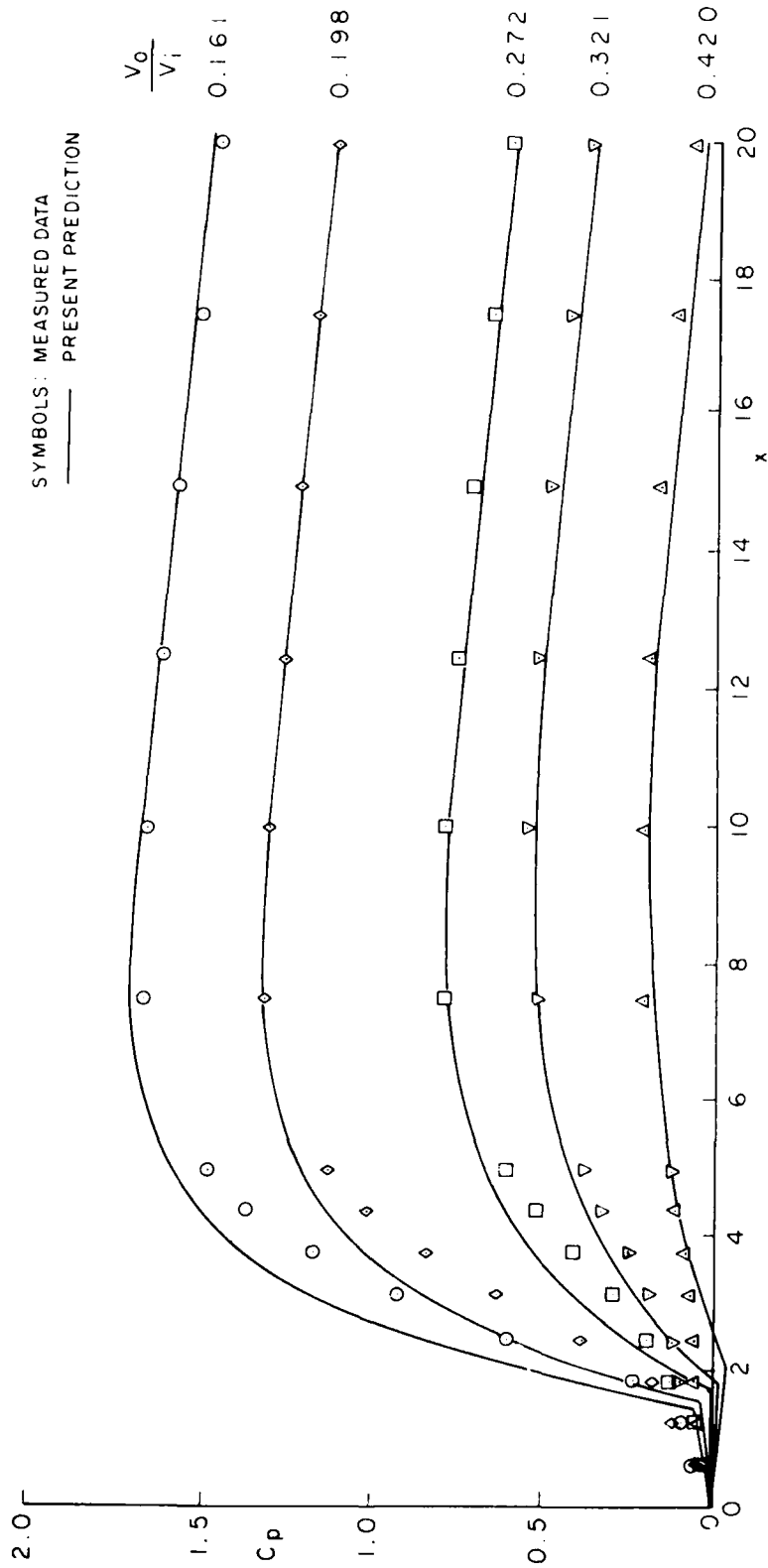


FIG. 12(c): PREDICTED AND MEASURED VALUES OF C_p COMPARED ($V_i > V_0$)

$V_1 > V_0$
 $\bar{D} = 0.529$

SYMBOLS: MEASURED DATA
—— PRESENT PREDICTION

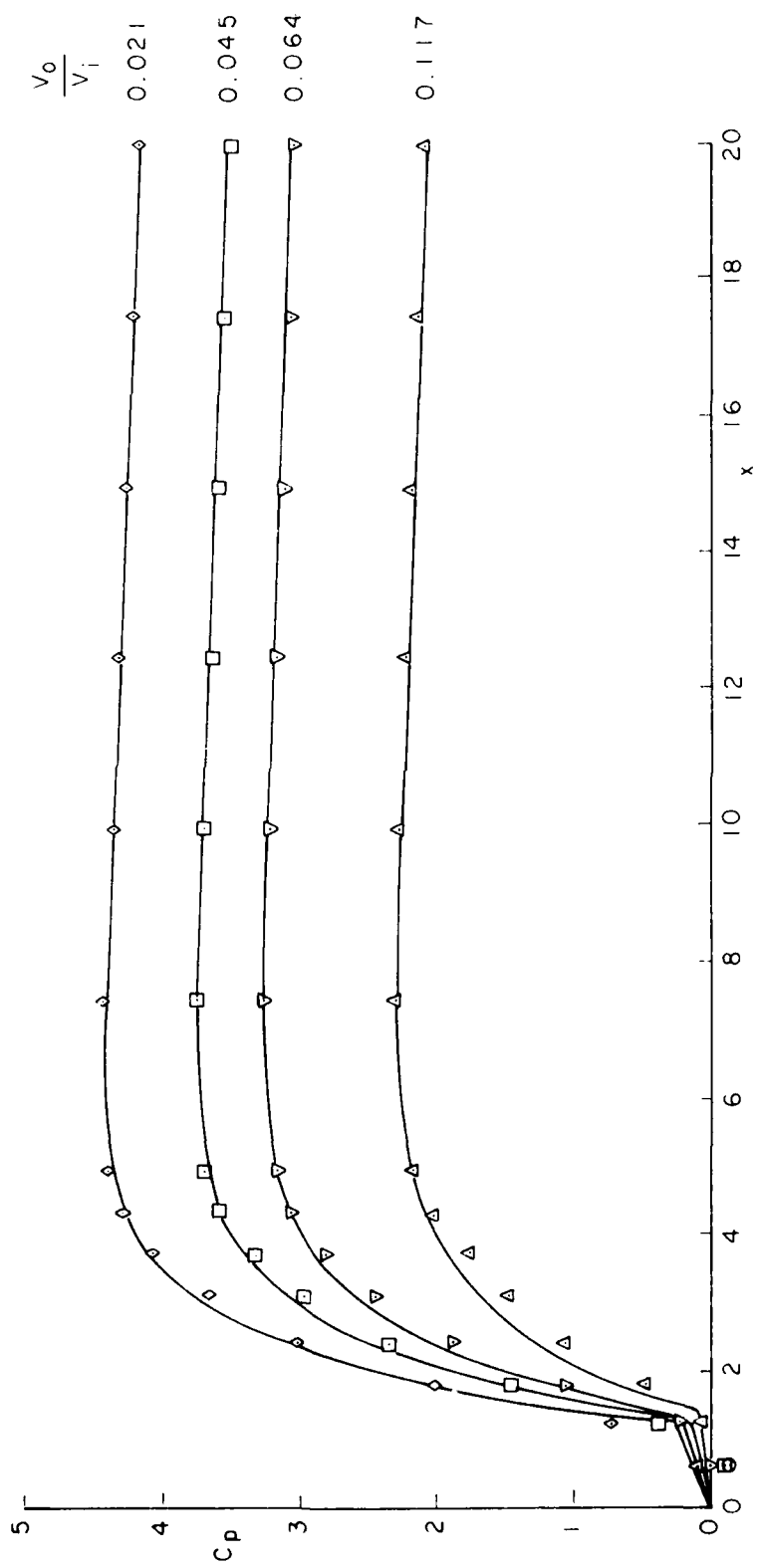


FIG. 12(d): PREDICTED AND MEASURED VALUES OF C_p COMPARED ($V_1 > V_0$)

$V_1 > V_0$
 $\frac{D}{\delta} = 0.273$

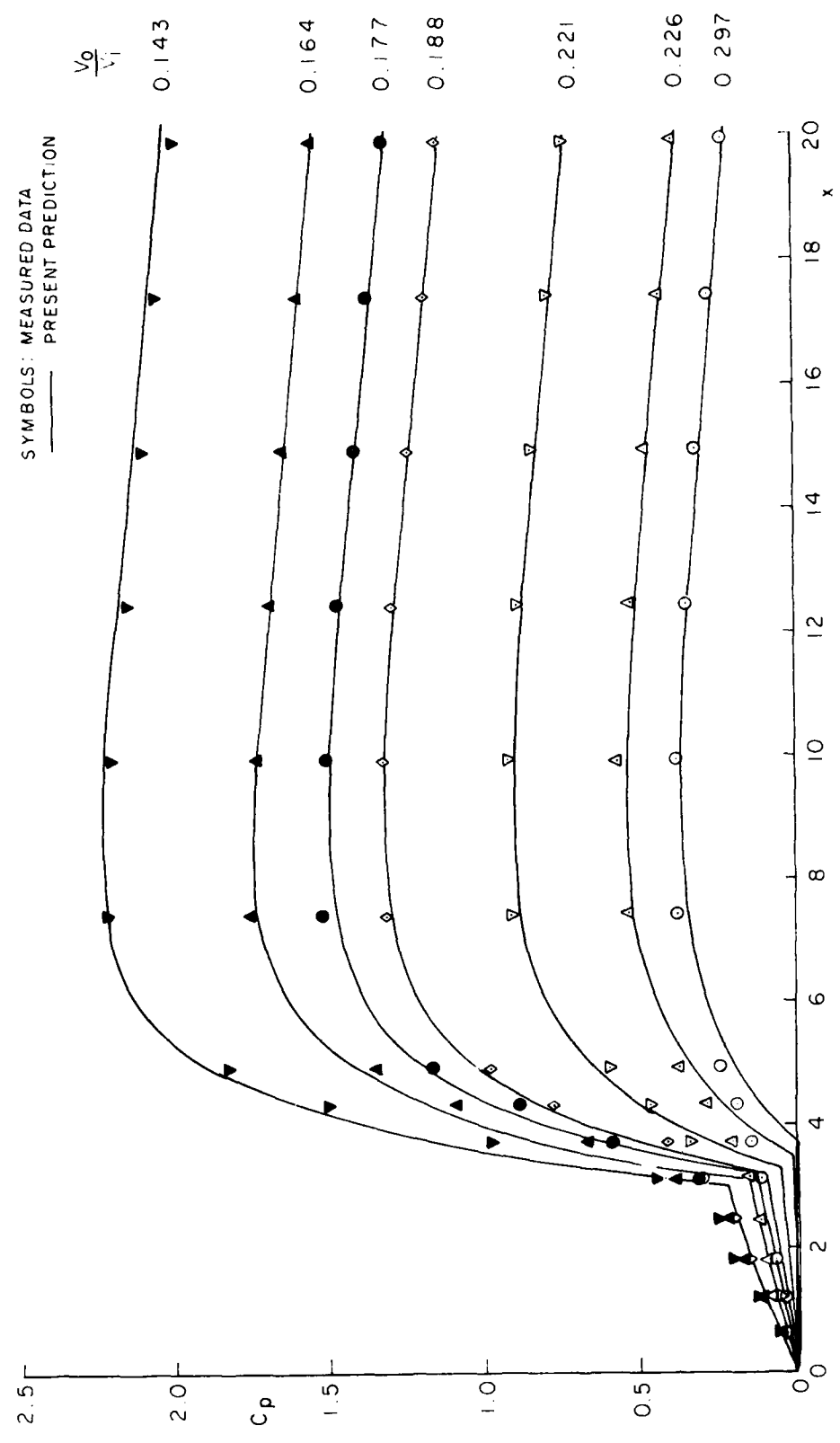


FIG. 12(e): PREDICTED AND MEASURED VALUES OF C_p COMPARED ($V_1 > V_0$)

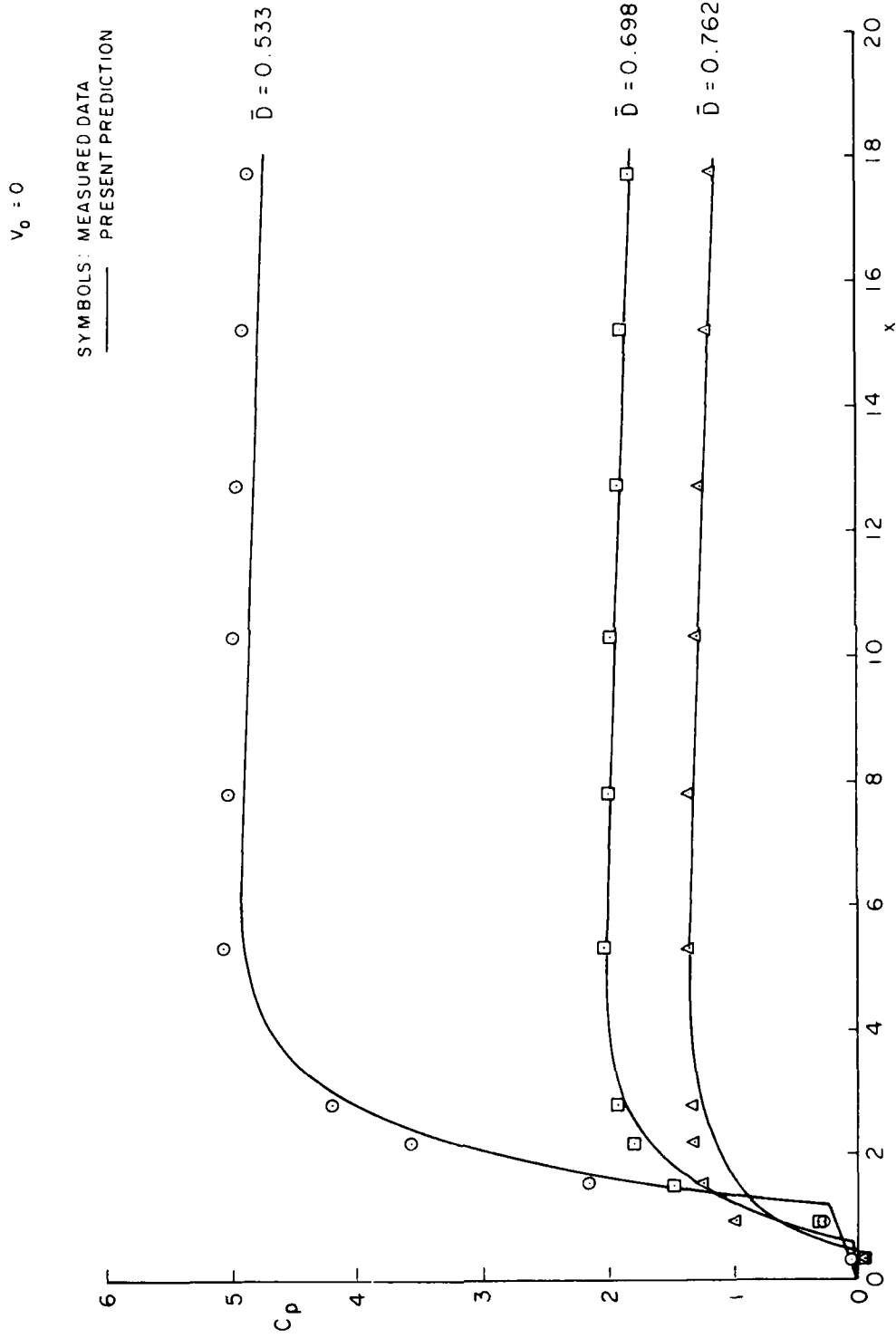


FIG. 12(f): PREDICTED AND MEASURED VALUES OF C_p COMPARED ($V_0 = 0$)

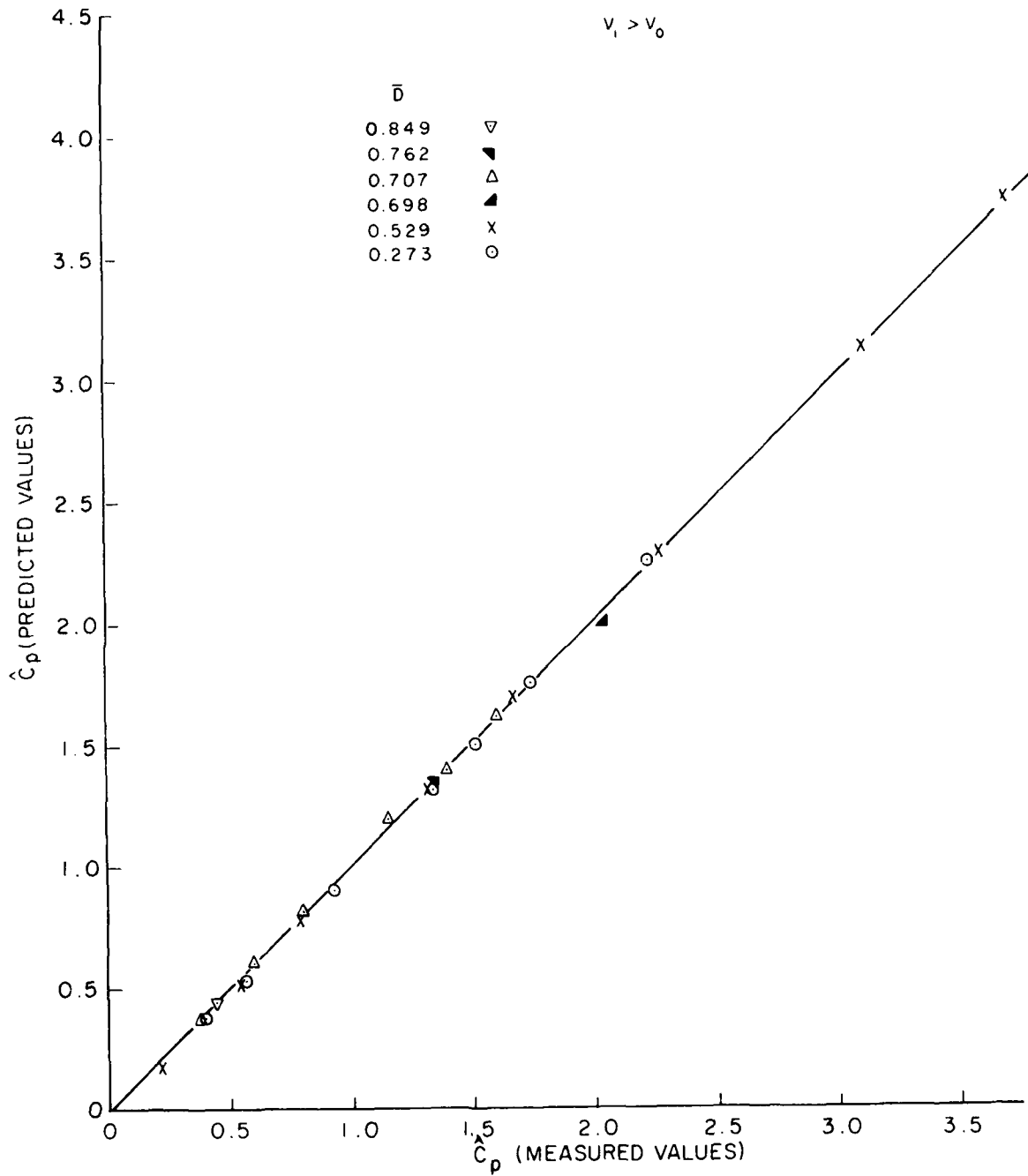


FIG. 13: PREDICTED AND MEASURED VALUES OF \hat{C}_p COMPARED ($V_1 > V_0$)

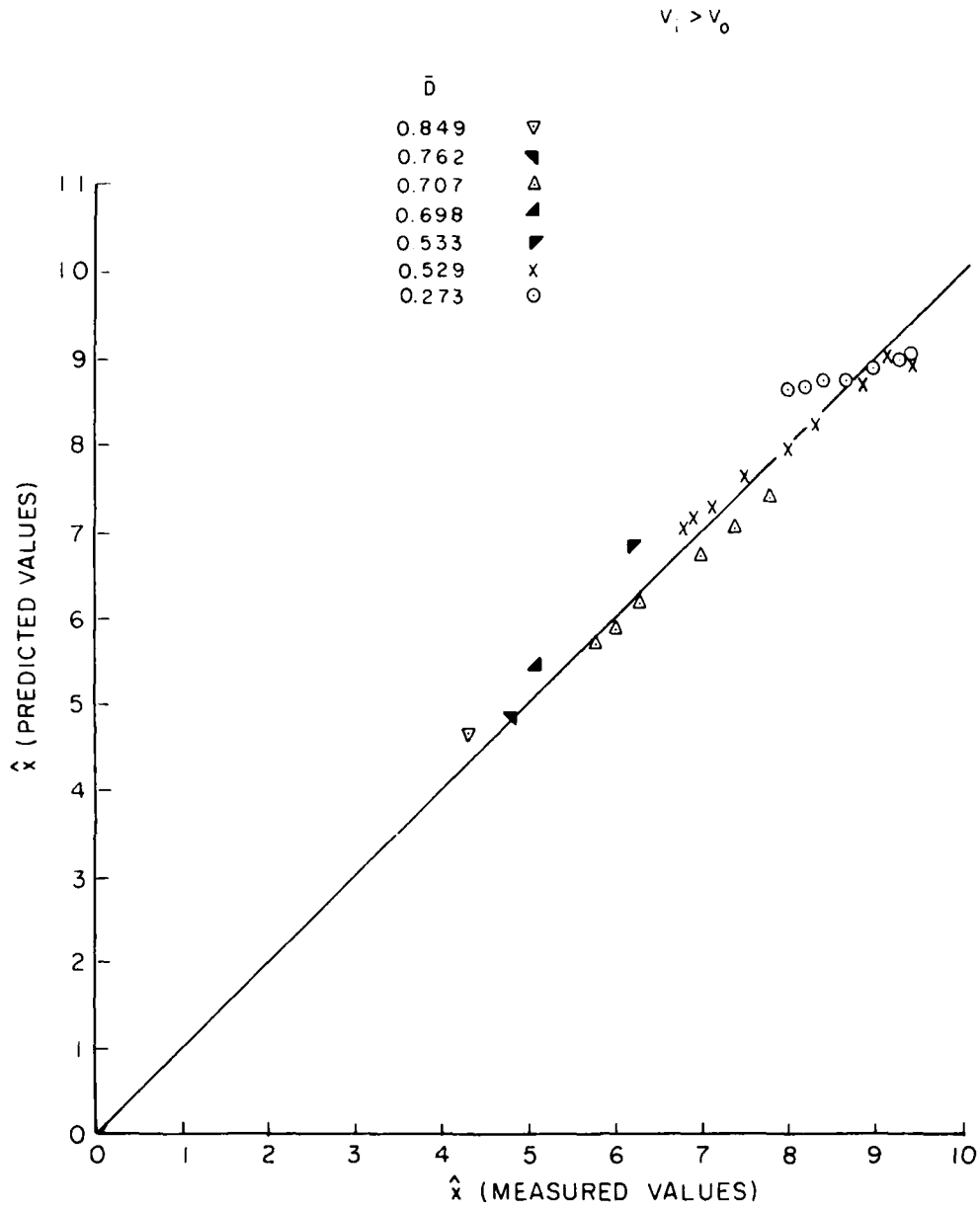


FIG. 14: PREDICTED AND MEASURED VALUES OF \hat{x} COMPARED ($V_i > V_o$)

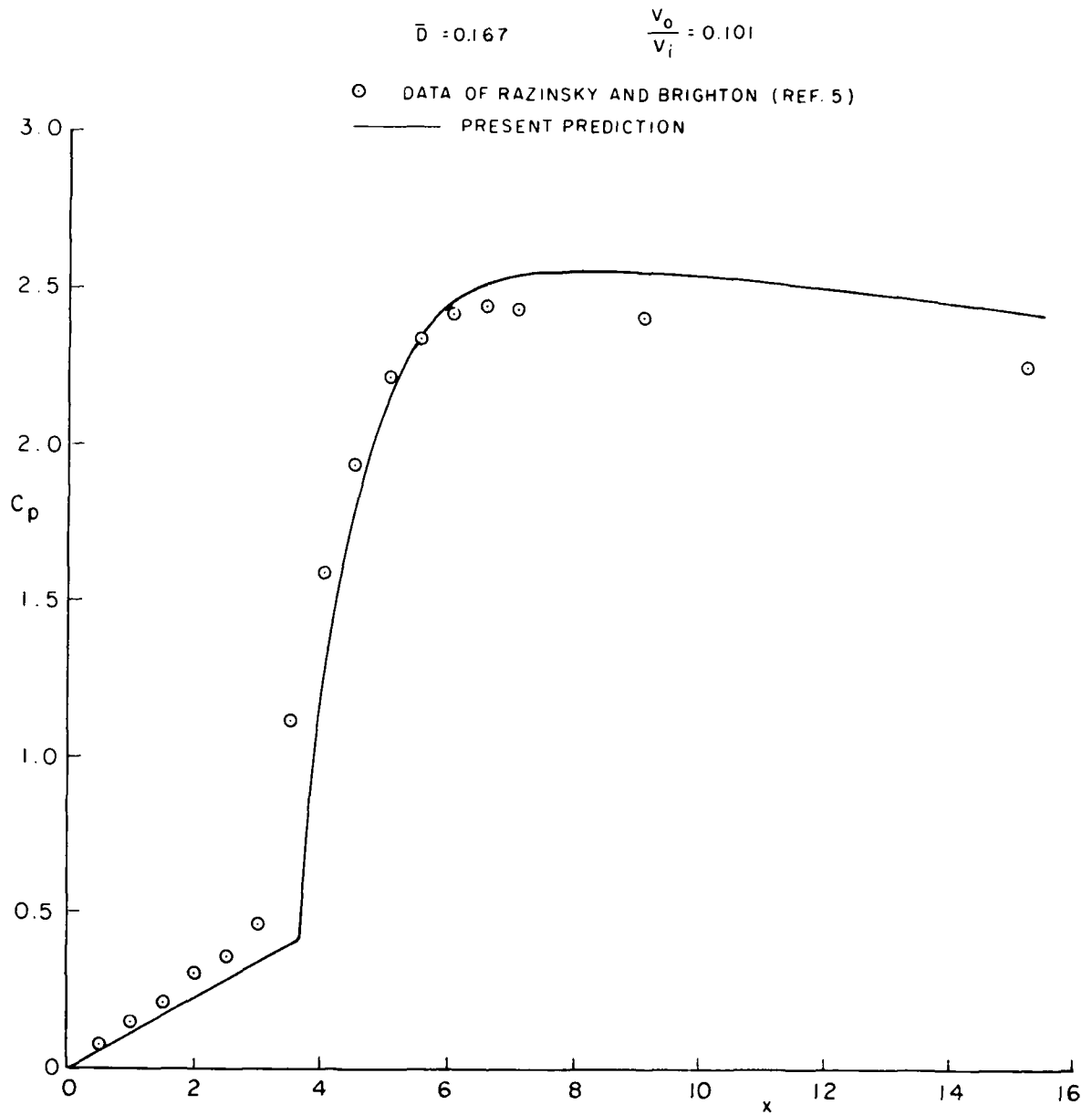


FIG. 15: DATA OF REFERENCE 5 COMPARED WITH PREDICTION OF PRESENT METHOD

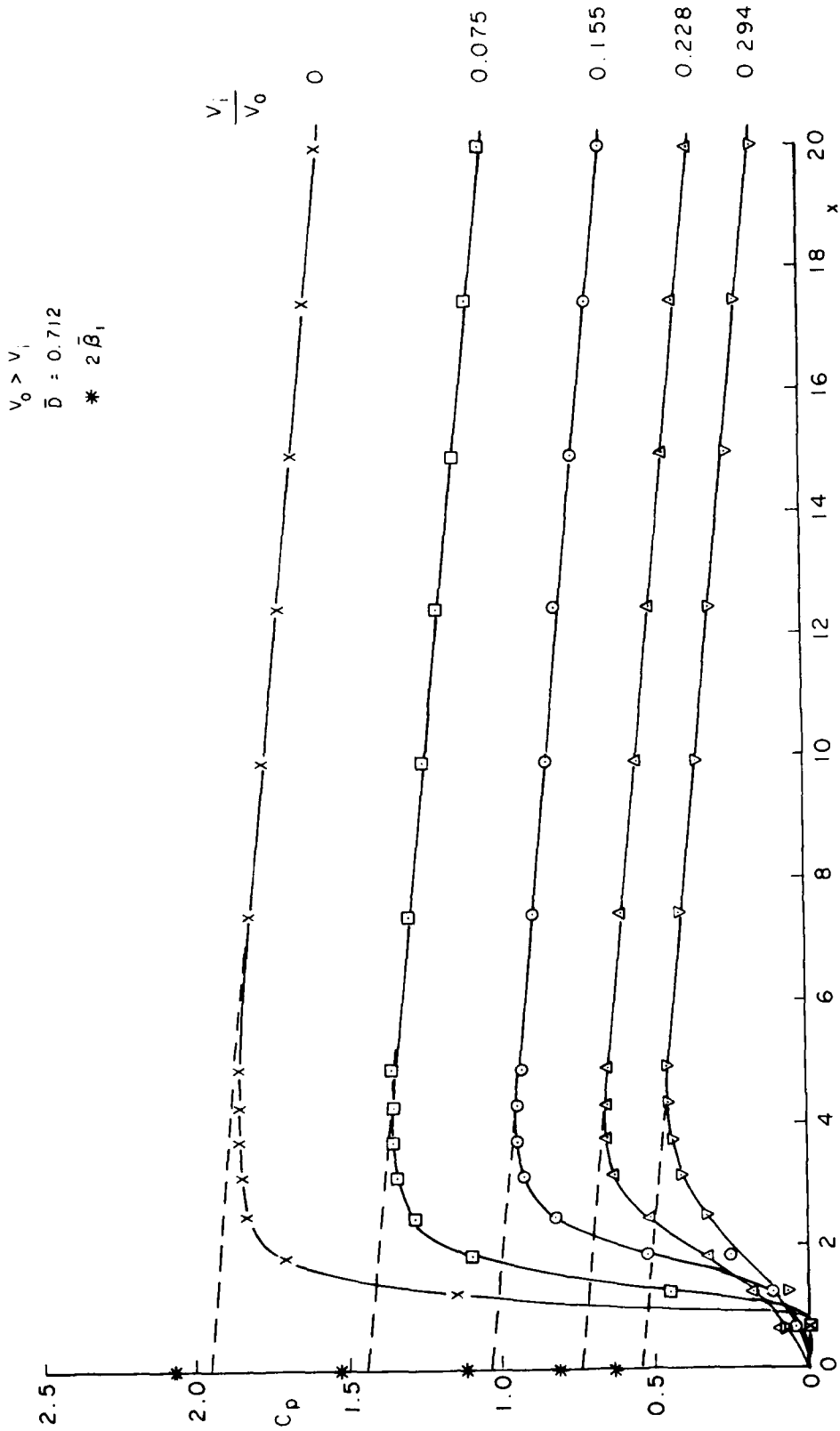


FIG. 16(a): MEASURED STATIC PRESSURE DISTRIBUTION ($V_0 > V_1$)

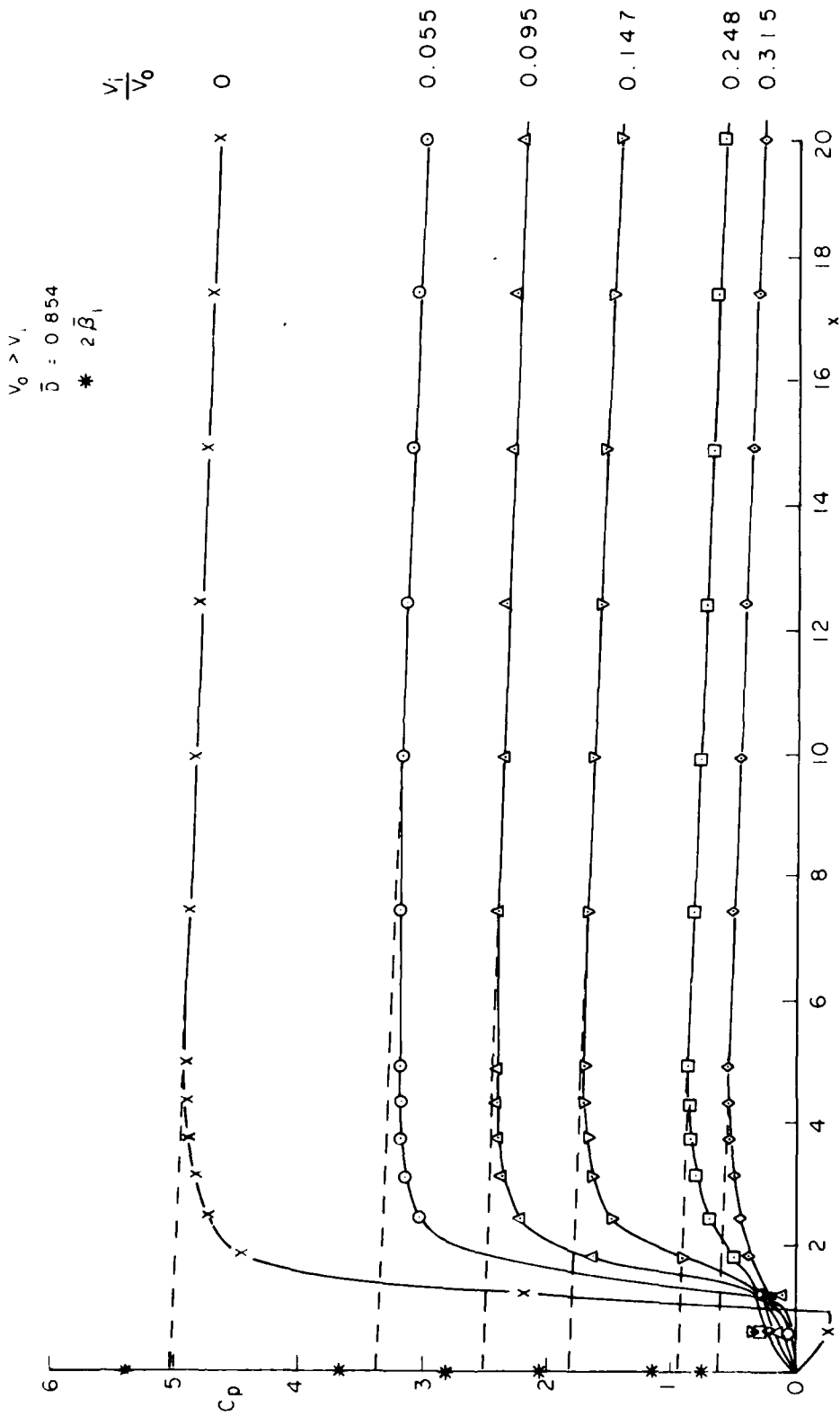


FIG. 16(b): MEASURED STATIC PRESSURE DISTRIBUTION ($V_0 > V_1$)

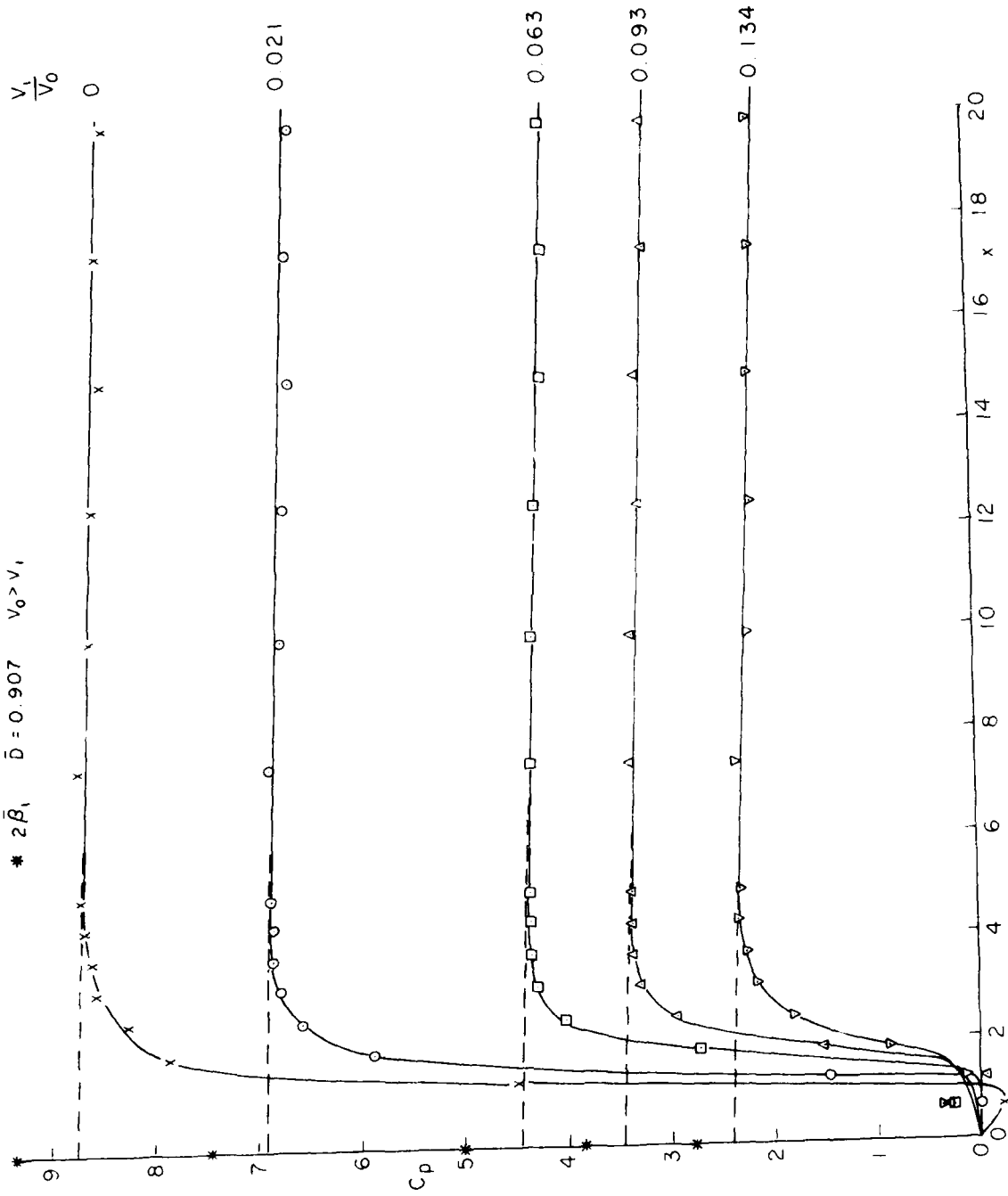


FIG. 16(c). MEASURED STATIC PRESSURE DISTRIBUTION ($V_0 > V_1$)

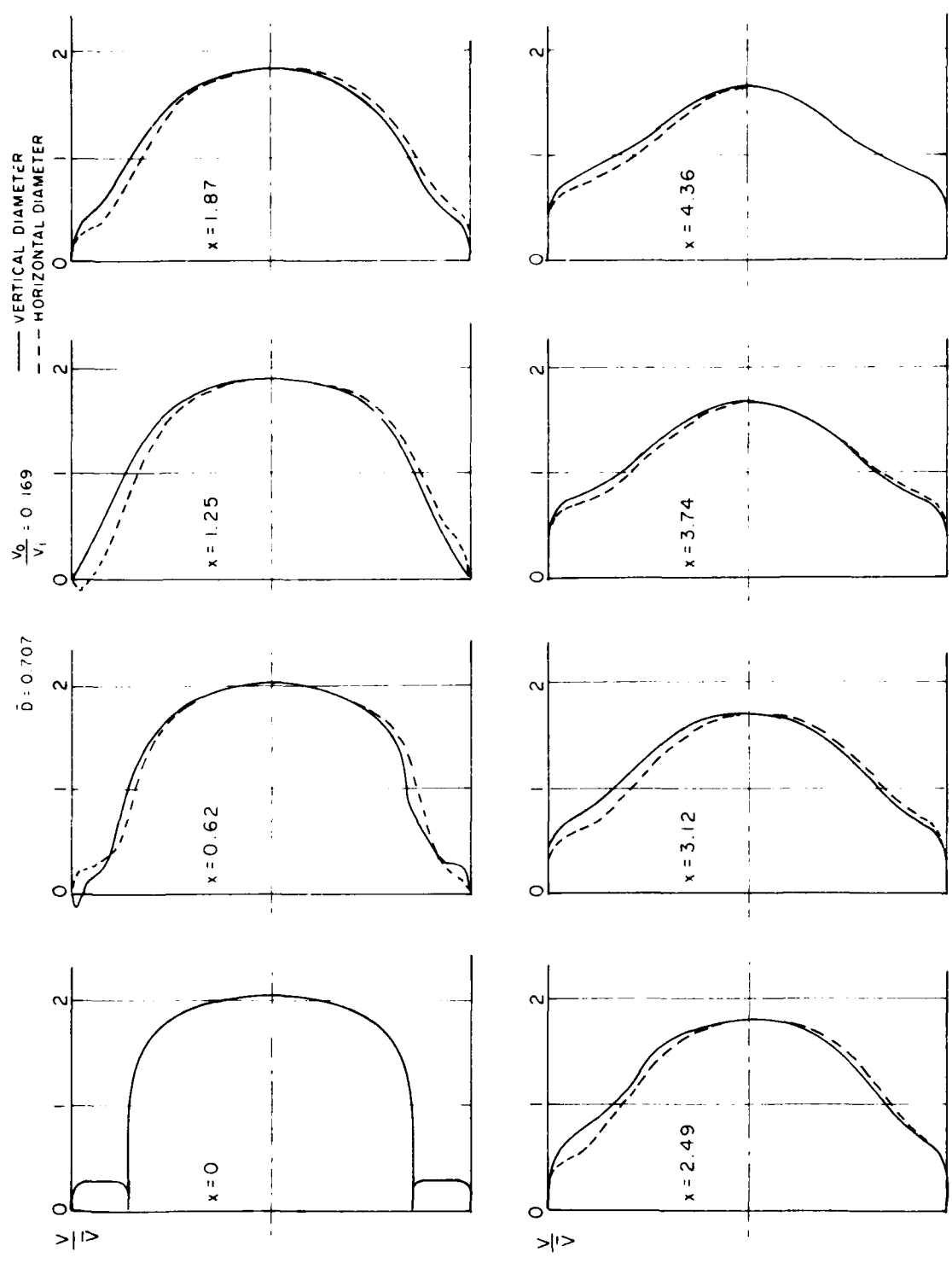


FIG. 17(a): MEASURED VELOCITY PROFILES IN MIXING PIPE ($V_1 \sim V_0$)

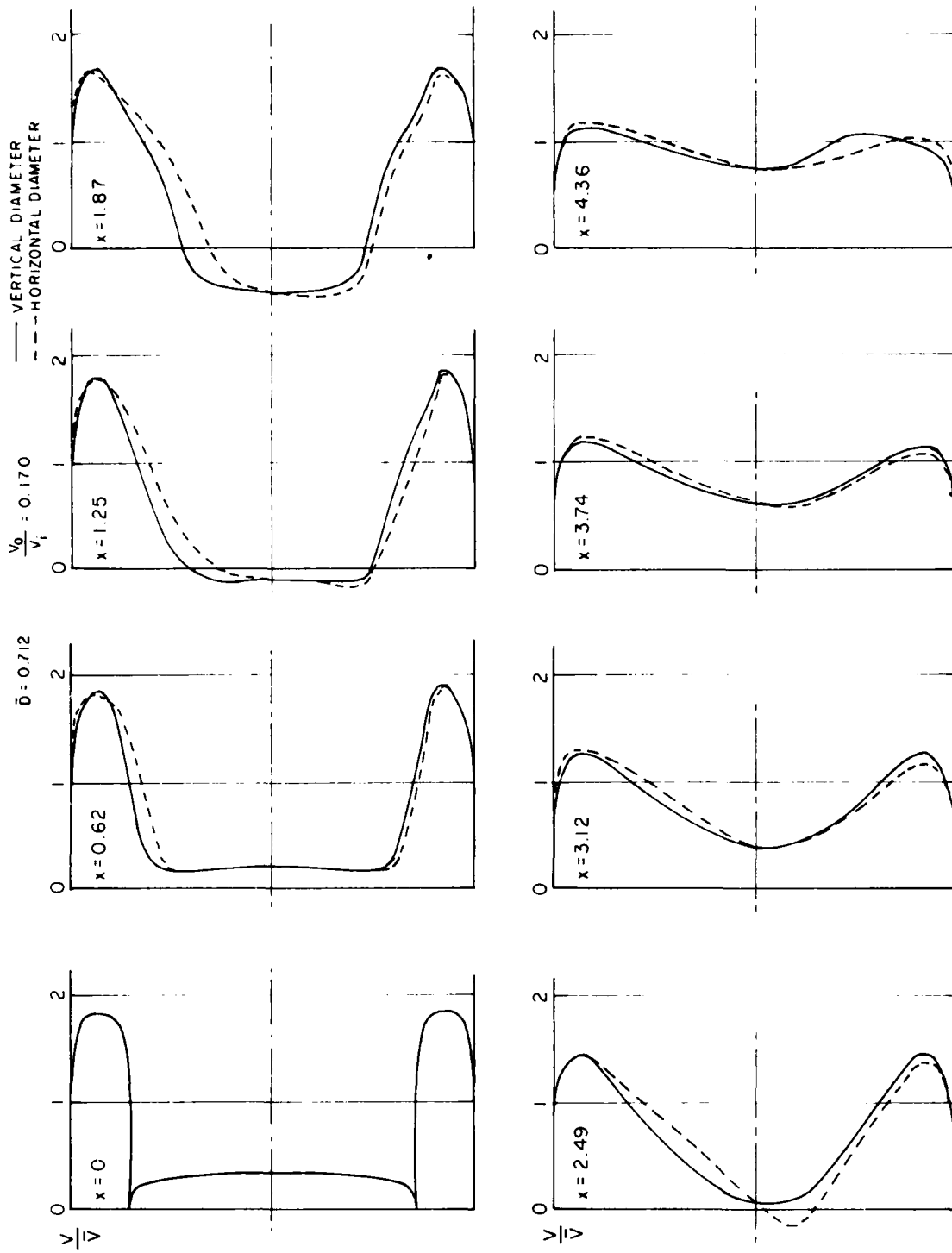


FIG. 17(b): MEASURED VELOCITY PROFILES IN MIXING PIPE ($V_0 > V_1$)

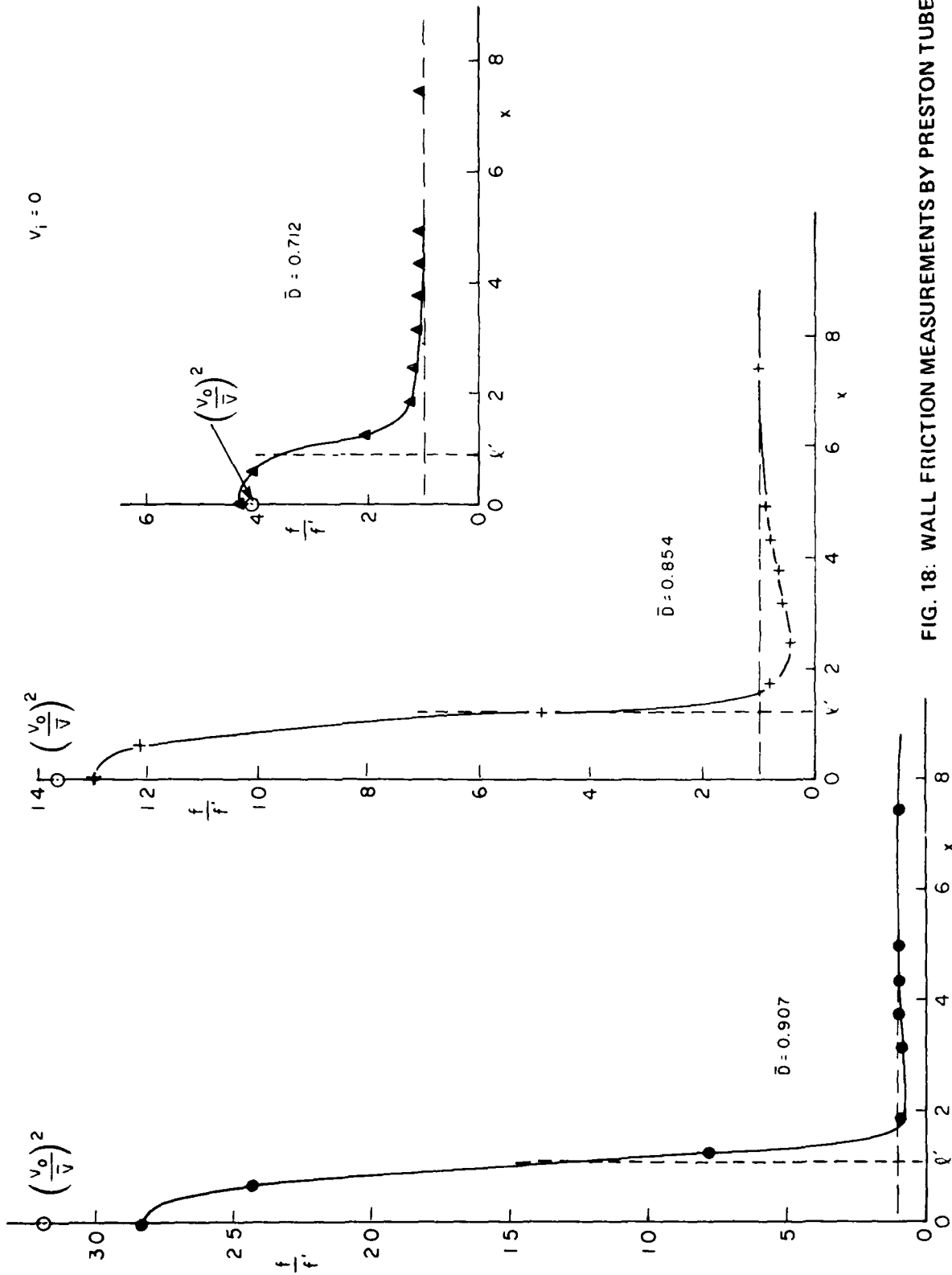


FIG. 18: WALL FRICTION MEASUREMENTS BY PRESTON TUBE

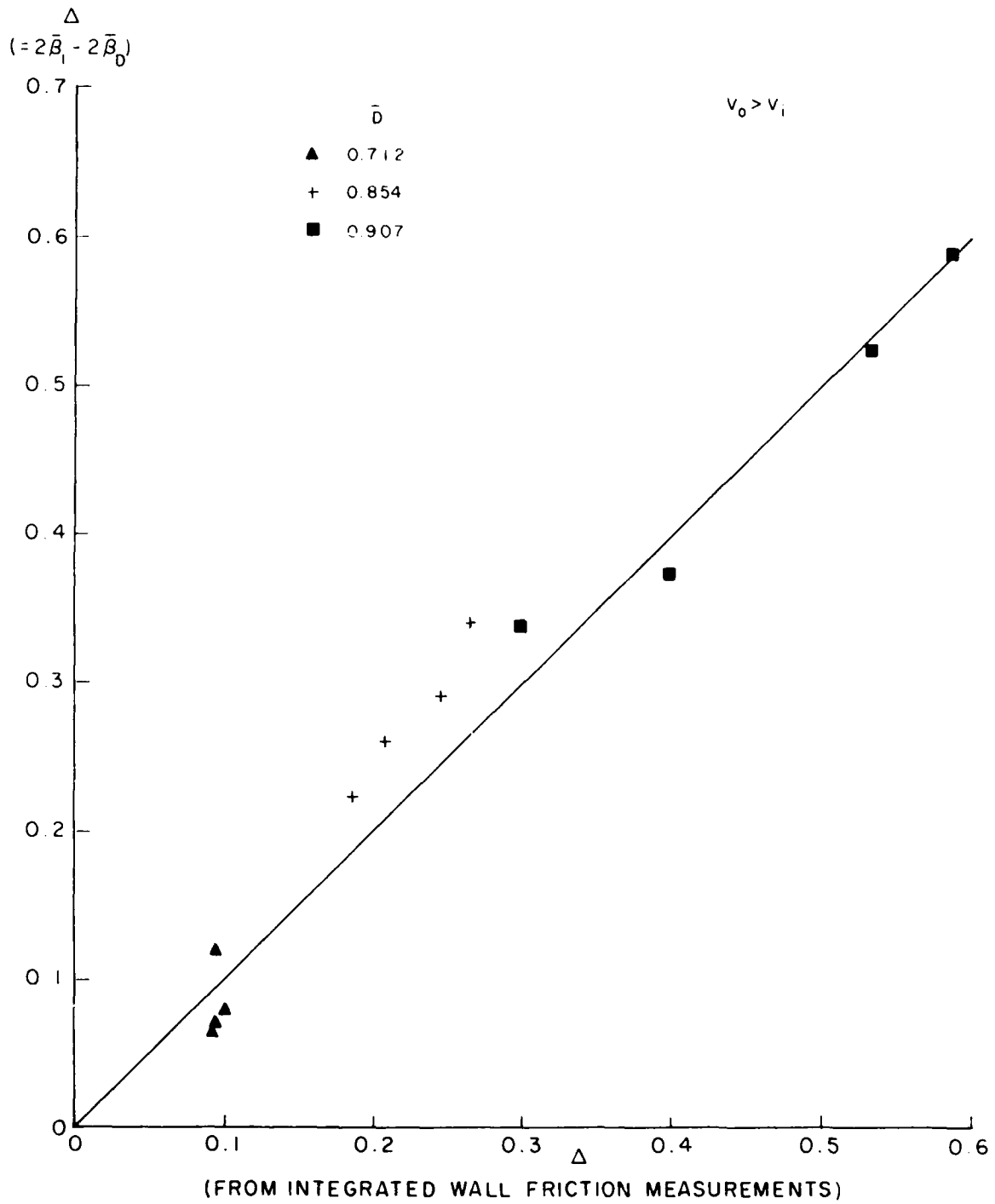


FIG. 19: ALTERNATIVE DERIVATIONS OF Δ COMPARED

$V_o > V_i$

- ● 0.907
- ▽ ▼ 0.854
- △ ▲ 0.712

OPEN SYMBOLS: $\Delta = 2\bar{\beta}_i - 2\bar{\beta}_0$

CLOSED SYMBOLS: Δ FROM FRICTION MEASUREMENTS

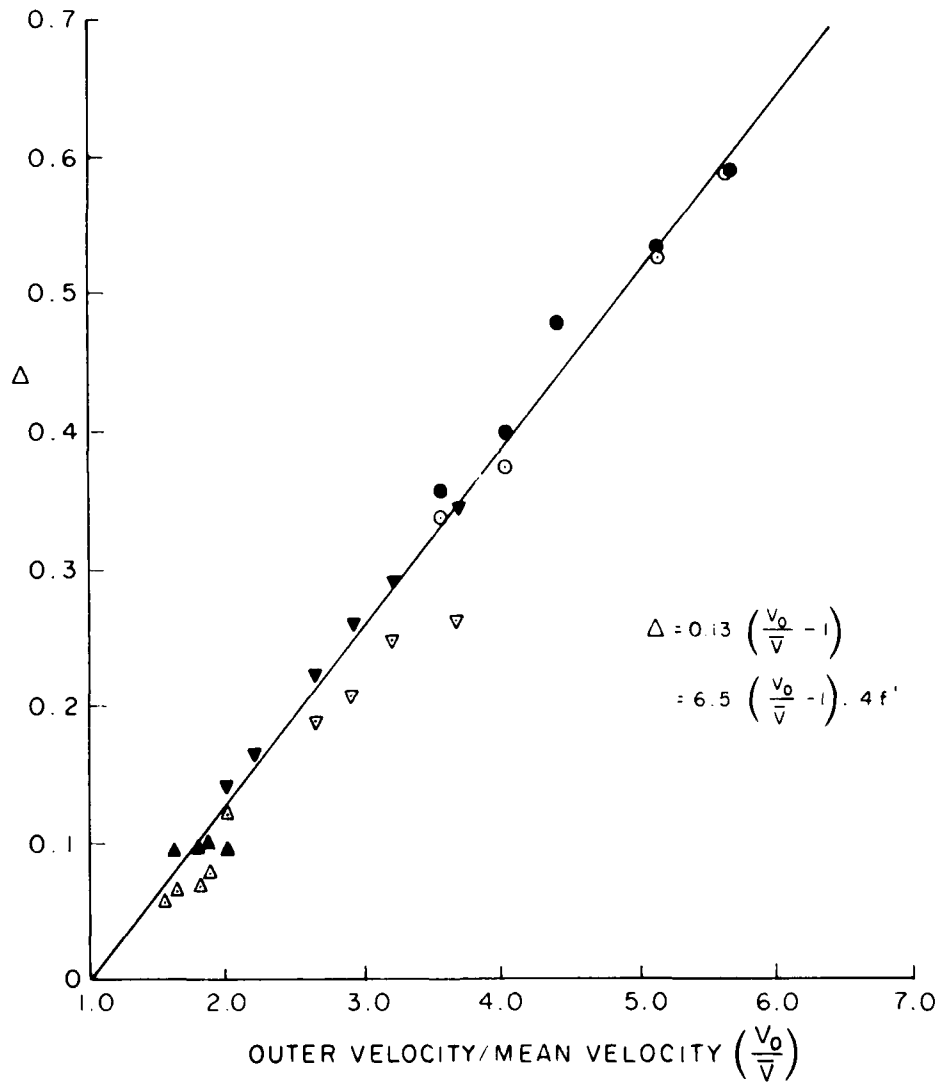


FIG. 20: CORRELATION OF DERIVED Δ VALUES

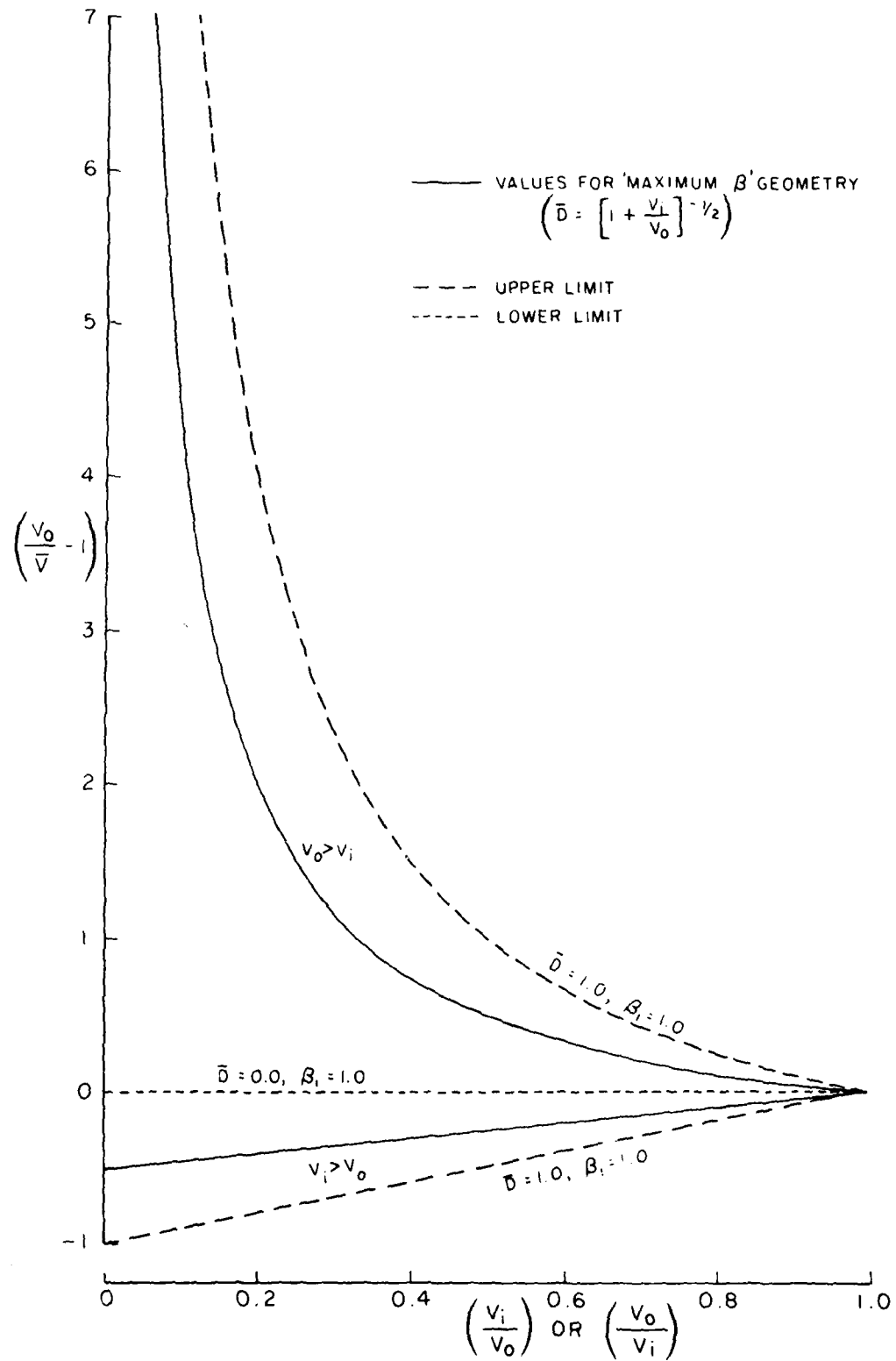


FIG. 21: $(V_0/\bar{V} - 1)$ FACTOR FOR 'MAXIMUM β ' GEOMETRY

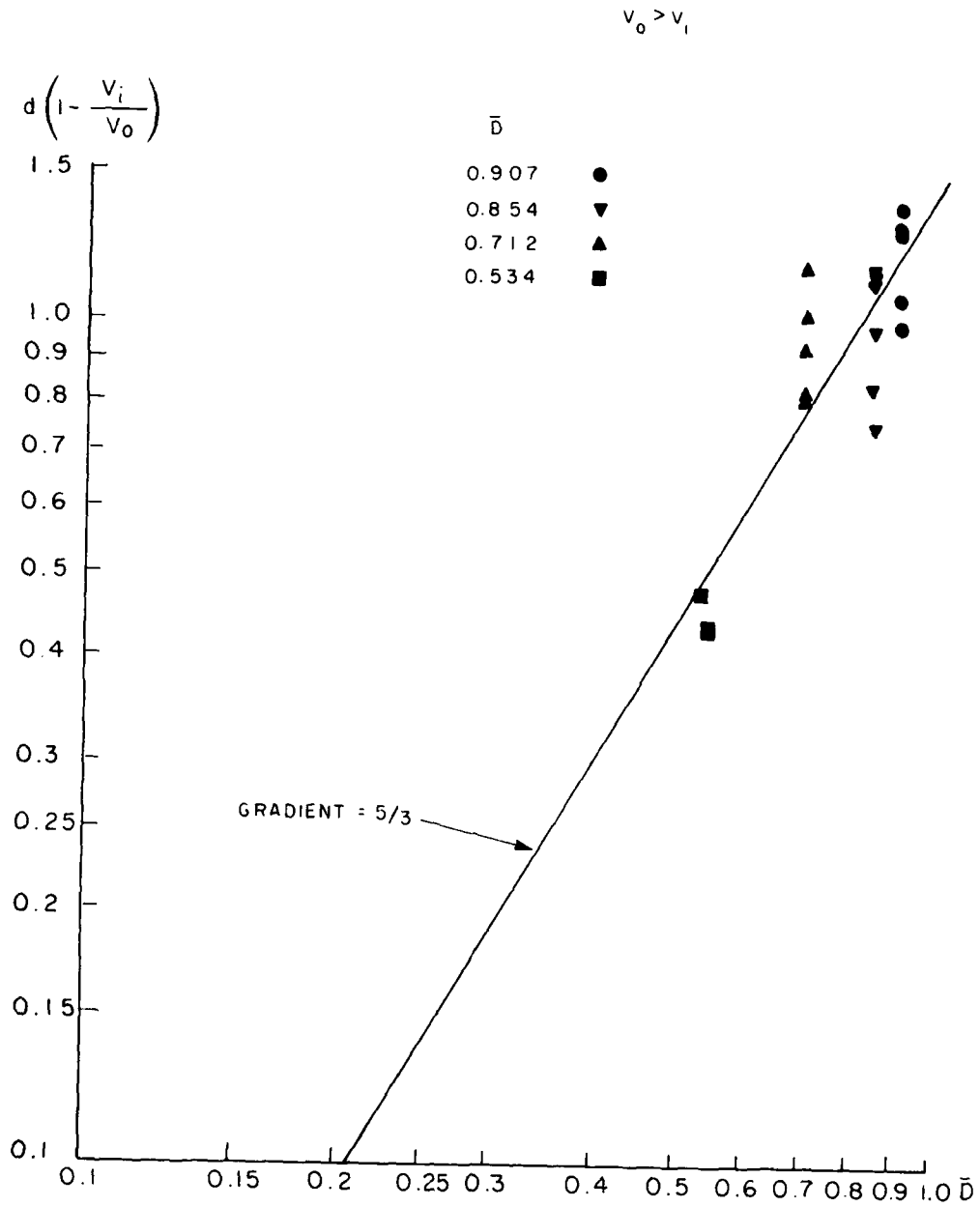


FIG. 22: CORRELATION OF DERIVED d VALUES WITH GEOMETRY ($v_0 > v_1$)

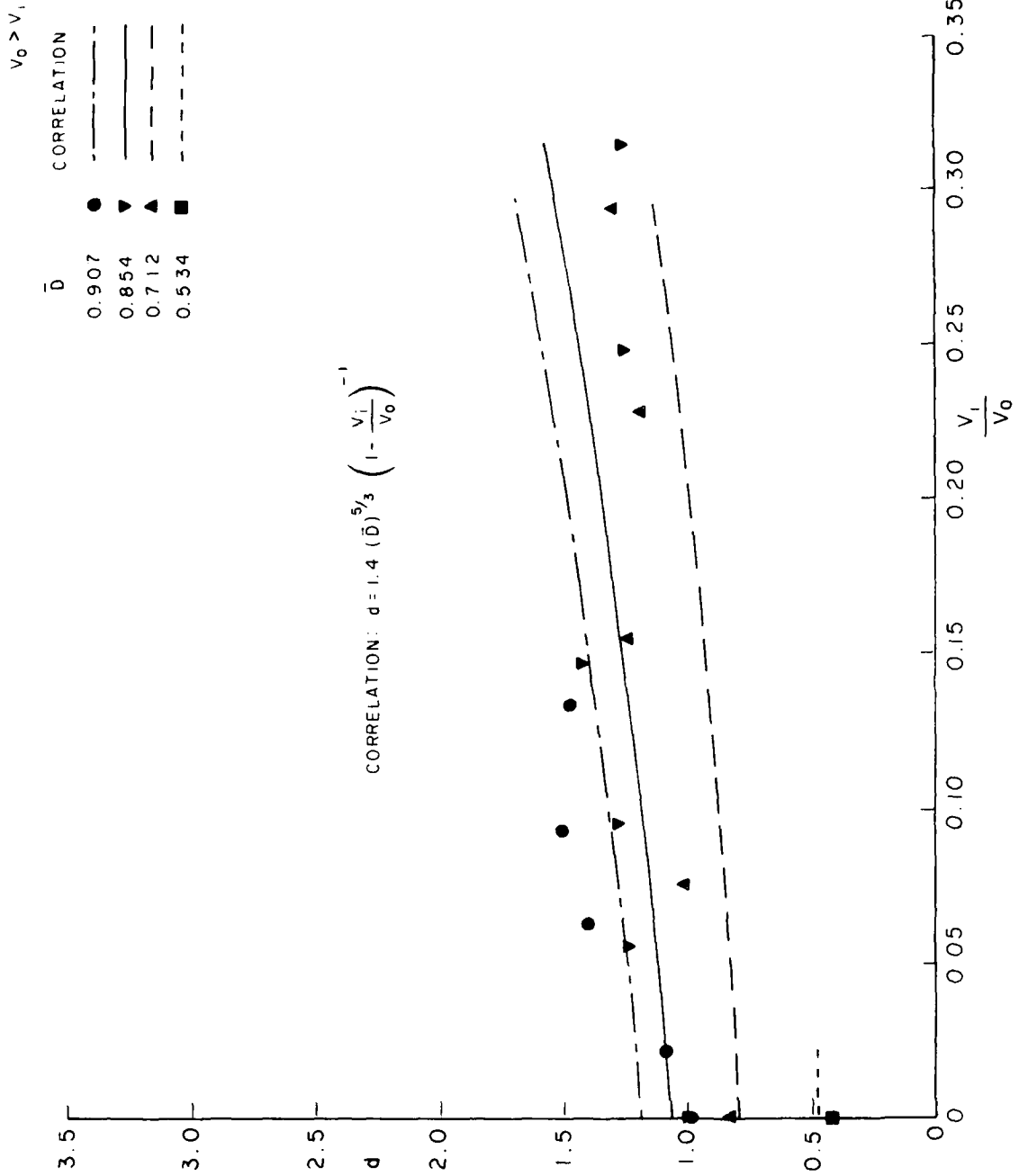


FIG. 23: FINAL CORRELATION OF DERIVED d VALUES ($V_0 > V_1$)

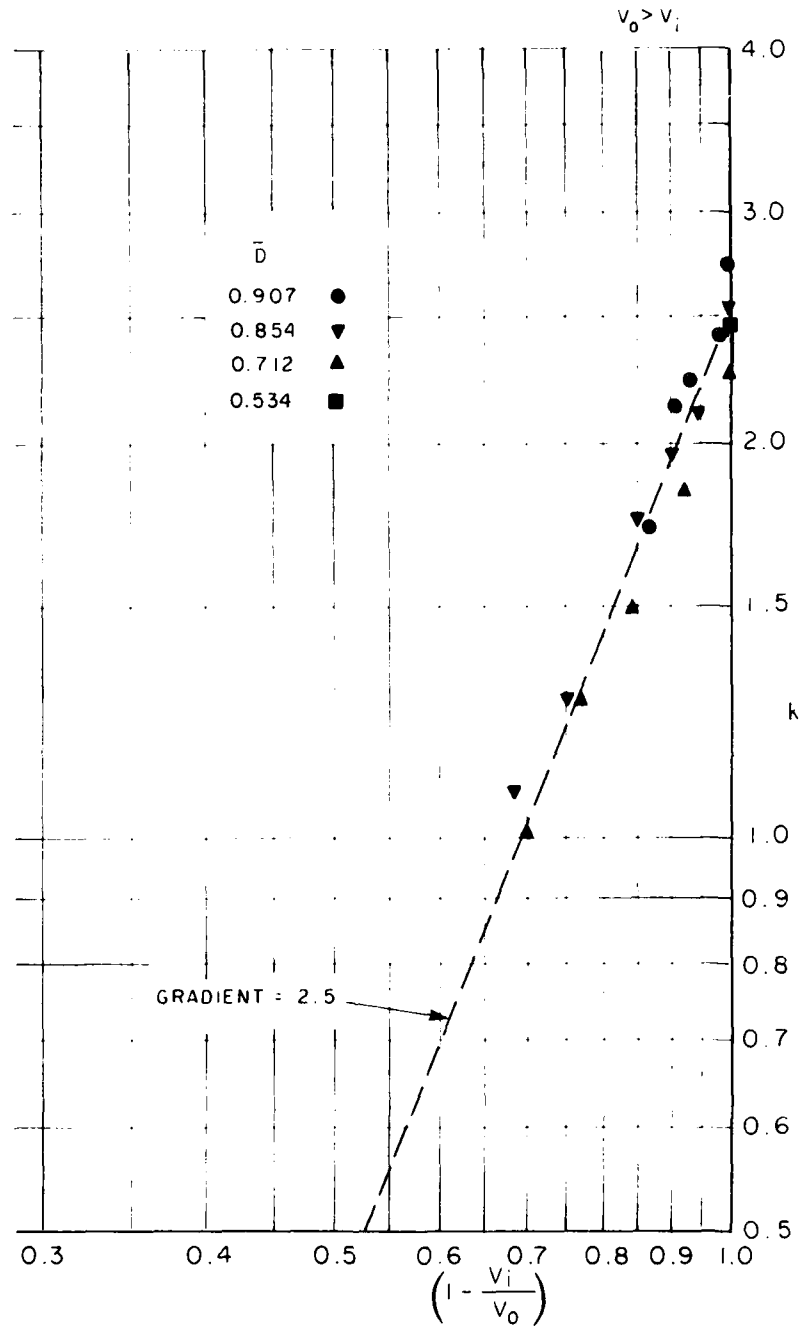


FIG. 24. CORRELATION OF DERIVED k VALUES WITH VELOCITY RATIO ($V_o > V_i$)

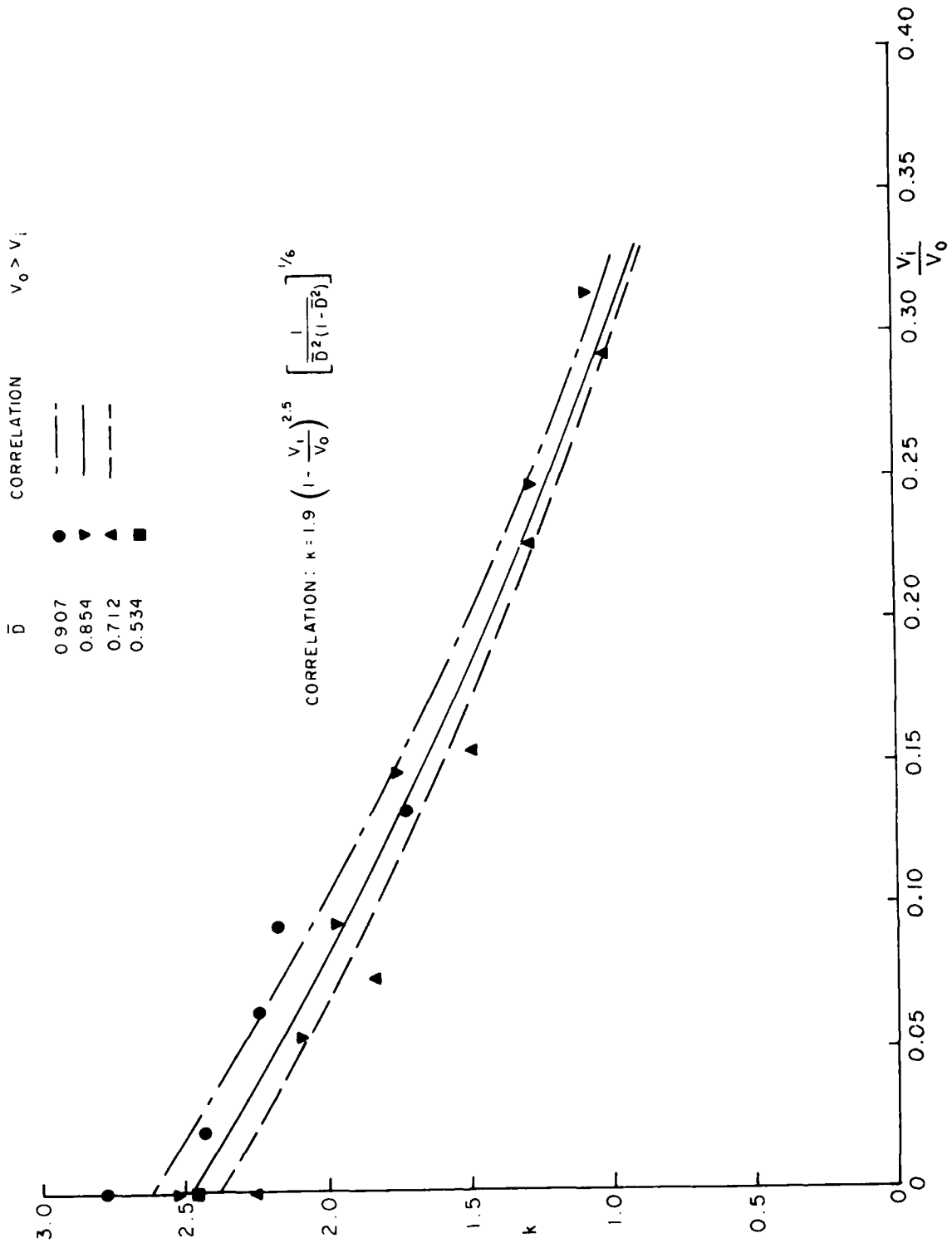


FIG. 25: FINAL CORRELATION OF DERIVED k VALUES ($V_o > V_i$)

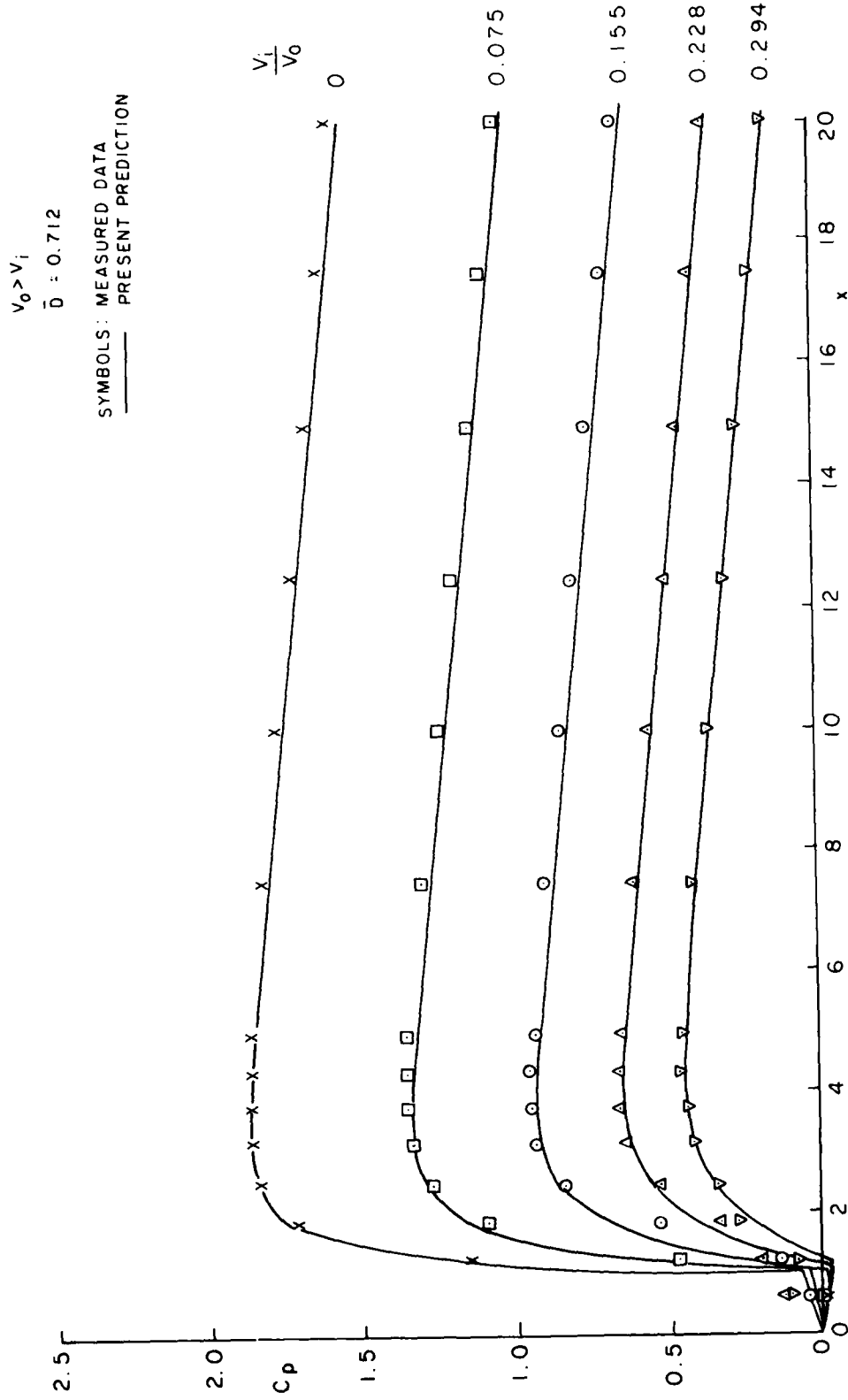


FIG. 26(a). PREDICTED AND MEASURED VALUES OF C_p COMPARED ($V_0 > V_i$)

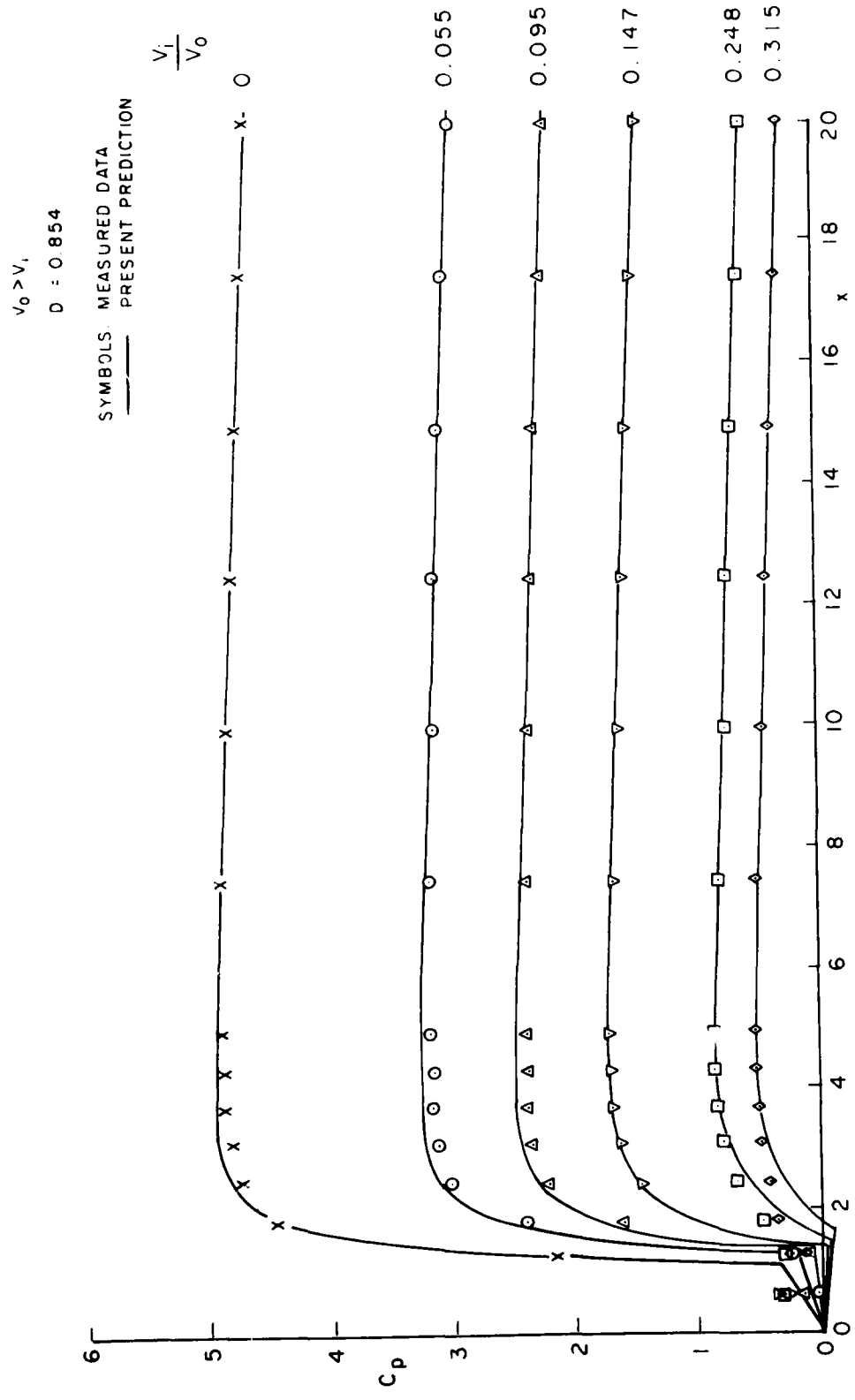


FIG. 26(b): PREDICTED AND MEASURED VALUES OF C_p COMPARED ($V_0 > V_1$)

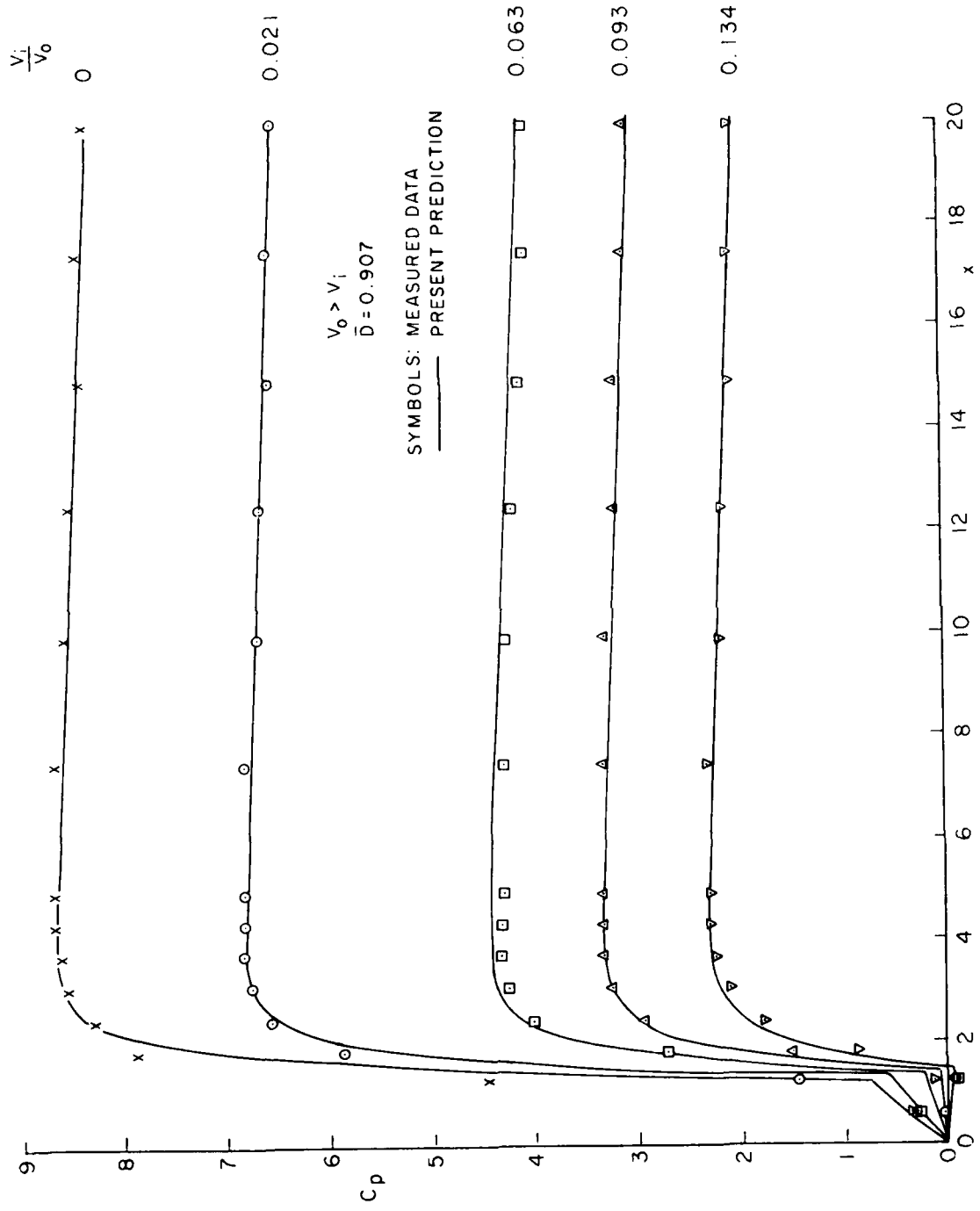


FIG. 26(c): PREDICTED AND MEASURED VALUES OF C_p COMPARED ($V_0 > V_i$)

(PREDICTED VALUES)

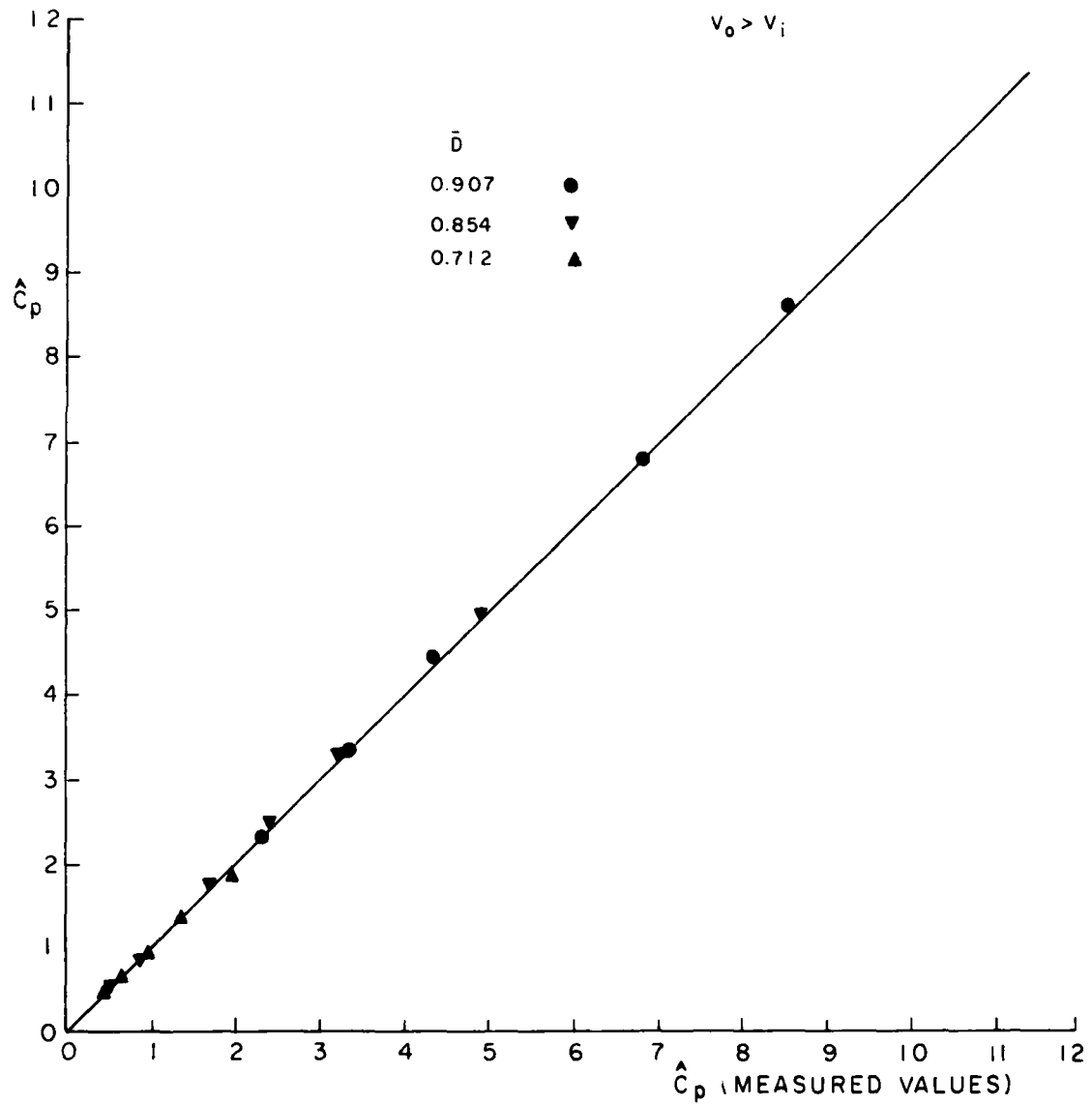


FIG. 27: PREDICTED AND MEASURED VALUES OF \hat{C}_p COMPARED ($V_o > V_i$)

(PREDICTED VALUES)

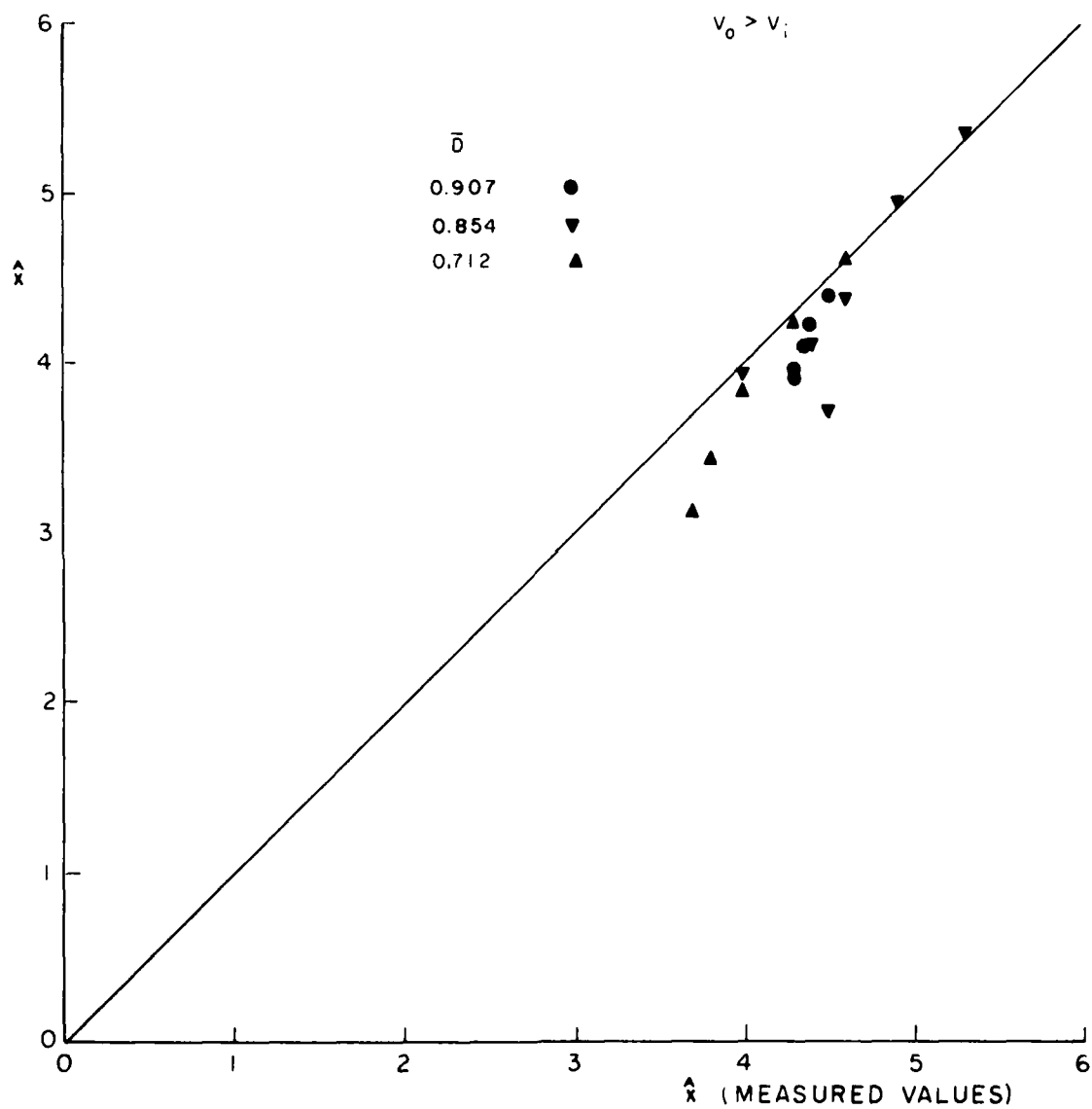


FIG. 28: PREDICTED AND MEASURED VALUES OF \hat{x} COMPARED ($V_0 > V_i$)

S = 25, 4f = 0.02

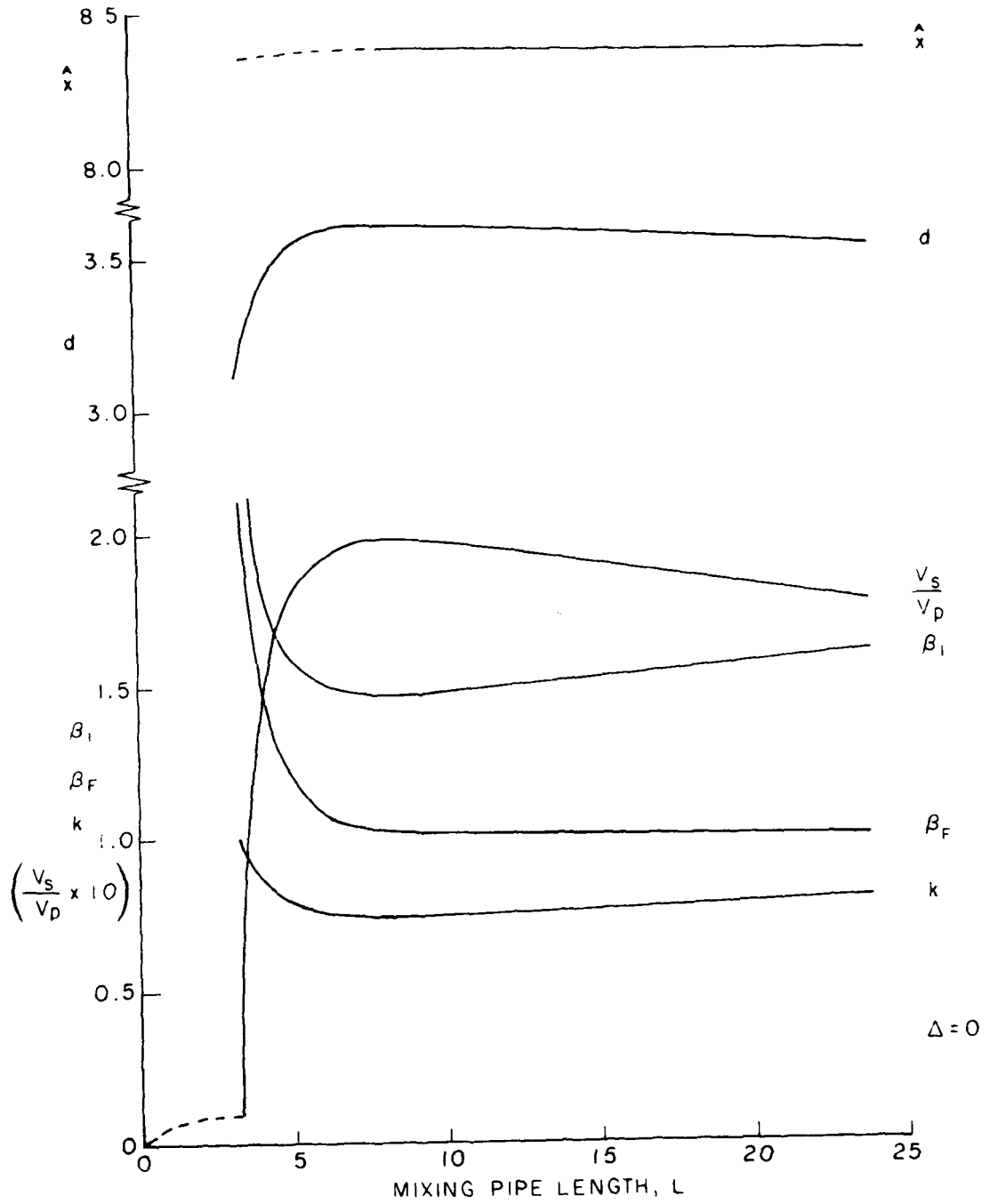


FIG. 29(a): RESULTS OF CALCULATION PROCEDURE APPLIED TO CENTRAL JET EJECTORS (S = 25)

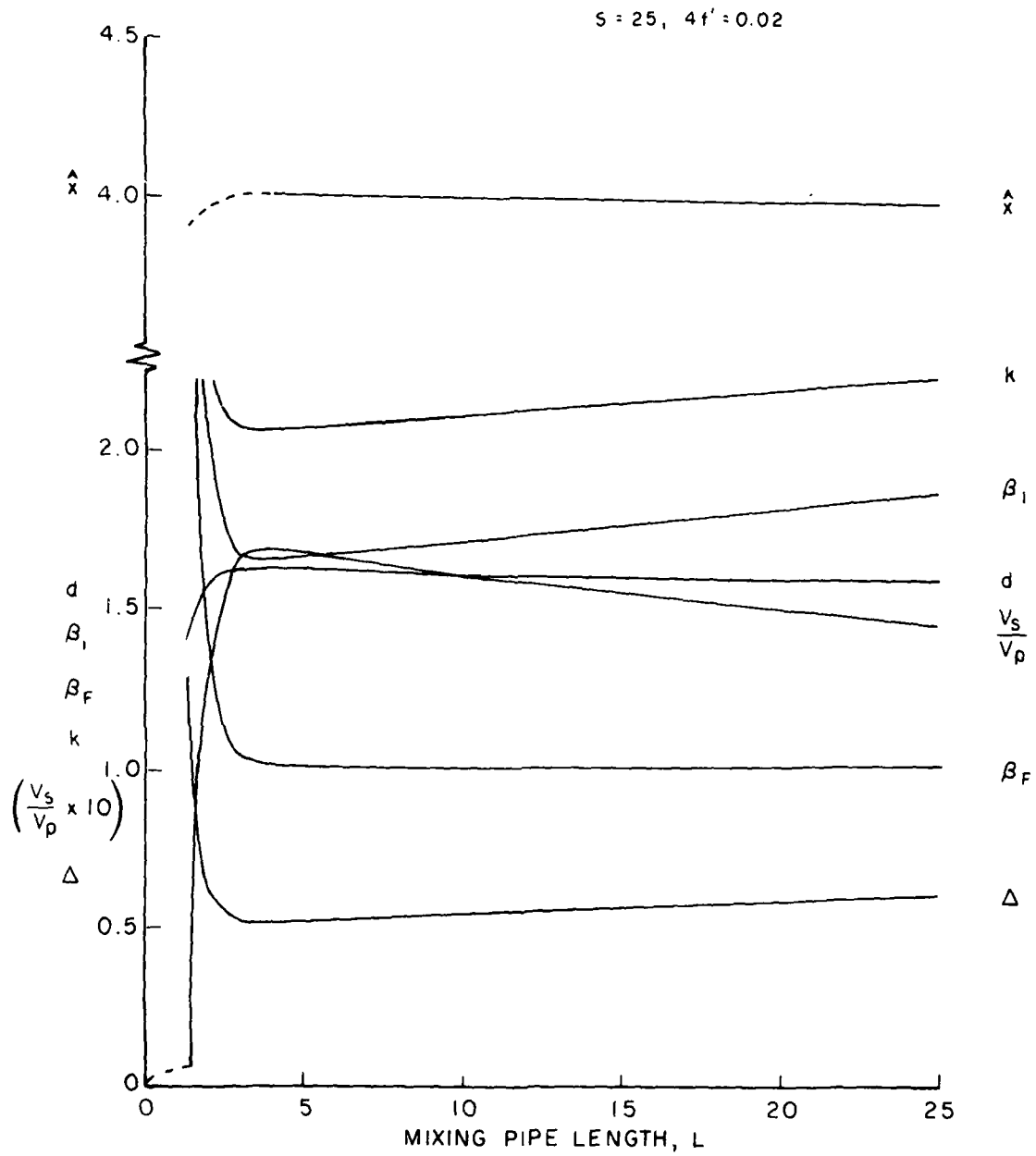


FIG. 29(b): RESULTS OF CALCULATION PROCEDURE APPLIED TO PARIETAL JET EJECTORS ($S = 25$)

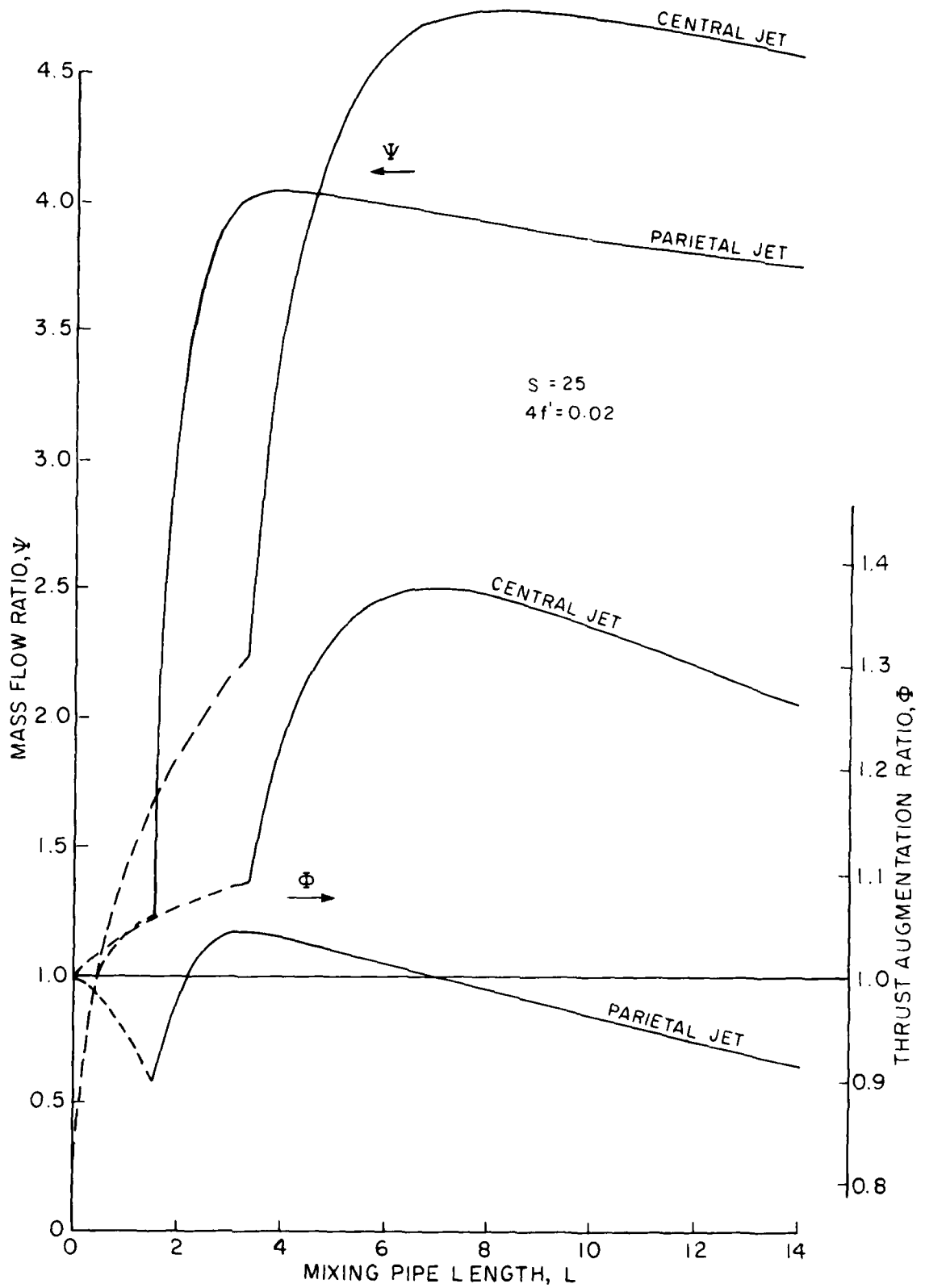


FIG. 30: EJECTOR PERFORMANCE CORRESPONDING TO CALCULATED RESULTS OF FIGURE 29

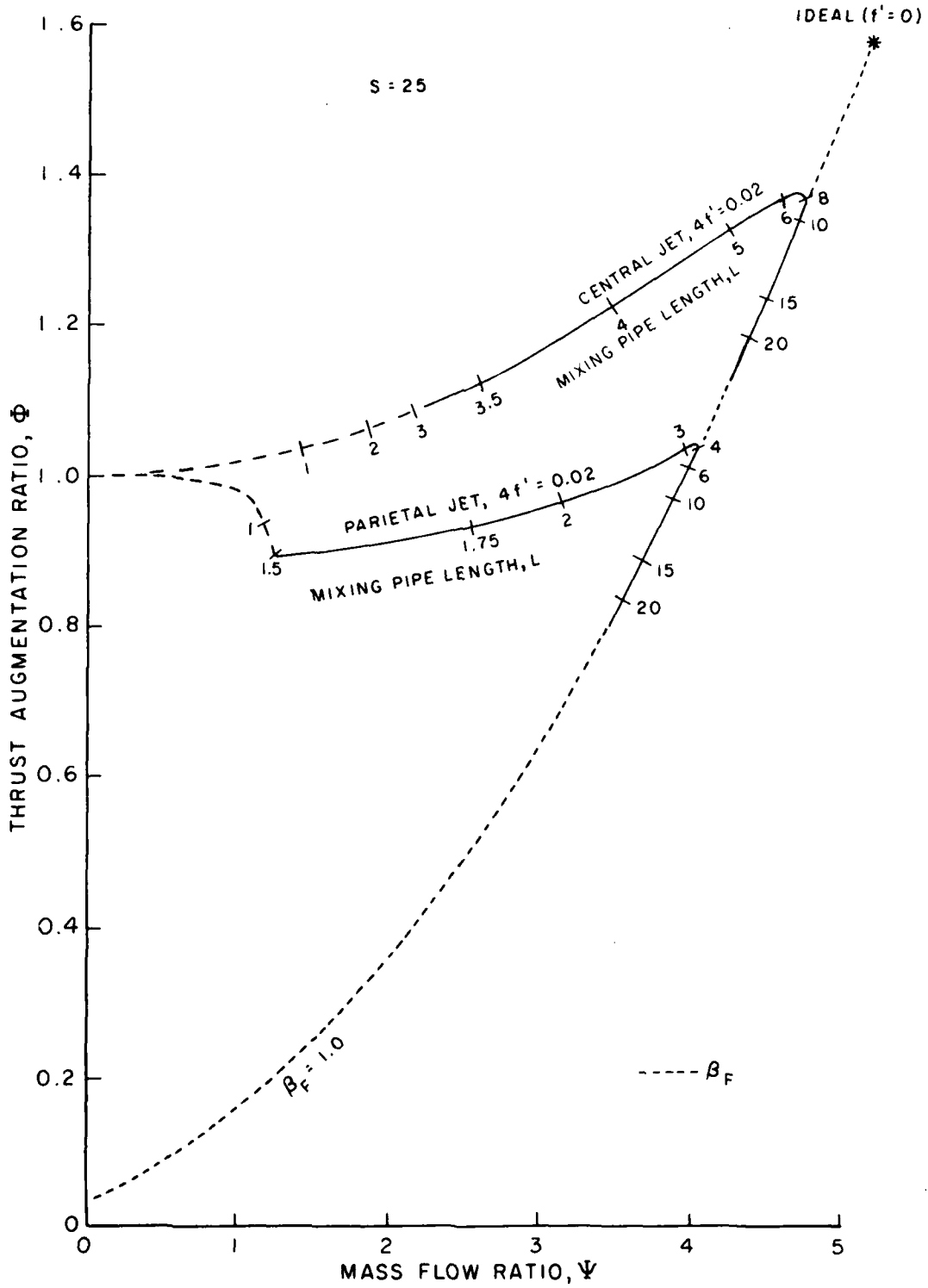


FIG. 31: PREDICTED PERFORMANCE OF CENTRAL AND PARIETAL JET EJECTORS ($S = 25$)

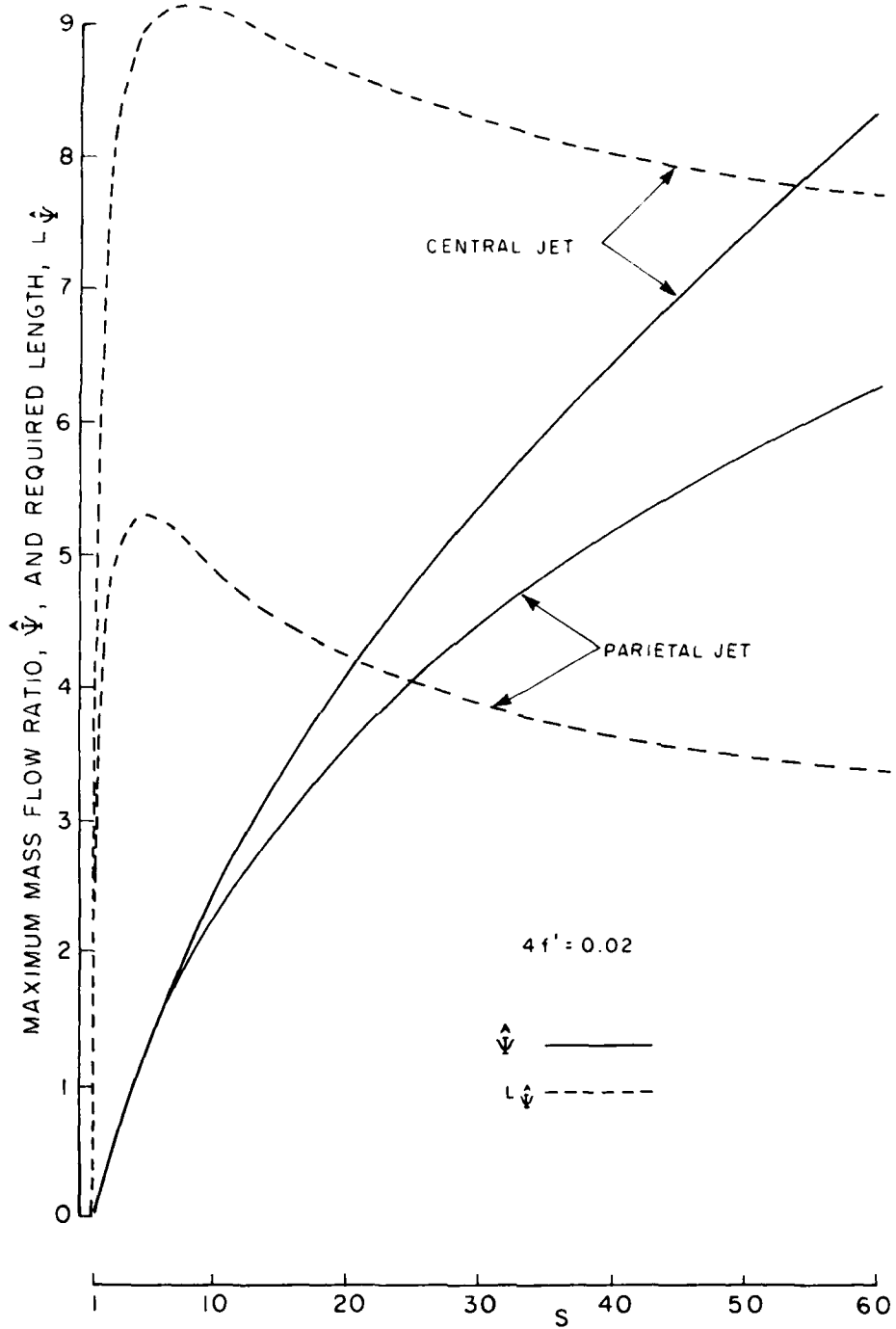


FIG. 32: PREDICTED MAXIMUM MASS FLOW RATIO AND REQUIRED LENGTH vs AREA RATIO

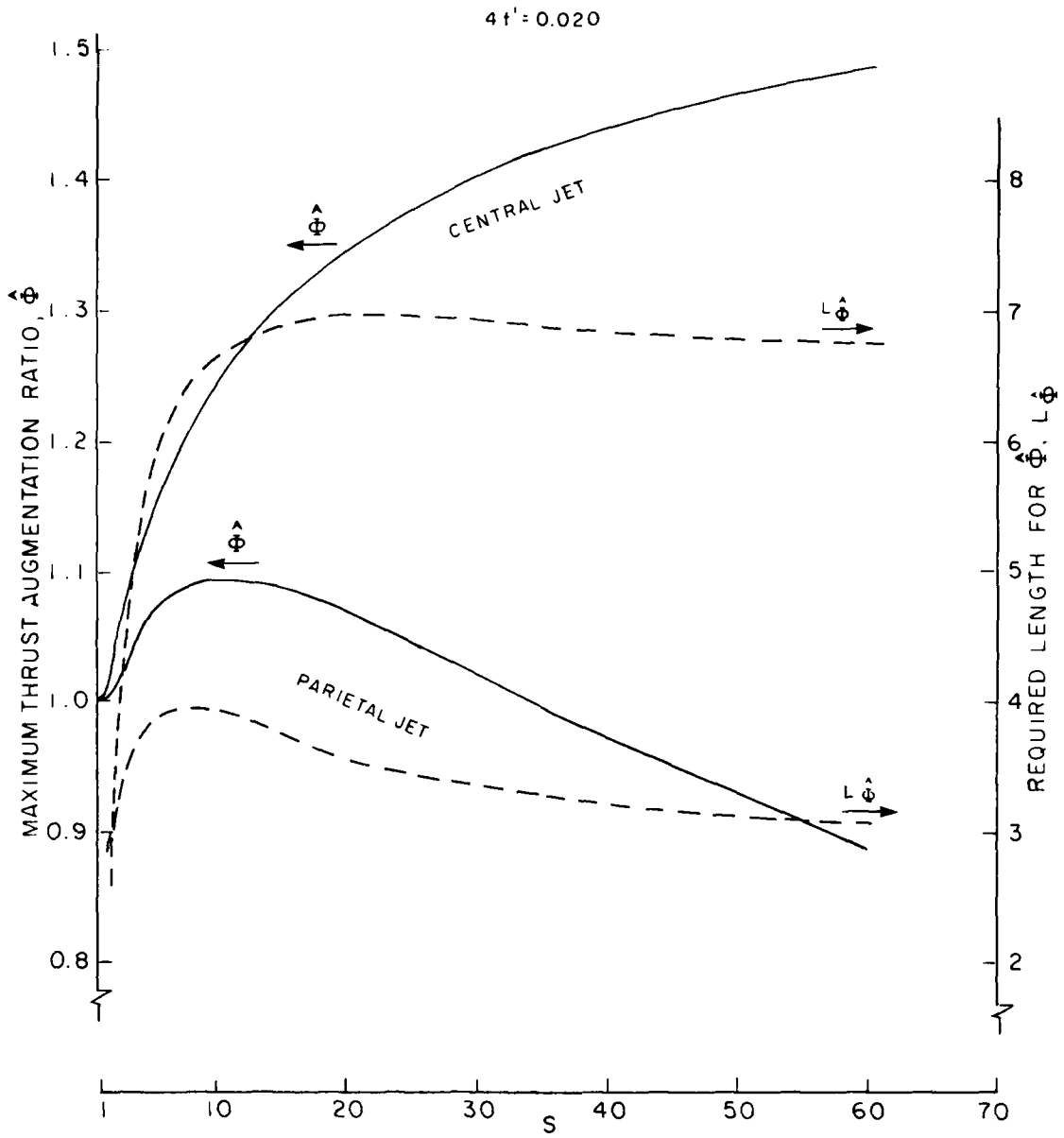


FIG. 33: PREDICTED MAXIMUM THRUST AUGMENTATION RATIO AND REQUIRED LENGTH vs AREA RATIO

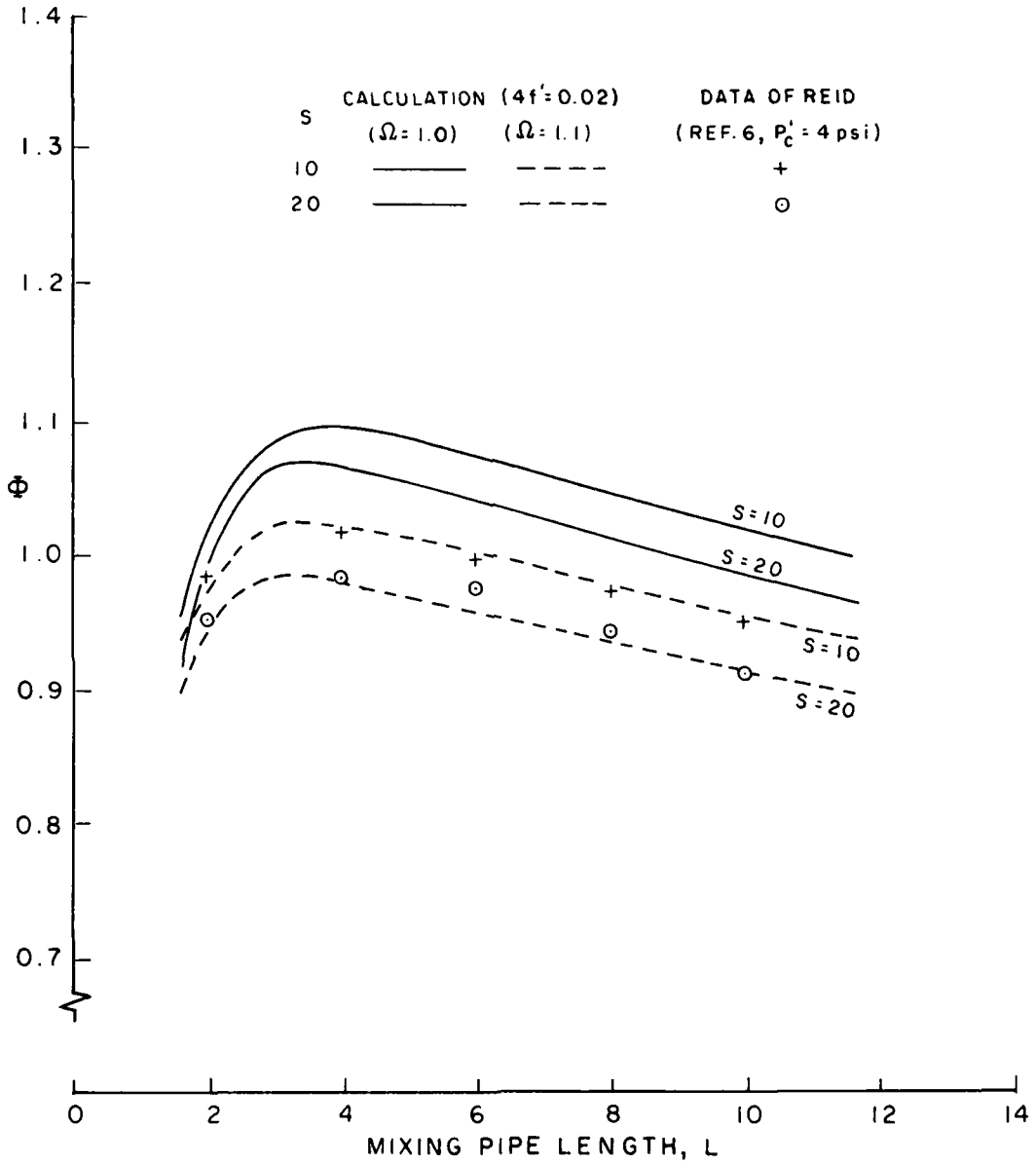


FIG. 34: PREDICTED PARIETAL EJECTOR PERFORMANCE COMPARED WITH MEASURED DATA OF REFERENCE 6 (S = 10 AND 20)

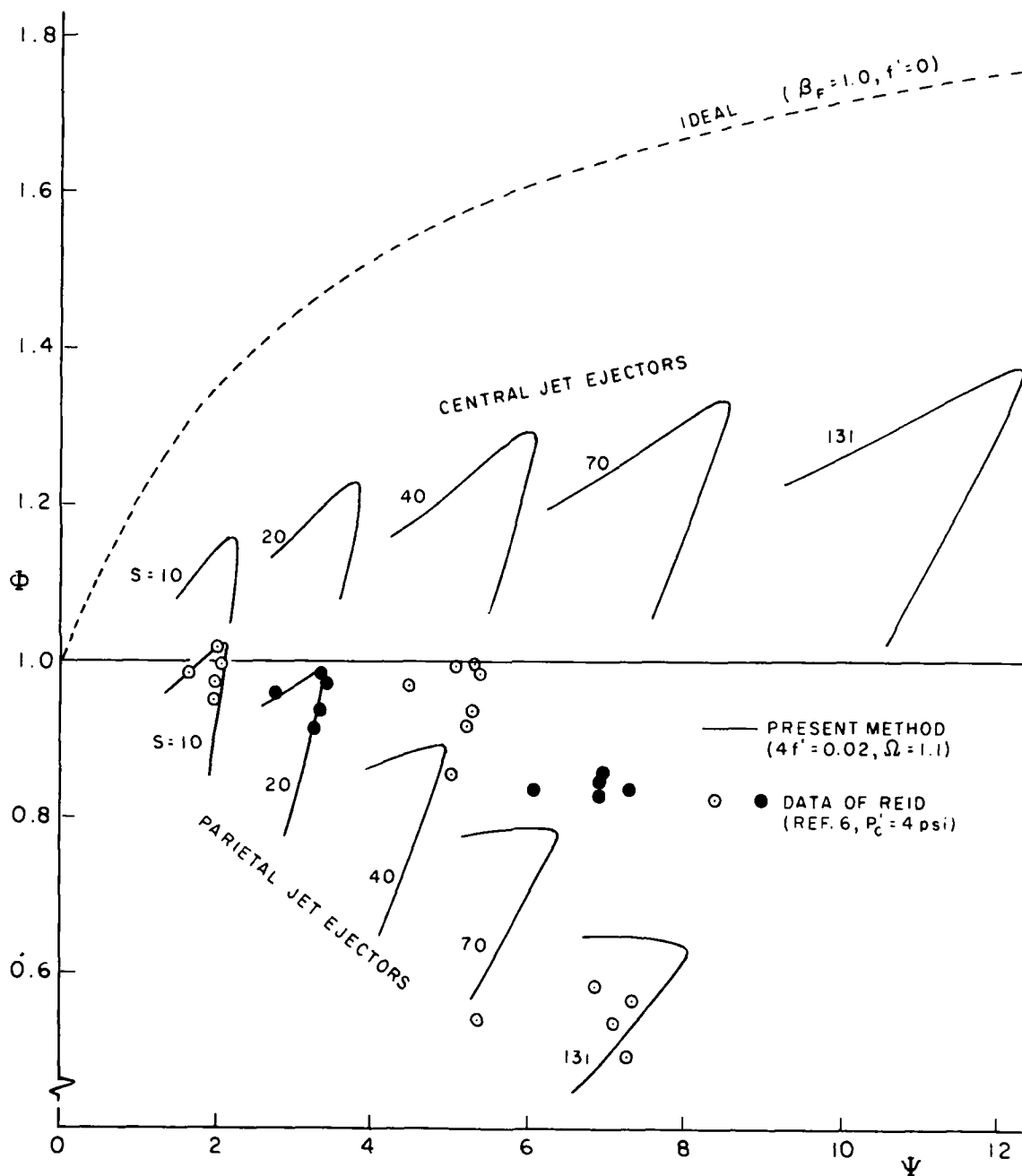


FIG. 35: PREDICTED PARIETAL EJECTOR PERFORMANCE COMPARED WITH MEASURED DATA OF REFERENCE 6 (S = 10 TO 131)

NRC, DME LR-602
National Research Council Canada, Division of Mechanical Engineering
CONFINED MIXING OF COAXIAL FLOWS
Tyler, R.A., Williamson, R.G., October 1980, 71 pp. (incl. figures)

An empirical approach is used to correlate the mixing of isothermal incompressible coaxial air flows in straight pipes of constant circular cross-section. An assumed decay function for kinetic momentum is correlated in terms of initial geometry and initial velocities of the mixing streams. The method allows the rapid estimation of quantities of engineering interest including the axial distribution of both static pressure and total momentum. The method has been tested against published data on thrust augmenting ejectors of the parietal type, and found to provide satisfactory reproduction of measured performance as affected by mixing pipe length and area ratio.

UNCLASSIFIED
1. Coaxial flow.
2. Turbulent mixing.
I. Tyler, R.A.
II. Williamson, R.G.
III. NRC, DME LR-602

NRC, DME LR-602
National Research Council Canada, Division of Mechanical Engineering
CONFINED MIXING OF COAXIAL FLOWS
Tyler, R.A., Williamson, R.G., October 1980, 71 pp. (incl. figures)

An empirical approach is used to correlate the mixing of isothermal incompressible coaxial air flows in straight pipes of constant circular cross-section. An assumed decay function for kinetic momentum is correlated in terms of initial geometry and initial velocities of the mixing streams. The method allows the rapid estimation of quantities of engineering interest including the axial distribution of both static pressure and total momentum. The method has been tested against published data on thrust augmenting ejectors of the parietal type, and found to provide satisfactory reproduction of measured performance as affected by mixing pipe length and area ratio.

UNCLASSIFIED
1. Coaxial flow.
2. Turbulent mixing.
I. Tyler, R.A.
II. Williamson, R.G.
III. NRC, DME LR-602

NRC, DME LR-602
National Research Council Canada, Division of Mechanical Engineering
CONFINED MIXING OF COAXIAL FLOWS
Tyler, R.A., Williamson, R.G., October 1980, 71 pp. (incl. figures)

An empirical approach is used to correlate the mixing of isothermal incompressible coaxial air flows in straight pipes of constant circular cross-section. An assumed decay function for kinetic momentum is correlated in terms of initial geometry and initial velocities of the mixing streams. The method allows the rapid estimation of quantities of engineering interest including the axial distribution of both static pressure and total momentum. The method has been tested against published data on thrust augmenting ejectors of the parietal type, and found to provide satisfactory reproduction of measured performance as affected by mixing pipe length and area ratio.

NRC No. 18861
UNCLASSIFIED
1. Coaxial flow.
2. Turbulent mixing.
I. Tyler, R.A.
II. Williamson, R.G.
III. NRC, DME LR-602

NRC, DME LR-602
National Research Council Canada, Division of Mechanical Engineering
CONFINED MIXING OF COAXIAL FLOWS
Tyler, R.A., Williamson, R.G., October 1980, 71 pp. (incl. figures)

An empirical approach is used to correlate the mixing of isothermal incompressible coaxial air flows in straight pipes of constant circular cross-section. An assumed decay function for kinetic momentum is correlated in terms of initial geometry and initial velocities of the mixing streams. The method allows the rapid estimation of quantities of engineering interest including the axial distribution of both static pressure and total momentum. The method has been tested against published data on thrust augmenting ejectors of the parietal type, and found to provide satisfactory reproduction of measured performance as affected by mixing pipe length and area ratio.

NRC No. 18861
UNCLASSIFIED
1. Coaxial flow.
2. Turbulent mixing.
I. Tyler, R.A.
II. Williamson, R.G.
III. NRC, DME LR-602

